

4-8-2011

Alternatives to Steel Grid Bridge Decks

Muhammad A. Saleem

Florida International University, msale005@fiu.edu

DOI: 10.25148/etd.FI11050304

Follow this and additional works at: <https://digitalcommons.fiu.edu/etd>

Recommended Citation

Saleem, Muhammad A., "Alternatives to Steel Grid Bridge Decks" (2011). *FIU Electronic Theses and Dissertations*. 372.
<https://digitalcommons.fiu.edu/etd/372>

This work is brought to you for free and open access by the University Graduate School at FIU Digital Commons. It has been accepted for inclusion in FIU Electronic Theses and Dissertations by an authorized administrator of FIU Digital Commons. For more information, please contact dcc@fiu.edu.

FLORIDA INTERNATIONAL UNIVERSITY

Miami, Florida

ALTERNATIVES TO STEEL GRID BRIDGE DECKS

A dissertation submitted in partial fulfillment of the

requirements for the degree of

DOCTOR OF PHILOSOPHY

in

CIVIL ENGINEERING

by

Muhammad Azhar Saleem

2011

To: Dean Amir Mirmiran
College of Engineering and Computing

This dissertation, written by Muhammad Azhar Saleem, and entitled Alternatives to Steel Grid Bridge Decks, having been approved in respect to style and intellectual content, is referred to you for judgment.

We have read this dissertation and recommend that it be approved.

Ton-Lo Wang

Girma Bitsuamlak

Syed M. Ahmed

Amir Mirmiran, Major Professor

Date of Defense: April 8, 2011

The dissertation of Muhammad Azhar Saleem is approved.

Dean Amir Mirmiran
College of Engineering and Computing

Interim Dean Kevin O'Shea
University Graduate School

Florida International University, 2011

© Copyright 2011 by Muhammad Azhar Saleem

All rights reserved.

DEDICATION

I dedicate this dissertation to my parents Muhammad Saleem (Late) and Mumtaz Jahan, my wife Sundas and our daughter Zainab. Without them this dream would not have been possible.

ACKNOWLEDGMENTS

I am grateful to my major advisor Dr. Amir Mirmiran, Dean of College of Engineering and Computing at the Florida International University for his support and guidance throughout my studies. The discussions I had with Dr. Mirmiran were a great source of learning and encouragement for me. I am truly thankful for his patience, support and valuable advices. I could not have completed this research without his help. I would also like to recognize and thank Dr. Ton-Lo Wang, Dr. Girma Bitsuamluk and Dr. Syed Ahmed for serving on my advisory committee.

I also want to acknowledge the help of Edgar Polo, Brandon Mintz, and Saad Ahmed together with all the personnel and graduate students at the Titan America Structures and Construction Testing Laboratory of the Florida International University. Special thanks to my friends Jun Xia and Wasif Ali who were always there to help me whenever I needed it.

The support of Florida Department of Transportation (FDOT) for providing funding, Lafarge North America for providing its UHPC (Ductal[®]), MMFX Technologies of Irvine, CA, for providing its HSS bars and FDOT Marcus Ansley Structures Research Laboratory for helping in fatigue tests are also acknowledged.

Last but not the least, I would like to thank to my parents, brothers and sisters in Pakistan for their endless support and encouragement.

ABSTRACT OF THE DISSERTATION
ALTERNATIVES TO STEEL GRID BRIDGE DECKS

by

Muhammad Azhar Saleem

Florida International University, 2011

Miami, Florida

Professor Amir Mirmiran, Major Professor

Most of the moveable bridges use open grid steel decks, because these are factory assembled, light-weight, and easy to install. Open grid steel decks, however, are not as skid resistant as solid decks. Costly maintenance, high noise levels, poor riding comfort and susceptibility to vibrations are among the other disadvantages of these decks. The major objective of this research was to develop alternative deck systems which weigh no more than 25 lb/ft², have solid riding surface, are no more than 4-5 in. thick and are able to withstand prescribed loading. Three deck systems were considered in this study: ultra-high performance concrete (UHPC) deck, aluminum deck and UHPC-fiber reinforced polymer (FRP) tube deck.

UHPC deck was the first alternative system developed as a part of this project. Due to its ultra high strength, this type of concrete results in thinner sections, which helps satisfy the strict self-weight limit. A comprehensive experimental and analytical evaluation of the system was carried out to establish its suitability. Both single and multi-unit specimens with one or two spans were tested for static and dynamic loading. Finite element models were developed to predict the deck behavior. The study led to the conclusion that the UHPC bridge deck is a feasible alternative to open grid steel deck.

Aluminum deck was the second alternative system studied in this project. A detailed experimental and analytical evaluation of the system was carried out. The experimental work included static and dynamic loading on the deck panels and connections. Analytical work included detailed finite element modeling. Based on the in-depth experimental and analytical evaluations, it was concluded that aluminum deck was a suitable alternative to open grid steel decks and is ready for implementation.

UHPC-FRP tube deck was the third system developed in this research. Prestressed hollow core decks are commonly used, but the proposed type of steel-free deck is quite novel. Preliminary experimental evaluations of two simple-span specimens, one with uniform section and the other with tapered section were carried out. The system was shown to have good promise to replace the conventional open grid decks. Additional work, however, is needed before the system is recommended for field application.

TABLE OF CONTENTS

CHAPTER	PAGE
1 INTRODUCTION.....	1
1.1 Problem Statement.....	1
1.2 Objectives of Research.....	2
1.3 Currently Available Light-Weight Bridge Decks.....	3
1.4 Research Methodology.....	4
1.5 Organization of Dissertation.....	5
References.....	7
2 ULTRA-HIGH PERFORMANCE CONCRETE BRIDGE DECK REINFORCED WITH HIGH STRENGTH STEEL.....	8
Abstract.....	8
2.1 Introduction.....	9
2.2 Significance of Research.....	12
2.3 System Design and Description.....	13
2.4 Experimental Program.....	14
2.5 Discussion of Test Results.....	17
2.5.1 Effect of End Anchorage.....	17
2.5.2 Effect of Multiple Webs.....	19
2.5.3 Effect of Continuity.....	20
2.5.4 Combined Effects of Multiple Webs and Continuity.....	21
2.6 Conclusions.....	22
References.....	24
3 STATIC AND FATIGUE PERFORMANCE OF ULTRA-HIGH PERFORMANCE CONCRETE BRIDGE DECK WITH HIGH-STRENGTH STEEL REBARS.....	40
Abstract.....	40
3.1 Introduction.....	41
3.2 Significance of Research.....	43
3.3 Experimental Work and Discussion.....	43
3.3.1 Shear Test for Connectors.....	44
3.3.2 Uplift Test for Connectors.....	45
3.3.3 Deck-to-Deck Connection Test.....	46
3.3.4 Lateral Distribution of Live Loads.....	47
3.3.5 Fatigue and Residual Strength Tests.....	49
3.4 Finite Element Analysis.....	52
3.5 Conclusions.....	53
References.....	55

4	DEVELOPMENT LENGTH OF HIGH STRENGTH STEEL REBARS IN ULTRA-HIGH PERFORMANCE CONCRETE.....	70
	Abstract.....	70
	4.1 Introduction.....	71
	4.2 Experimental Program.....	74
	4.2.1 Loading and Instrumentation.....	75
	4.2.2 Embedment length.....	76
	4.3 Test Results and Discussions.....	77
	4.3.1 Pullout test.....	77
	4.3.2 Beam tests.....	80
	4.4 Comparison with ACI 318-08 and ACI 408R-03.....	81
	4.5 Summary and Conclusions.....	82
	References.....	84
5	EXPERIMENTAL EVALUATION OF ALUMINUM BRIDGE DECK SYSTEM.....	100
	Abstract.....	100
	5.1 Introduction.....	102
	5.2 Review of Previous Work.....	103
	5.3 Loading Requirements.....	105
	5.4 Experimental Work.....	106
	5.4.1 Flexural Tests.....	106
	5.4.2 Shear Test for Connectors.....	108
	5.4.3 Uplift Test for Connectors.....	110
	5.4.4 Lip Test (Tongue and Groove Test).....	110
	5.4.5 Fatigue and Residual Strength Tests.....	111
	5.4.6 Coupon Tests.....	113
	5.5 Finite Element Analysis.....	113
	5.6 Conclusions.....	114
	References.....	116
6	TUBE-BASED COMPOSITE DECK SYSTEM FOR MOVEABLE BRIDGES.....	133
	Abstract.....	133
	6.1 Introduction.....	133
	6.2 Literature Review.....	134
	6.3 Preliminary Design.....	135
	6.4 Experimental Work.....	136
	6.4.1 Uniform Section Deck Specimen.....	137
	6.4.2 Tapered Section Deck Specimen.....	137
	6.5 Conclusions.....	138
	References.....	140
7	SUMMARY AND CONCLUSIONS.....	149
	7.1 UHPC Bridge Deck.....	149

7.2 Aluminum Bridge Deck.....	151
7.3 UHPC-FRP Bridge Deck.....	152
VITA.....	154

LIST OF TABLES

TABLE	PAGE
Table 2.1 Proportions of UHPC Constituent Materials.....	27
Table 2.2 Mechanical Properties of UHPC.....	27
Table 2.3 Test Matrix.....	28
Table 3.1 Test Matrix.....	57
Table 4.1 Proportions of UHPC Constituent Materials.....	87
Table 4.2 Test Matrix.....	88
Table 4.3 Summary of Pullout Tests Results.....	89
Table 4.4 Summary of Beam Tests Results.....	90
Table 5.1 Test Matrix.....	118

LIST OF FIGURES

FIGURE	PAGE
Figure 1.1 Open Rectangular and Diagonal Steel Grating for Bridge Decks.....	1
Figure 1.2 Re-Welding of Joints Broken due to Fatigue.....	2
Figure 1.3 Sandwich Plate System.....	4
Figure 2.1 Schematics of Single Unit Deck Panel.....	29
Figure 2.2 Idealized Stress-Strain Relationship of UHPC for Preliminary Specimen Design.....	30
Figure 2.3 Stress~Strain Curve for High Strength Steel.....	30
Figure 2.4 Finite Element Analysis: (a) FE Model, and (b) Deflection Response.....	31
Figure 2.5 Configuration of End Anchorages.....	32
Figure 2.6 Schematics of Test Specimens and Loading Configurations: (a) 1T1S; (b) 4T1S; (c) 1T2S; and (d) 3T2S.....	33
Figure 2.7 Testing of Specimen 1T1S-A with End Anchor Plate: (a) Test Setup, (b) Shear-Bond Failure, and (c) Load-Deflection Response.....	34
Figure 2.8 Testing of Specimen 1T1S-U without End Anchorage: (a) Shear-Bond Failure, (b) Measure of Shear Crack, and (c) Load-Deflection Response.	34
Figure 2.9 Testing of Specimens 1T1S-H with 180o Hook: (a) Shear Failure of Specimen 1, (b) Shear Failure of Specimen 2 (Shown Upside Down), and (c) Load-Deflection Responses.....	35
Figure 2.10 Testing of Specimen 4T1S-H: (a) Test Setup, (b) Punching Shear Pattern, and (c) Load-Deflection Responses.....	36
Figure 2.11 Testing of Specimen 1T2S-H: (a) Test Setup, (b) Shear Failure, and (c) Load-Deflection Responses.....	37
Figure 2.12 Testing of Specimen 3T2S-H: (a) Test Setup, (b) Punching Shear Pattern, and (c) Load-Deflection Responses for the North Span	38
Figure 2.13 Load-Steel Strain Responses for Specimen 3T2S-H.....	39

Figure 3.1 Schematics of Single-Unit Deck Panel.....	58
Figure 3.2 Testing of Deck-to-Girder Connection for Shear: (a) Test Setup; (b) Mode of Failure; (c) Schematics of Connection; and (c) Load-Displacement Responses.....	59
Figure 3.3 Testing of Deck-to-Girder Connection for Uplift: (a) Test Setup; (b) Mode of Failure; and (c) Load-Displacement Responses.....	60
Figure 3.4 Testing of Deck-to-Deck Connection: (a) Test Setup; (b) Mode of Failure; (c) Schematics of the Connection; and (d) Load-Deflection Responses.....	61
Figure 3.5 Average Distribution Factors for Various Specimens.....	62
Figure 3.6 Lateral Distribution of Load: (a) 5T1S; (b) 4T1S; (c) 4T2S; and (d) Deck-to-Deck Connection Specimen.....	63
Figure 3.7 Loading Configuration and Instrumentation Plan for the Fatigue Test.....	64
Figure 3.8 Fatigue Test: (a) Test Setup; and (b) Growth of Deflection under Fatigue Loading.....	65
Figure 3.9 Residual Strength Test with Load on Edge of Deck-to-Deck Connection: (a) Test Setup; (b) Shear Cracks; (c) Longitudinal Cracks; and (d) Load-Deflection Responses.....	66
Figure 3.10 Residual Strength Test with Load on Top of Deck-to-Deck Connection: (a) Test Setup; (b) Shear Cracks; (c) Longitudinal Cracks; and (d) Load-Deflection Responses.....	67
Figure 3.11 Stress-Strain Relationships: (a) UHPC; and (b) MMFX Steel.....	68
Figure 3.12 FE Analysis of Specimen 4T2S: (a) FE model; and (b) Comparison of Experimental and Analytical Results.....	69
Figure 4.1 Schematics of the Proposed UHPC-HSS Deck System.....	91
Figure 4.2 Stress-Strain Relationships for: (a) UHPC; and (b) MMFX Steel.....	92
Figure 4.3 Pullout Test: (a) Schematics of Specimens; and (b) Specimens Ready for Casting.....	93
Figure 4.4 Schematics of Beam Specimens with Instrumentation.....	94

Figure 4.5 Typical Load-Slip Responses for #3 Rebar Pullout Specimens.....	95
Figure 4.6 Typical Load-Strain Responses for #3 Rebar Pullout Specimens.....	95
Figure 4.7 Typical Load-Slip Responses for #7 Rebar Pullout Specimens.....	96
Figure 4.8 Typical Load-Strain Responses for #7 Rebar Pullout Specimens.....	96
Figure 4.9 Modes of Failure in Pullout Specimens.....	97
Figure 4.10 Variation of Crack Lengths in Pullout Specimens with respect to Embedment Lengths.....	98
Figure 4.11 Typical Load-Deflection Responses of Beam Specimens.....	98
Figure 4.12 Modes of Failure in Beams Specimens.....	99
Figure 4.13 Variation of Unbonded Lengths of Rebars with respect to Embedment Lengths in Beam Specimens.....	100
Figure 4.14 Comparisons of Test Data from Present Study with ACI 318-08 and ACI 408R-03.....	100
Figure 5.1 Aluminum Bridge Deck Panel: (a) Unit Cross Section; and (b) Assembled Deck.....	119
Figure 5.2 Test Setup for: (a) Simple-Span Panel; and (b) Two-Span Continuous Panel.....	120
Figure 5.3 Simple-Span Panel: (a) Deformed shape; and (b) Mid-Span Load- Deflection Response.....	121
Figure 5.4 Two-Span Continuous Panel: (a) Deformed Shape; (b) Mid-Span Load- Deflection Response.....	122
Figure 5.5 Simple-Span Inverted Panel: (a) Deformed Shape; (b) Mid-Span Load- Deflection Response.....	123
Figure 5.6 Shear Test for Connectors: (a) Test Setup; (b) Load-Displacement Response.....	124
Figure 5.7 Uplift Test for Connectors: (a) Test Setup; (b) Failure Pattern; and (c) Load-Deflection Responses.....	125

Figure 5.8 Lip Test: (a) Test Setup; (b) Failure Pattern; and (c) Load-Deflection Response.....	126
Figure 5.9 Instrumentation Plan and Loading Configuration for the Fatigue Test.....	127
Figure 5.10 Fatigue Test: (a) Test Setup; and (b) Growth of Maximum Deflection under Fatigue Loading.....	128
Figure 5.11 Residual Strength Test on Lip Joint: (a) Test Setup; and (b) Load-Deflection Responses.....	129
Figure 5.12 Residual Strength Test between Lip Joints: (a) Test Setup; and (b) Load-Deflection Responses.....	130
Figure 5.13 Tension Test: (a) Test Specimen; (b) Ruptured Specimen; (c) Stress-Strain Response.....	131
Figure 5.14 Comparison of Experimental and Analytical Load-Strain Responses: (a) Simple-Span Panel; and (b) Two-Span Continuous Panel.....	132
Figure 6.1 Stress-Strain Response of Glass FRP Tubes.....	142
Figure 6.2 Geometry of Deck Sections: (a) Uniform Section, and (b) Tapered Section.....	143
Figure 6.3 Stress-Strain Relationship for UHPC.....	144
Figure 6.4 Instrumentation Plan for the Uniform Section UHPC-FRP Deck Specimen.....	144
Figure 6.5 Test Setup for the Uniform Section UHPC-FRP Deck Specimen.....	145
Figure 6.6 Flexural Cracks near Ultimate Load.....	145
Figure 6.7 Load-Deflection and Load-Slippage Responses.....	145
Figure 6.8 Load-Strain Responses.....	145
Figure 6.9 Instrumentation Plan for the Tapered Section UHPC-FRP Deck Specimen.....	146
Figure 6.10 Test Setup for the Tapered Section UHPC-FRP Deck Specimen.....	147
Figure 6.11 Failure Pattern.....	147

Figure 6.12 Compression Failure..... 147

Figure 6.13 Un-cracked Tension Face..... 147

Figure 6.14 Slippage of FRP Tubes..... 147

Figure 6.15 Load-Deflection and Load-Slippage Responses..... 148

Figure 6.16 Load-Strain Responses..... 148

Figure 6.17 Load-Strain Response..... 148

Figure 6.18 Load-Strain Responses..... 148

LIST OF ABBREVIATIONS

1T1S	Single-T Simple-Span
1T2S	Single-T Two-Span
3T2S	Three-T Two-Span
4T1S	Four-T Simple-Span
ACI	American Concrete Institute
ADT	Average Daily Traffic
ASTM	American Society for Testing and Materials
DF	Distribution Factor
DOF	Degree of Freedom
FDOT	Florida Department of Transportation
FE	Finite Element
FRC	Fiber Reinforced Concrete
FRP	Fiber Reinforced Polymer
HSS	High-Strength Steel
LRFD	Load and Resistance Factor Design
NSC	Normal Strength Concrete
PVC	Polyvinyl Chloride
SCC	Self-Compacting Concrete
SPS	Sandwich Plate System
UHPC	Ultra-High Performance Concrete

1. INTRODUCTION

1.1 Problem Statement

Open grid steel decks are commonly used on moveable bridges (Figure 1.1) because they are light weight, factory assembled and easy to install. Self-weight of moveable bridge decks is typically limited to 25 lb/ft², which makes the open grid steel deck a suitable choice because these decks, on average, weigh between 14 and 25 lb/ft². Also, deck crowning, scuppers, and drains are not required, since rain water drains through the openings in the deck.

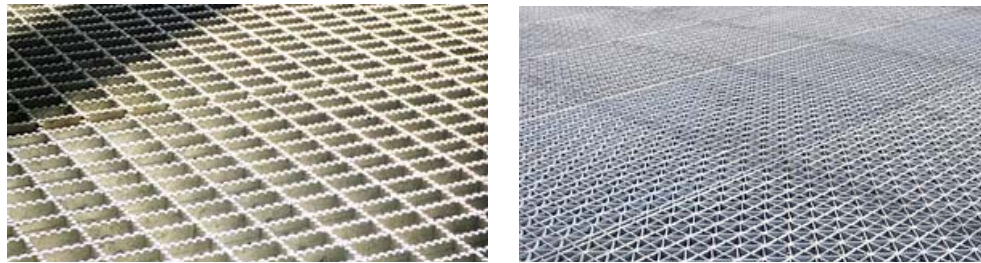


Figure 1.1 Open Rectangular and Diagonal Steel Grating for Bridge Decks

The open grid steel decks, however, have the following disadvantages:

1. Poor rideability: not as skid resistant as decks with a solid riding surface;
2. Damage prone and costly to maintain and repair;
3. High noise levels; and
4. Susceptible to vibrations and poor riding comfort

Since these bridge decks can polish over time, their skid resistance can further deteriorate to unacceptable levels without an active maintenance program, leading to poor rideability. Noise is another potential concern in some urban areas. Baseline acoustic testing by Florida Atlantic University (Takkasila and Reddy 1996) measured noise levels radiating from these bridge decks at levels that may cause public concern.

In addition, open grid steel decks may develop fatigue problems, leading to breakage of the deck welds. Experience at Florida Department of Transportation (FDOT) District 6 indicates that at times part or the entire panel may come loose (Figure 1.2), and often requires welding at least once a year (communications with Mr. Ryan Fisher, Moveable Structures Project Manager, FDOT District 6).



Figure 1.2 Re-Welding of Joints Broken due to Fatigue

Due to the safety, maintenance, and environmental concerns pertaining to open grid steel decks, research is needed into alternative deck systems that address the rideability concerns while meeting the strict self-weight limit (25 lb/ft^2) on these types of bridges.

1.2 Objectives of Research

The main objective of this research is to investigate promising alternatives to open grid steel decks. The alternative decks should have the following attributes:

1. Solid riding surface;
2. Weigh no more than 25 lb/ft^2 ;

3. Have no more than 4-5 in. thickness to fit within current structures;
4. Have a capacity to withstand AASHTO LRFD HS 20 truck loading; and
5. Ability to span at least 4 ft between supporting stringers

1.3 Currently Available Light-Weight Bridge Decks

Open Grid Steel Decks: First time used in 1920, open grid steel decks became more popular in the 1950's and were redesigned and reintroduced in the 1980's (Huang 2002). Three types of open grid steel decks are in use: unfilled system, concrete-filled system, and unfilled composite system (Exodermic™). Unfilled system is used with or without roughened surface. Filled system is either filled with concrete to the full depth of the grid or partial depth (ASTM Standard D 5484-99). Unfilled composite system consists of reinforced concrete slab composite with an unfilled grid (Exodermic™ brochure).

Sandwiched Plate System (SPS): The SPS was developed by Intelligent Engineering Limited of Buckinghamshire, U.K (Figure 1.3). It consists of two metal plates and an elastomeric core, which is sandwiched between the plates (Kennedy et al. 2002). SPS has improved fatigue and corrosion resistance, because most of the fatigue and corrosion prone details are removed from it (www.ie-sps.com). SPS is compatible with all types of wearing surfaces. While its first application was on Shenley Bridge in Quebec, Canada, SPS has by now been implemented in U.S., U.K. and Germany (Tyuryayeva 2006). FDOT considered SPS for the Mathews Bridge in Jacksonville.

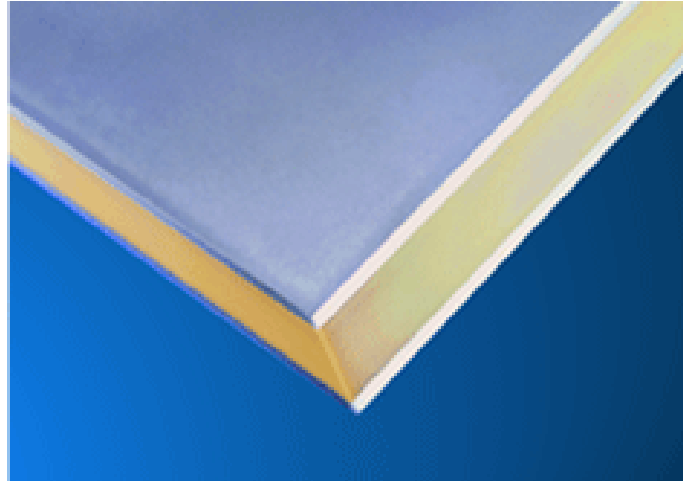


Figure 1.3 Sandwich Plate System
(Source: <http://www.ie-sps.com>)

Fiber Reinforced Polymer (FRP) Bridge Decks: An FRP bridge deck weighs approximately 80% less than a concrete deck (Mu et al. 2006). Therefore, FRP decks can be extremely advantageous for movable bridges, in which self-weight is most of the times the governing design criterion. During the last fifteen years, several old bridge decks have been replaced by FRP decks. At present, a total of nine state DOTs are using FRP, decks including Illinois, Maryland, North Carolina, Delaware, Kansas, New York, Ohio, and Oregon. An existing timber bridge deck of a moveable bridge in Oregon was replaced by and FRP deck (Hong and Hastak 2006). Recently developed FRP decks include DuraSpan[®] Bridge Deck, ZellComp[®] Decking System, Strongwell[®] FRP Bridge Deck, Honeycomb Sandwich Panels, and KSCI[®] FRP Composite Bridge Deck.

1.4 Research Methodology

The following three proposed deck systems are evaluated experimentally to ensure their feasibility and to assess their serviceability and ultimate capacity:

1. Ultra-high performance concrete (UHPC) deck;

2. Aluminum deck panels made by SAPA Group of Sweden; and
3. UHPC-fiber reinforced polymer (FRP) tube deck

Two types of bridge deck configurations are used; simple-span and two-span continuous. The simple-span specimens are subjected to a single load at their mid-span, whereas the two-span specimens are loaded with two loads, one in each span. Fatigue tests are also performed on select specimens. Deck-to-deck and deck-to-girder connections are also tested individually before using them in the full-scale specimens. Depending on the type of materials used, ancillary tests are carried out to determine the material properties of the constituents; for example, compressive strength and modulus of rupture of concrete, and tensile strength and modulus of elasticity of steel rebars and aluminum. Analytical models are also developed to predict the behavior of the above mentioned deck systems. The predicted responses are also compared with the experimental results.

1.5 Organization of Dissertation

This dissertation is divided into seven chapters including this first chapter of introduction. Chapters 2 through 6, each represents a paper published, in press, or in review. Chapter 2 covers the experimental evaluation of UHPC deck including the static flexural tests under HS 20 truck wheel load. Chapter 3 presents the experimental results of connection details as well as fatigue testing of UHPC deck. It also includes the outcome of analytical modeling of the deck system using the general purpose finite element program ANSYS[®]. Chapter 4 comprises of pullout and beam test results conducted to establish the development length of high-strength steel in UHPC. Chapter 5 presents the experimental evaluation of the second alternative deck system made of

aluminum. The experimental results include flexural tests, deck-to-girder and deck-to-deck connection tests, and fatigue and residual strength test. Chapter 6 consists of test results of the third deck system made of FRP tubes and UHPC. Chapter 7 provides the conclusions of the present study and recommendations for the future research.

References

AASHTO LRFD Bridge Design Specifications, 2005, Interim Revisions, American Association of State Highway and Transportation Officials, Washington, D.C.

ASTM D5484, 1999, "Standard Specification for Steel Grid Bridge Flooring." ASTM International, West Conshohocken, PA.

Exodermic™ Brochure, Exodermic™ Bridge Deck Inc., North Baltimore, OH.

Hong, T., and Hastak, M., 2006, "Construction, Inspection, and Maintenance of FRP Deck Panels." *Journal of Composites for Construction*, ASCE, Volume 10, Issue 6, pp. 561-572.

Huang, H., Chajes, M. J., Mertz, D. R., Shenton, H.W., Kalikin, V. N., 2002, "Behavior for Open Steel Grid Deck for Bridges" *Journal of Constructional Steel Research*, Volume 58, pp. 819-842

ie-sps.com accessed on April 14, 2011

Kennedy, D. G. L., Dorton, R. A., Alexander, S. D. B., 2002, "The Sandwich Plate System for Bridge Decks" International Bridge Conference, Pittsburgh, PA.

Mu, B., Wu, H., Yan, A., Warnemuende, K., Fu, G., Gibson, R.F., and Kim, D., 2006, "FEA of Complex Bridge System with FRP Composite Deck." *Journal of Composite for Construction*, ASCE, Volume 10, Issue 1, pp. 79-86.

Takkasila, M., and Reddy, H., 1996, "Structural Modification of Bascule Bridges for Noise Mitigation." Florida Atlantic University, Boca Raton, FL.

Tyuryayeva, Y., 2006, "Study of Noise Mitigation and Skid Resistance in Florida Bascule Bridge Decks" MSc. Project, Florida International University, Miami, FL.

2. ULTRA-HIGH PERFORMANCE CONCRETE BRIDGE DECK REINFORCED WITH HIGH STRENGTH STEEL

Muhammad Azhar Saleem, Amir Mirmiran, Jun Xia, and Kevin Mackie

Accepted for publication in the ACI Structural Journal

Abstract

Currently there is a need to develop light-weight bridge deck systems with solid riding surfaces to replace the open grid steel decks from moveable bridges. Open grid steel decks present several problems including poor rideability, high noise levels, susceptibility to fatigue damage, and high maintenance costs. There is a great opportunity to use advanced materials such as ultra-high performance concrete (UHPC) to develop new light-weight bridge deck systems. UHPC is increasingly making its way into bridge engineering applications.

In this study, a low profile UHPC deck system has been developed that satisfies the strength and serviceability requirements, addresses the concerns with open grid steel decks, and meets the strict self-weight requirements for movable bridges. The detailed experimental study shows that the proposed system has great potential to serve as an alternative to open grid steel decks. Standard 180° hook on both ends of flexural reinforcement help avoid bond failure. Establishment of development length of high strength steel for UHPC, deck-to-deck connection, deck-to-girder connection and fatigue performance are still needed to be investigated before the system would be ready for implementation.

2.1 Introduction

According to National Bridge Inventory (2008), there are 71,466 structurally deficient and 79,922 functionally obsolete bridges in the United States (U.S.). A majority of these bridges need deck repairs (Naaman and Chandrangsou 2004). Therefore, there is a vital need to develop light-weight bridge deck systems that could be used to rehabilitate a critical component in the aging infrastructure. Moveable bridges are also a victim of deterioration, and require urgent repair and restoration. Open grid steel decks are commonly used on moveable bridges because they are light weight and easy to install. Self-weight of moveable bridge decks is typically limited to 25 lb/ft² (1.2 kN/m²), which makes the open grid steel deck a suitable choice because these decks, on average, weigh between 14 and 25 lb/ft² (0.67 and 1.2 kN/m²). However, these decks have major shortcomings including poor rideability, high maintenance cost, high noise levels, and susceptibility to fatigue damage (Mirmiran et al. 2009).

A new type of ultra-high performance concrete (UHPC) waffle slab deck was developed that includes a solid riding surface and is within the acceptable self-weight limit for moveable bridge decks. The unit weight of UHPC (156 lb/ft³ or 2500 kg/m³) is similar to that of conventional concrete but with much higher strength. Therefore, it results in shallower sections and ultimately lower self-weight than an equivalent capacity conventional concrete deck. The proposed UHPC deck has a low profile of only 5 in. (127 mm) depth, which is compatible with the open grid steel decks that typically span a 4 ft (1,219 mm) girder spacing. This paper presents the experimental characterization of the proposed deck system.

UHPC is an advanced structural material composed of a high-strength cementitious matrix and steel fibers (Habel et al. 2007), with better durability and higher tensile strength than other cementitious materials (Habel 2006, Graybeal 2007). The most distinguishing characteristics of UHPC are the lack of coarse aggregate, the use of fibers, and the low water/cement ratio. The use of silica fumes, ground quartz and only fine aggregates creates a dense matrix with minimal voids, which in turn results in a significant increase in strength as compared to regular concrete which has both fine and coarse aggregates. The fibers in the matrix are designed to provide bond at the micro level and help control the cracks. The fibers act as micro-reinforcement, similar to mild steel reinforcement in conventional reinforced concrete at the macro level (Perry 2003, Harris and Roberts-Wollmann 2005). UHPC has 4-8 times higher compressive strength than conventional concrete. Heat treatment of UHPC with steaming at 90° C (194° F) and 95 percent relative humidity for 48 hours significantly enhances compressive strength and modulus of elasticity, decreases creep coefficient, and almost eliminates long-term shrinkage (Graybeal 2006). Graybeal and Hartmann (2003) found the tensile strength of UHPC ranging from 0.9 to 1.7 ksi (6.2 to 12 MPa) with various curing regimes. Harris and Roberts-Wollmann (2005) argued that the high tensile strength of UHPC is achieved as a result of the interaction of steel fibers at the microscopic level and their ability to sustain load after the onset of cracking. In addition, UHPC achieves flexural strengths ranging from 5.0 to 7.2 ksi (35 to 50 MPa) based on standard flexural beam tests (Perry and Zakariassen 2003).

Several UHPC products are available in the market. The one used for this project is Ductal[®], which is developed from the joint research of three French companies;

Bouygues, Lafarge, and Rhodia. Its constituent materials include cement, silica fumes, ground quartz, sand, steel fibers (2% by volume), super-plasticizer, and water. The straight high-strength steel fibers have a 0.008 in. (0.2 mm) diameter and a ½ in. (13 mm) length. The critical fiber volume fraction to achieve the homogeneous distribution is about 0.4% to 0.5% (Vodicka et al. 2004). Taerwe et al. (1999) also achieved the homogeneous distribution for up to 8% fiber volume fraction when using short steel fibers. Therefore 2% of steel fiber volume fraction is a suitable amount to achieve a homogeneous distribution without compromising the workability of the cement paste. Proportion of the constituent materials used in this research is presented in Table 2.1.

In recent years, UHPC has been used in the construction of highway and pedestrian bridges (Blais 1999, Hajar 2003, Graybeal 2006) in the U.S., New Zealand, South Korea, Japan, and Australia. Naaman and Chandransu (2004) developed a UHPC deck with only one layer of steel rebars at the bottom instead of four (two bottom; two top). They concluded that by using UHPC instead of conventional concrete, about 70% of the reinforcement could be eliminated and a significant reduction in crack widths could be achieved. Graybeal (2007), Perry (2007), and Toutlemonde (2007) have also developed bridge decks with UHPC but with higher self weights, which exceed the limits for moveable bridges. Nonetheless, test results on these decks have demonstrated the feasibility of UHPC as a promising material for bridge deck applications. Harris and Roberts-Wollmann (2005) evaluated the punching shear capacity of UHPC slabs by testing twelve 45 x 45 in. (1,143 x 1,143 mm) slabs of various thicknesses. They concluded that 1 in. (25.4 mm) thickness of UHPC deck is sufficient to prevent the punching shear failure under 8 x 20 in. (203 x 508 mm) wheel load of 37.2 kips (166 kN).

Naaman et al. (2007) stated that the punching shear resistance increases significantly by adding fibers, because they develop tensile strain-hardening, and minimize the spalling of concrete cover at large deformations.

A major cause of early deterioration in reinforced concrete structures is the corrosion of reinforcing bars (Sahmaran et al. 2008). To mitigate this issue, high-strength steel (HSS) bars of MMFX Technologies of Irvine, CA, were used in the proposed deck system. These uncoated, high-strength, and corrosion-resistant microcomposite bars are made from a low-carbon chromium alloy steel. The corrosion resistance of this type of rebar has been tested through accelerated laboratory deterioration tests, and the results show a generally good corrosion resistance compared to black bars (Hartt et al. 2007). Field applications of MMFX include reinforcement in bridge decks by Iowa and Kentucky Departments of Transportation. Delaware Department of Transportation also considered using these bars in its I-95 Service Road Bridge 1-712-B in 2005 (Chajes et al. 2005).

2.2 Significance of Research

Rehabilitation of aging infrastructure in North America is an enormous challenge faced by transportation agencies. Advanced materials such as UHPC can provide alternative solutions. No prior research has focused on developing lightweight UHPC systems for moveable bridges with strict weight, geometric, and strength constraints. The proposed waffle slab UHPC-HSS deck system is shown experimentally to meet these requirements, and has the potential to replace the open grid steel decks currently in use on most moveable bridges. The concept has potential applications in other types of bridges that require a lightweight deck.

2.3 System Design and Description

The proposed waffle deck system is composed of longitudinal and transverse ribs. Longitudinal ribs span between the girders and act as primary load-carrying members for the deck. The smaller transverse ribs run parallel to the direction of traffic and connect the longitudinal ribs. The schematic of a single unit of the proposed deck is shown in Figure 2.1.

The simplified stress-strain relation of UHPC (Graybeal 2006), as shown in Figure 2.2, was used for the preliminary design of the deck, with a modulus of elasticity of 8,000 ksi (55.2 GPa), and tensile and compressive strengths of 1.13 and 28 ksi (7.8 and 193 MPa), respectively. The ultimate strains in compression and tension are 0.0035 and 0.007 respectively. Some researcher has suggested smaller values for the ultimate tensile strain for UHPC prepared with smooth steel fibers. However, calculations have shown that there is no noticeable difference in initial stiffness, ultimate sectional moment capacity, or the ultimate curvature due to different ultimate tensile strains. This discussion will be presented in another paper related to the analytical evaluation of the proposed bridge deck system. Mechanical properties as provided by the manufacturer are shown in Table 2.2. An elastic-perfectly plastic model was used for the HSS rebars, with a yield strength of 75 ksi (517 MPa). The stress strain curve for the HSS rebar is shown in Figure 2.3. Based on the self-weight limit of 25 lb/ft² (1.2 kN/m²) a series of cross sections were developed and a sensitivity analysis was performed to help with the sizing of the proposed deck system. Factors considered included reinforcement ratio, flange width and thickness, and rib depth and thickness in both directions. A flange thickness of 1.25 in. (31.75 mm) was selected according to Harris and Roberts-Wollmann (2005) to

avoid punching shear failure. The overall depth was limited to 5 in. (127 mm) to be compatible with current open grid steel decks. The section was designed as singly-reinforced, with one No. 7 (No. 22M) bar at a minimum clear cover of ½ in. (13 mm).

In order to decide the minimum number of webs of the deck system that should be used in the experimental investigation, a preliminary finite element analysis was performed using MSC.Patran/Nastran. Four node shell elements were used for both the webs and slabs while truss elements were used for steel reinforcement. The truss elements shared the nodes with the quad elements representing the webs to simulate a perfect bond between the reinforcement and concrete. All materials were treated as elastic in this stages and corresponding modulus of elasticity and Poisson's ratio were used in the program. The distributed load was applied on the top of the deck piece at center on a 10 x 20 in. (508 x 254 mm) rectangular region to represent the loading patch. The deck was simply supported at the two edges. The maximum deflection of the deck system versus the different number of webs the deck piece consisted is plotted in Fig 2.4. It was found that the load can be transferred transversely as far as up to 2 webs on either side of the web being loaded, so this geometric configuration was used for the experiments. The distribution factor, which is defined as the percentage of the total load resisted by the central deck unit, can be estimated based on the deflections of all webs, and the result turned out to be around 36% for a five-web deck model.

2.4 Experimental Program

The primary objective of the experimental work was to evaluate the behavior of the proposed deck at service and ultimate loading conditions, as well as to investigate its failure modes. The experimental program included testing single and multi-unit deck

panels with simple and two-span configurations. Specimens were prepared in five separate castings without any heat treatment (see Table 2.3). Formwork for the specimens was initially made of plywood. However, later castings were carried out with styrofoam forms, for their ease to cut, assemble, and transport.

Since the concrete has self compacting characteristics, no internal or external vibrations were applied during the casting. Material was introduced from one end of the formwork and was allowed to flow to the other end. Whenever more material was required it was introduced behind the leading edge of the flowing material. The same casting method was used for all specimens to maintain a similar fiber distribution. One simple-span specimen was cut after testing to examine the spatial distribution of the fibers. It was observed that the fibers tend to align with the formwork (Fehling and Bunje 2008), which may cause a non-homogenous distribution of the fibers. Initially, it was intended to apply heat treatment for curing, but the required temperature of 90°C (194°F) could not be achieved. Therefore, the traditional method of moist curing was used instead. The specimens were sealed with plastic sheets for 28 days to prevent the loss of moisture. The strengths achieved without heat treatment were still sufficient to satisfy the ultimate load requirements.

Initially, four single-T simple-span (1T1S) specimens were tested with three different end anchorage options (Figure 2.5) for the bottom flexural rebars: (a) 2 x 2 in. (51 x 51 mm) welded steel plate; (b) 180° hook; and (c) no anchorage. Based on test results, it was decided to use the 180° hook for the end anchorage in subsequent specimens. The deck design was then expanded to four-T simple-span (4T1S), single-T two-span (1T2S), and three-T two-span (3T2S) specimens. The specimen test matrix is

summarized in Table 2.3 and schematics of test specimens and loading configurations are shown in Figure 2.6. Table 2.3 also describes the compressive strengths for various batches. Compressive strengths were obtained by testing 4 in. diameter and 8 in. long cylinders. In order to insure uniform distribution of load, edges of the cylinders were grounded before testing. Load was applied at a rate of 35 psi/sec.

The simple-span specimens were subjected to a single load, whereas the two-span specimens were loaded simultaneously at the middle of each span. Loads were applied on an AASHTO prescribed footprint of 20 x 10 in. (508 x 254 mm) for an HS 20 truck dual-tire wheel, using a neoprene pad with a steel plate on top and with the longer side oriented perpendicular to the traffic. The simple-span specimens had a 4 ft (1,219 mm) center-to-center (c/c) spacing between the supporting steel girders. The same arrangement was used for two-span specimens. The distance between the two loading pads was 4 ft (1,219 mm), which is more critical than the standard wheel base of 6 ft (1,829 mm) for an HS truck. Both the panel and beam actions were examined at service and ultimate load levels.

String potentiometers with 12 in. (305 mm) range and strain gauges were installed at critical locations to acquire the deflection and strain data. A hydraulic actuator with a 235 kip (1,046 kN) capacity was used to apply the load. A displacement control procedure was adopted for all tests at a rate of 0.015 in./min (0.38 mm/min). All instruments were connected to a data acquisition system with a sampling frequency of 1 Hz. The target live load was 37.2 kips (166 kN), including the dynamic impact factor and load factor, based on the AASHTO LRFD recommendations (2005). The supporting girders were W24x68 (W610x101), which are typically used in moveable bridges.

2.5 Discussion of Test Results

All specimens were continuously monitored during the tests, and any excessive cracking or deflection, and significant load drop was considered as sign of failure and an indicator to stop the test. The dominant mode of failure in all specimens was beam shear. In the multi-unit specimens (4T1S and 3T2S) beam shear failure was followed by the punching shear failure near the ultimate load. The results are grouped in terms of the effects of end anchorage, number of webs, and the continuity on the system performance.

2.5.1 Effect of End Anchorage

The load-deflection response, test setup, and mode of failure for Specimen 1T1S-A with welded anchor plate are shown in Figure 2.7. While minor flexural cracks were observed at mid-span, they did not grow significantly with the increase of load. In contrast, large shear cracks developed at both ends between the supporting girders and the loading pad. Breaking sounds from the pullout of the steel fibers could be heard at frequent intervals throughout the test. The failure took place due to the fracture of the weld between the end plate and the rebar at 40 kips (178 kN), with a maximum deflection of 1 in. (25.4 mm). Failure was sudden with a loud sound, and quite notable from the sudden load drop with no increase in deflection. Nonetheless, the specimen exceeded the target load. Readings from the top strain gauge affixed to concrete at mid-span right under the loading pad were deemed inaccurate due to the loading pad restrictions. The maximum compressive strain at the edge of the loading pad reached 0.0037, slightly higher than the crushing strain of concrete.

Figure 2.8 presents the failure pattern and load-deflection response of the Specimen 1T1S-U without any end anchorage. The first shear crack appeared at 21.3 kips

(94.8 kN). The response began to soften near the ultimate load of 33 kips (147 kN) with a deflection of 0.71 in. (18 mm) at the peak load. The test was stopped when the deflection reached 1.16 in. (29.5 mm), and the load dropped by 63% to 12.3 kips (54.7 kN). Flexural cracks were deemed insignificant, as the mode of failure was a combination of bond and shear failure. The failure, however, was more ductile than the specimen with welded anchor plate. Shear cracks appeared near both supports, and gradually widened. A large shear crack opened more than $\frac{3}{4}$ in. (19 mm) and moved towards the top flange, which subsequently crushed. The extension of the shear crack into the top flange is possibly due to the absence of end anchorage. The ultimate load for this specimen was less than the target load, emphasizing the need for end anchorage. The maximum compressive strain at the edge of the loading pad was 0.014, about four (4) times higher than the specimen with the welded anchor plate. The apparent reason for such a high strain is the extension of shear crack into the flange.

Specimens 1T1S-H1 and 1T1S-H2 were made with the ACI standard 180° hooks, based on the results of the first two tests. Figure 2.9 shows the load-deflection responses and modes of failure for both specimens. The hooks seemingly improved force transfer across the shear cracks, such that the failure of Specimen 1T1S-H1 was no longer a bond failure. The first shear crack appeared at 22.3 kips (99 kN). Two major shear cracks appeared at both ends and gradually opened up with the increase of load. Although the hooks averted the bond failure, the ultimate load was the same as the specimen with welded anchor plate, i.e., 40 kips (178 kN) with a slightly less deflection of 1.04 in. (26.4 mm) at the peak load. However, the reason for the lower strength was attributed to the

lower compressive strength of the batch. The maximum steel strain reached 0.0067, equivalent to a stress level of 132 ksi (910 MPa).

A second specimen with 180° hook was considered necessary because the first test did not provide a realistic estimate of the ultimate load due to its lower material strength. Specimen 1T1S-H2 developed the first shear crack at 26 kips (116 kN), and reached a peak load of 47 kips (209 kN) with a deflection of 1.05 in. (26.7 mm) at the peak load. The failure was relatively more ductile than Specimen 1T1S-H1, as the maximum steel strain reached 0.0096, equivalent to a stress level of 143 ksi (986 MPa).

The first four specimens clearly showed the feasibility of the proposed system as an alternative to open grid steel deck. All specimens with 180° hooks exceeded the target load of 37.2 kips (166 kN). The test program was therefore expanded to multiple spans and multiple units to understand both the negative moment behavior and the transverse load distribution.

2.5.2 Effect of Multiple Webs

Specimen 4T1S-H with 180° hooks and 4 equivalent webs was tested over a simple span to determine the transverse load distribution among the webs. The first shear crack appeared at 40 kips (178 kN), and then gradually grew wider, leading to the punching of the top flange. The deck failed at 85 kips (378 kN), i.e., twice the target load, with a center rib deflection of 0.85 in. (26.1 mm) at the peak load. The test was stopped when the load dropped by about 30% to 60 kips (267 kN) at a maximum deflection of 1.22 in. (31 mm). Figure 2.10 shows the load-deflection responses measured under each rib.

The strain in the transverse rebar at mid-span was 0.0116, which is nearly three (3) times that of the longitudinal steel, mainly because of the lower stiffness of transverse ribs. Most of the load was taken by the three interior ribs, as shown in the load-deflection responses. The load distribution between the ribs can be calculated based on the rebar strains at the bottom, which are 0.001, 0.0025, and 0.004, respectively for the exterior, interior, and central ribs at the ultimate load. The distribution factor for the center unit is calculated by dividing its rebar strain (0.004) with the sum of rebar strains (0.011) in all five webs. It comes out to be 0.364, which means 36.4% of the total load is carried by the central unit. This value is very close to that derived earlier from the elastic FE analysis at the design phase. After the load drop, the load was taken primarily by the central rib. The drop in the load-deflection curve is attributed to the yielding of the transverse No. 4 (No. 13M) rebar, which caused a change in the transverse load distribution. Punching shear failure occurred when the entire load was fully concentrated on the central rib.

2.5.3 Effect of Continuity

Specimen 1T2S-H with 180° hooks and a single web was tested over two equal spans to assess the continuity behavior of the proposed deck. Figure 2.11 shows the test setup, mode of failure, and load-deflection responses. The first shear crack appeared at 24 kips (107 kN) near the interior support. At later stages, shear cracks also appeared near the exterior supports with some flexural cracks at the two mid-spans. Initially, it was planned to load the specimen beyond the plastic hinge formation at the interior support. However, the test was stopped at 55 kips (245 kN) when the spreader beam was about to touch the specimen due to excessive deflections of the deck. A slight difference was observed between the load-deflection responses of the two spans. When the strain in the

top rebar reached 0.0025 at the interior support, both the load-deflection and the load-strain curves began to soften significantly. This may be attributed to the top rebar losing its bond strength at the cracked region.

2.5.4 Combined Effects of Multiple Webs and Continuity

Figure 2.12 shows the test setup, mode of failure, and load-deflection responses of Specimen 3T2S-H, with 180° hooks, three webs and two spans. No visible shear or flexural crack appeared before reaching the service load level of 42.6 kips (189.6 kN). Mid-span deflection at service load was 0.2 in. which is equal to span/240. This value is higher than what is allowed by AASHTO. Since all the specimens were tested without deck-to-girder connections therefore higher deflections are expected. Similar to the previous specimens, shear was the dominant mode of failure, and flexural cracks were minimal. The first flexural crack was observed at the top of interior support section at 49 kips (218 kN). It was followed by several shear cracks on the two interior ribs near the interior support. These cracks continued to grow, ultimately leading to the punching shear of the flange. As the punching began, the top flexural crack at the support section closed. The ultimate load was 147 kips (654 kN), i.e., 73.5 kips (327 kN) for each span with deflections of 1 in. (25.4 mm) and 0.77 in. (19.6 mm) at the peak load, for the north and south spans, respectively. The ultimate load for each span is almost twice the target load of 37.2 kips (166 kN).

Load-deflection curves show that the majority of the load was taken by the two interior ribs as the loading pad was placed on top of the deck at the location between them. The top concrete strain at mid-span did not reach its ultimate value of 0.0035. However, the bottom compressive strain at the interior support section was very high

(i.e., 0.016), indicating the crushing of concrete. The strain gauges at the interior support section on the top steel bars were damaged at around 90 kips (401 kN) when the strain was 0.0036. The crack that appeared in the top flange at the interior support section at 49 kips (218 kN) likely penetrated to the level of top steel bars and damaged the strain gauges. Similar to Specimen 4T1S-H, the transverse steel strain was high. The maximum transverse steel strain reached 0.027 which is 3.55 times the maximum longitudinal bottom steel strain of 0.0076 (see Figure 2.13). Overall, the specimen performed very well and easily achieved its target load.

2.6 Conclusions

A thorough experimental characterization of the UHPC deck system demonstrates its great potential to serve as an alternative to open grid steel decks for light-weight or moveable bridges. The proposed deck addresses the environmental concerns of open grid steel decks, while meeting the self-weight limit of moveable bridges. The ultimate load capacity of all specimens exceeded the target load for the bridge deck. The governing mode of failure in most specimens was shear, except for the first two specimens which suffered from shear-bond failure. The shear failure observed in this research is not abrupt and catastrophic, which is different from the commonly seen shear failure mode. Shear cracks, additional beam deflection, and rotation at the cracked section were seen as signs prior to the ultimate shear failure. Use of ACI standard 180° hooks at both ends of flexural reinforcement helped effectively avoid bond failure. For the multi-T simple-span and two-span specimens, most of the load was taken by the ribs present either under or near the loading pad, which ultimately led to punching through the slab. The load distribution factor for the web directly under the load is about 36%.

While the proposed deck system seems to be very promising, the following additional work is still needed before any field implementation: (a) establishment of development length and effectiveness of hooks and mechanical anchorages; (b) determination of the transverse load distribution between the ribs; (c) design of connections with supporting steel stringers and between the adjacent panels; and (d) fatigue performance of the deck and its connections.

References

- AASHTO LRFD Bridge Design Specifications, 2005, American Association of State Highway and Transportation Officials, Washington, D.C.
- ACI Committee 318, 2005, "Building Code Requirements for Structural Concrete (ACI 318-05)," American Concrete Institute, Farmington Hills, MI.
- Blais, P.Y., and M. Couture, September-October 1999, "Precast, Prestressed Pedestrian Bridge-World's First Reactive Powder Concrete Structure" *PCI Journal*, pp. 60-71
- Chajes, M. J., McNally, M., Richardson, D.R., Wenczel, G.C., and Liu, W., 2005, "MMFX Rebar Evaluation for I-95 Service Road Bridge 1-712-B." *Final Report*, Delaware Center for Transportation, University of Delaware. Newark, DE.
- Fehling, E., and Bunje, K., 2008, "The Gartnerplatzbrücke Design of first Hybrid UHPC-Steel Bridge across the River Fulda in Kassel, Germany." *Proceedings of Second International Symposium on Ultra High Performance Concrete*, Germany, pp. 581-588.
- Graybeal, B. A., 2006, "Structural Behavior of Ultra-High Performance Concrete Prestressed I-Girders," *Final Report*, Federal Highway Administration, McLean, VA.
- Graybeal, B. A., 2007, "Compressive Behavior of Ultra-High-Performance Fiber-Reinforced Concrete," *ACI Materials Journal*, V. 104, No. 2, pp. 146-152.
- Graybeal, B. A., and Hartmann, J.L., 2003, "Strength and Durability of Ultra-High Performance Concrete," *Proceedings of the 2003 PCI National Bridge Conference*, Orlando, FL, pp. 20.
- Habel, K., Denarié, E. and Brühwiler, E., 2007, "Experimental Investigation of Composite Ultra-High-Performance Fiber-Reinforced Concrete and Conventional Concrete Members," *ACI Structural Journal*, V. 104, No. 1, pp. 93-101.
- Habel, K., Viviani, M., Denarié, E. and Brühwiler, E., 2006, "Development of the Mechanical Properties of an Ultra-High Performance Fiber Reinforced Concrete (UHPRFC)," *Cement and Concrete Research*, V. 36, pp. 1362-1370.
- Hajar, Z., A. Simon, D. Lecointre, and Petitjean, J., 2003, "Construction of the First Road Bridges Made of Ultra-High-Performance Concrete," *Proceedings of 2003 International Symposium on High Performance Concrete*, Orlando, FL, pp. 18.

- Harris, D.K., and Roberts-Wollmann, C.L., 2005, "Characterization of the Punching Shear Capacity of Thin Ultra-High Performance Concrete Slabs," *Final Report*, Virginia Transportation Research Council, Charlottesville, VA.
- Hartt, W.H., Powers, R.G., Lysogoroski, D.K., Liroux, V., and Virmani, Y.P., 2007, "Corrosion Resistant Alloys for Reinforced Concrete," *Final Report*, Federal Highway Administration, McLean, VA.
- Mirmiran, A., Saleem, M.A., Mackie, K. and Xia, J., 2009, "Alternatives to Steel Grid Decks," *Final Report*, Florida Department of Transportation, Tallahassee, FL.
- Naaman, A. E., and Chandrangsou, K., 2004, "Innovative Bridge Deck System Using High-Performance Fiber-Reinforced Cement Composites," *ACI Structural Journal*, V. 101, No. 1, pp. 57-64.
- Naaman, A. E., Likhitruangsilp, V. and Montesinos, G. P., 2007, "Punching Shear Response of High-Performance Fiber-Reinforced Cementitious Composite Slabs," *ACI Structural Journal*, V. 104, No. 2, pp. 170-179.
- National Bridge Inventory, Federal Highway Administration, 2008.
- Perry, V., 2003, "A Revolutionary New Material for New Solutions," *Technical Forum Presentation*, Lafarge North America.
- Perry, V., 2007, "Innovative Field Cast UHPC Joints for Precast Deck Panel Bridge Superstructures - CN Overhead Bridge at Rainy Lake, Ontario," *CSCE 2007 Annual General Meeting & Conference*, Canada.
- Perry, V.H., and Zakariassen, D., 2003, "Overview of UHPC Technology, Materials, Properties, Markets and Manufacturing," *Proceedings of the 2003 Concrete Bridge Conference*, Orlando, FL.
- Sahmaran, M., Li, V. C. and Andrade, C., 2008, "Corrosion Resistance Performance of Steel-Reinforced Engineered Cementitious Composite," *ACI Materials Journal*, V. 105, No. 3, pp. 243-250.
- Taerwe, L., De Schutter, G., Van Gysel, A., Vyncke, J. and Schaerlaekens, S., 1999, "Quantification of Variations in the Steel Fibre Content of Fresh and Hardened Concrete," *Proceedings of 3rd International RILEM Workshop on High Performance Fiber Reinforced Cement Composites*, Germany, pp. 213-222.
- Toutlemonde, F., 2007, "Fatigue Performance of UHPFRC Ribbed Slab Applied as a Road Bridge Deck Verified According to the Eurocodes," *Proceedings of 5th International Conference on Concrete under Severe Conditions*, France.

Vodicka, J., Spura, D. and Kratky, J., 2008 “Homogeneity of Steel Fiber Reinforced Concrete (SFRC),” *Proceedings of 6th International RILEM Symposium on Fibre Reinforced Concretes*, Varenna, Italy, Vol. 1, pp. 537–544.

Table 2.1 Proportions of UHPC Constituent Materials*

Constituent Materials	Percentage by Weight (%)	Weight Relative to Cement
Cement	28.6	1.00
Silica Fume	9.3	0.33
Ground Quartz	8.5	0.30
Fine Sand	41.1	1.44
Steel Fibers	6.4	0.22
Superplasticizer	0.5	0.02
Water	5.6	0.20
Sum	100	

* Source: <http://www.lafargenorthamerica.com> (May 1, 2008)

Table 2.2 Mechanical Properties of UHPC*

Density	156 lb/ft ³ (2500 kg/m ³)
Compressive Strength	22-26 ksi (150-180 MPa)
Tensile Strength	1.2 ksi (8 MPa)
Modulus of Elasticity	7250 ksi (50,000 MPa)
Flexural Strength	4.4-5.8 ksi (30-40 MPa)
Poisson Ratio	0.2
Shrinkage	<0.00001 in/in
Creep factor	0.3
Thermal expansion coefficient	0.0000118 in/in/°C

* Source: <http://www.lafargenorthamerica.com> (February 22, 2009)

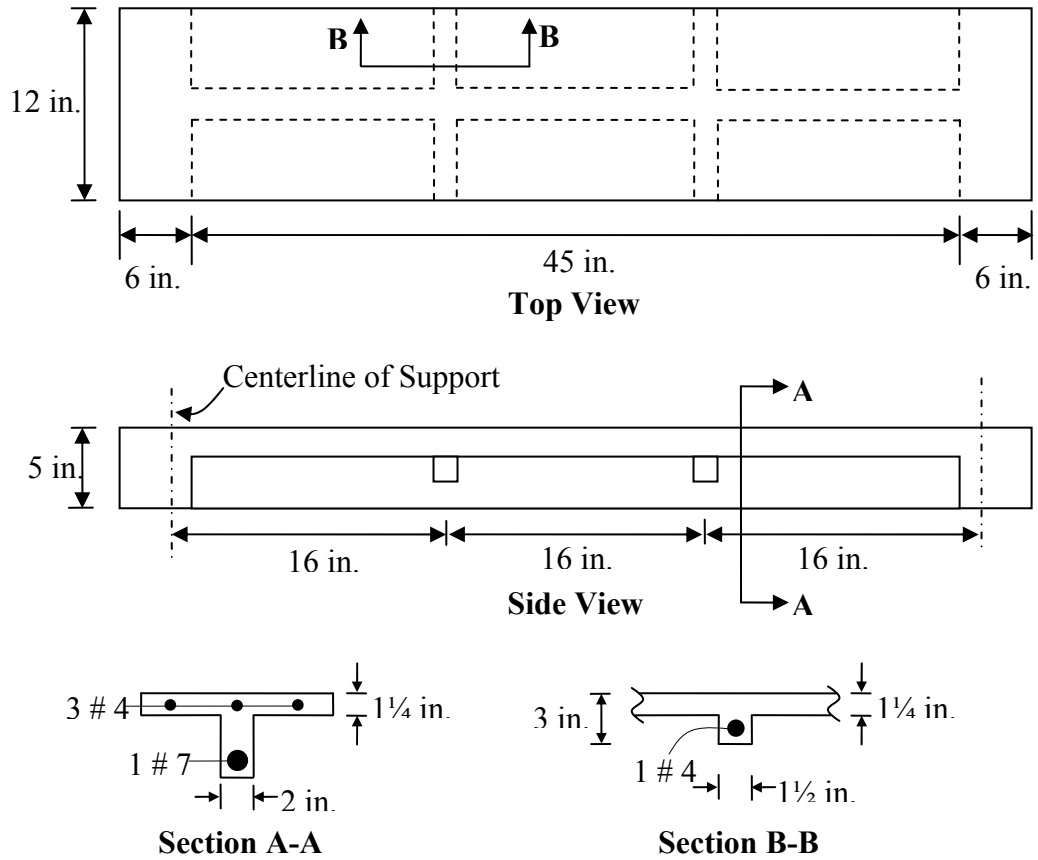
Table 2.3 Test Matrix

No.	Specimen Name	Quantity	28-Day Compressive Strength, ksi (MPa)	Flexural Reinforcement	End Anchorage
1	1T1S*-A	1	28 (193)	1 No. 7**	Anchored
2	1T1S-U	1	28 (193)	1 No. 7	Un-anchored
3	1T1S-H1	1	18 (124)	1 No. 7	180° Hook
4	1T1S-H2	1	27 (186)	1 No. 7	180° Hook
5	4T1S-H	1	26 (179)	1 No. 7 (in each rib)	180° Hook
6	1T2S-H	1	22 (152)	1 No. 7	180° Hook
7	3T2S-H	1	27 (186)	1 No. 7 (in each rib)	180° Hook

*1T1S means single-T simple-span deck specimen with 4 ft (1,219 mm) span length

**1 No. 7 of U.S. Customary rebar = 1 No. 22 SI rebar

A = Anchored, U = Un-anchored, H = 180° Hook



Note: 1 in. = 25.4

Figure 2.1 Schematics of Single Unit Deck Panel

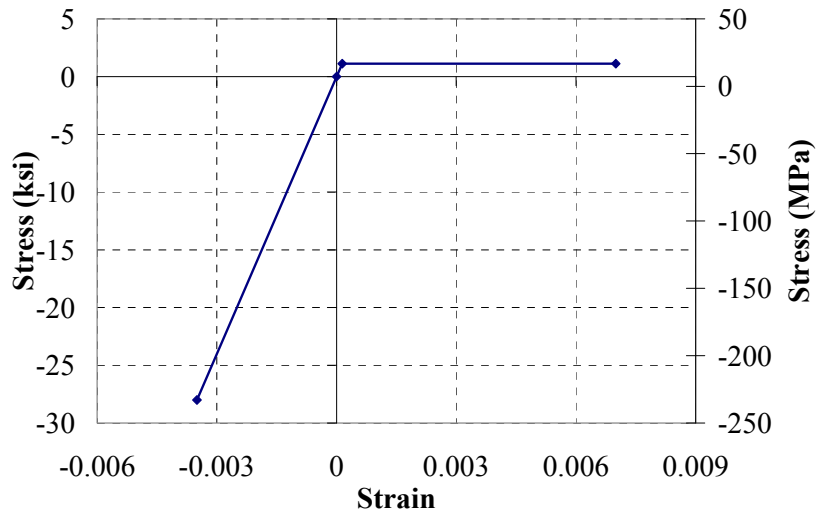


Figure 2.2 Idealized Stress-Strain Relationship of UHPC for Preliminary Specimen Design

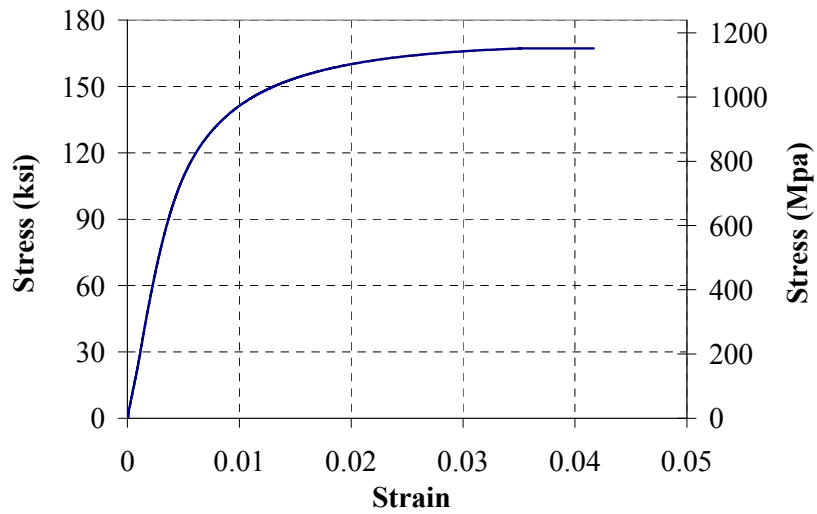


Figure 2.3 Stress-Strain Curve for High Strength Steel

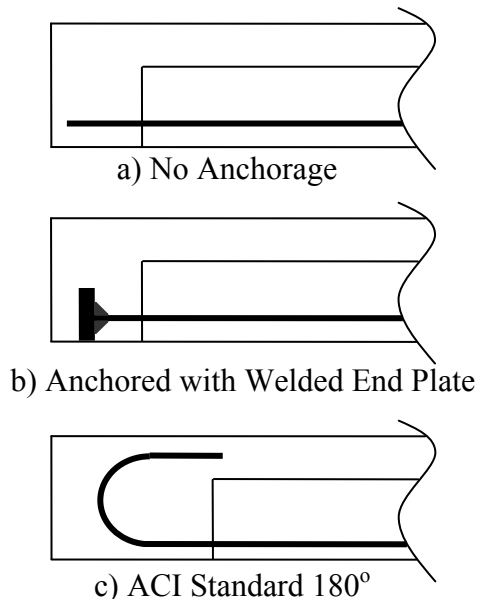


Figure 2.5 Configuration of End Anchorages

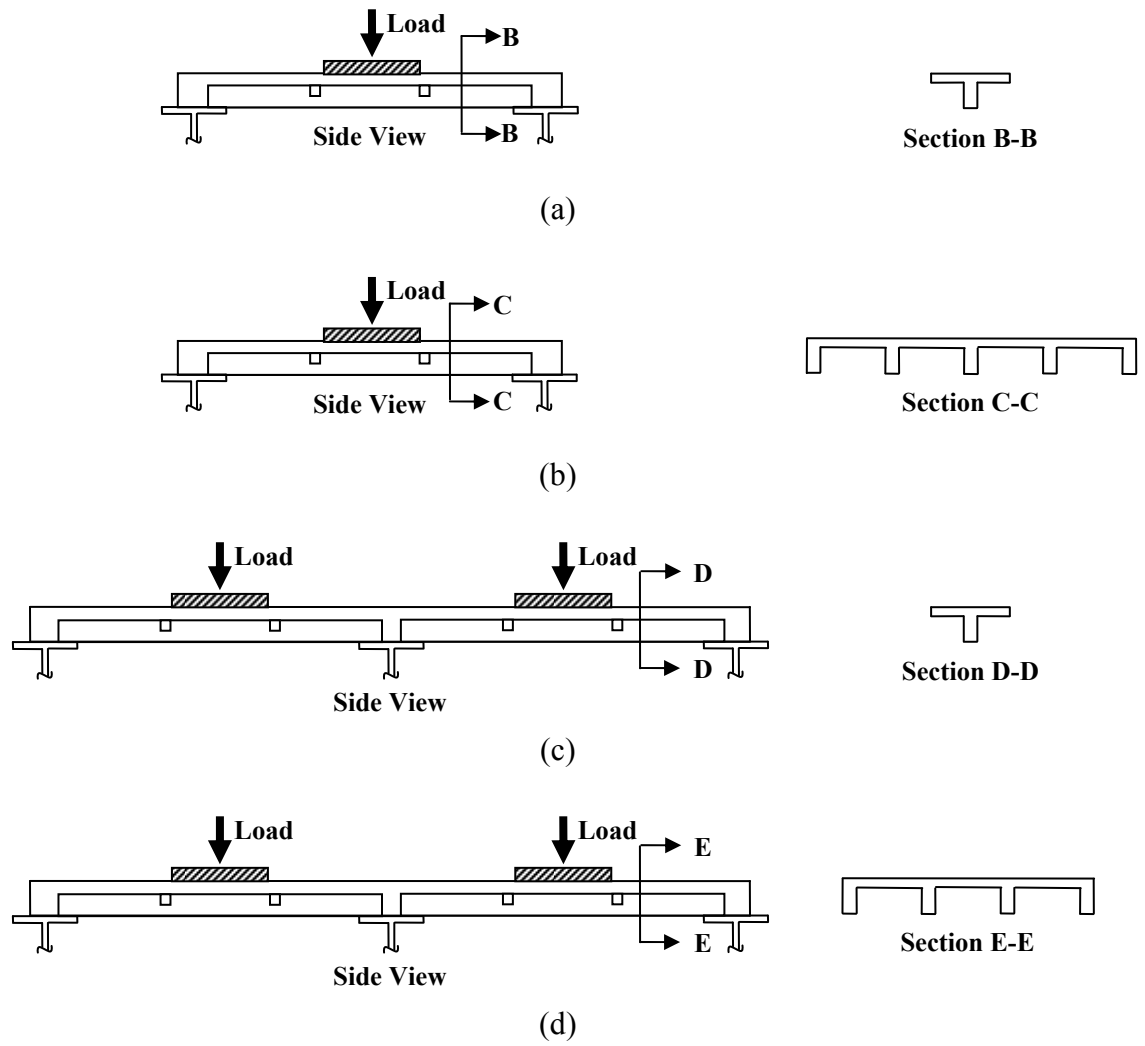
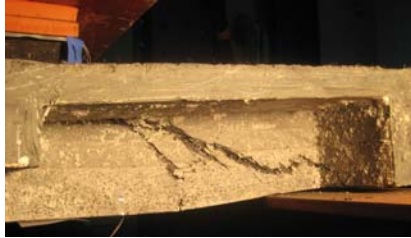


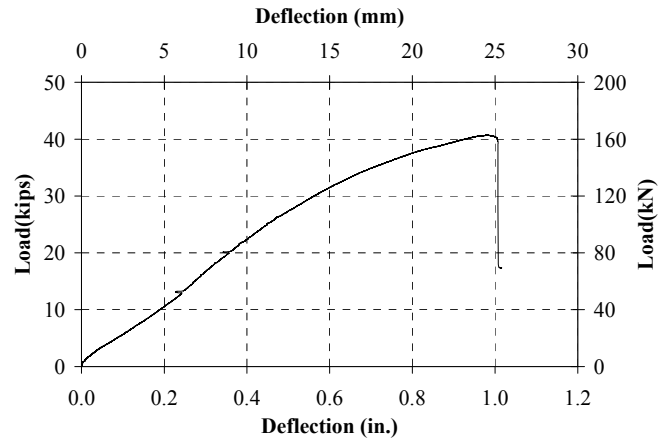
Figure 2.6 Schematics of Test Specimens and Loading Configurations: (a) 1T1S; (b) 4T1S; (c) 1T2S; and (d) 3T2S



(a)



(b)



(c)

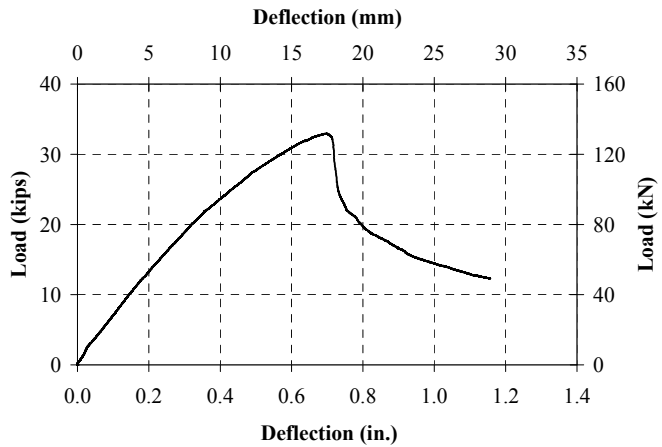
Figure 2.7 Testing of Specimen 1T1S-A with End Anchor Plate: (a) Test Setup, (b) Shear-Bond Failure, and (c) Load-Deflection Response



(a)



(b)



(c)

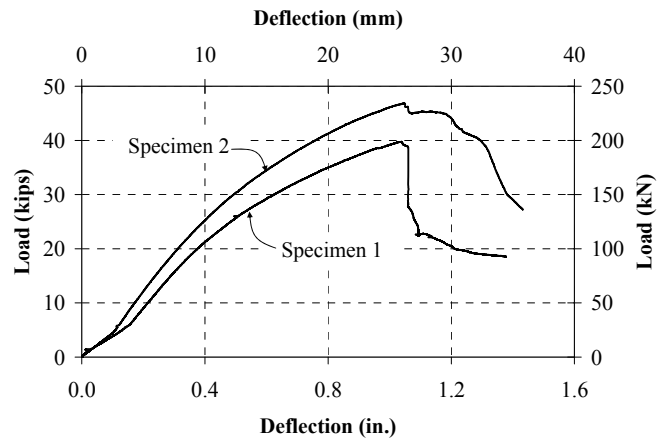
Figure 2.8 Testing of Specimen 1T1S-U without End Anchorage: (a) Shear-Bond Failure, (b) Measure of Shear Crack, and (c) Load-Deflection Response



(a)



(b)



(c)

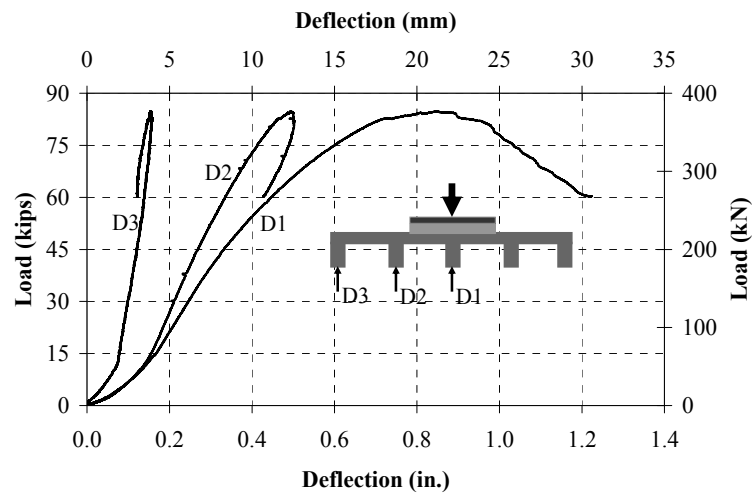
Figure 2.9 Testing of Specimens 1T1S-H with 180° Hook: (a) Shear Failure of Specimen 1, (b) Shear Failure of Specimen 2 (Shown Upside Down), and (c) Load-Deflection Responses



(a)

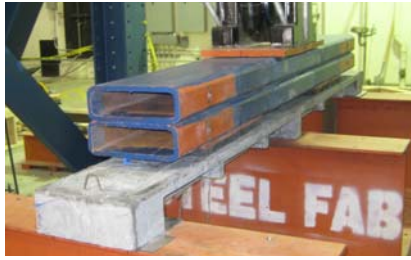


(b)



(c)

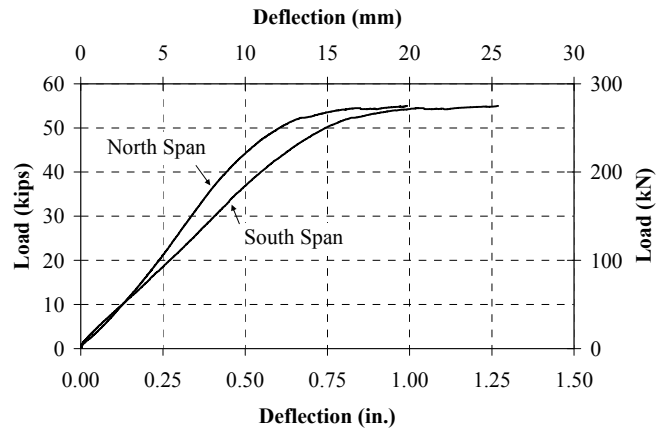
Figure 2.10 Testing of Specimen 4T1S-H: (a) Test Setup, (b) Punching Shear Pattern, and (c) Load-Deflection Responses



(a)



(b)



(c)

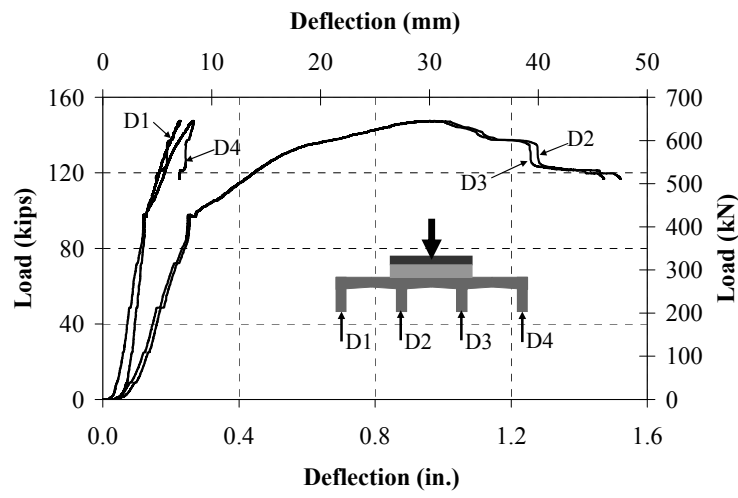
Figure 2.11 Testing of Specimen 1T2S-H: (a) Test Setup, (b) Shear Failure, and (c) Load-Deflection Responses



(a)



(b)



(c)

Figure 2.12 Testing of Specimen 3T2S-H: (a) Test Setup, (b) Punching Shear Pattern, and (c) Load-Deflection Responses for the North Span

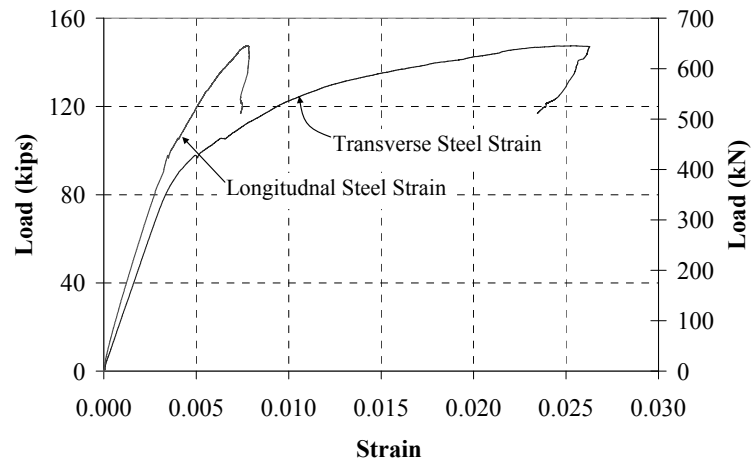


Figure 2.13 Load-Steel Strain Responses for Specimen 3T2S-H

3. STATIC AND FATIGUE PERFORMANCE OF ULTRA-HIGH PERFORMANCE CONCRETE BRIDGE DECK WITH HIGH-STRENGTH STEEL REBARS

Muhammad A. Saleem, Amir Mirmiran, Jun Xia, and Kevin Mackie

A Paper Prepared for ACI Structural Journal

Abstract

Earlier studies have shown the feasibility of ultra-high performance concrete (UHPC) bridge deck as an alternative to open grid steel decks. However, design of connections and the response of UHPC deck to fatigue loading were yet to be investigated prior to field investigation. Deck-to-girder connection is subjected to shear from braking forces, and to uplift from wind loads. Deck-to-deck connection, which is designed as tongue and groove, transfers the load from one panel to the other as the vehicles move along the bridge. Therefore, it was imperative to verify the strength of the connections against potential loading combinations. This paper presents the experimental and analytical results of the study which includes the deck-to-girder connection test for shear and uplift forces, deck-to-deck connection test, multi-unit specimen tests to determine the lateral distribution of live loads, and full-scale test for fatigue loading and residual strength. The fatigue and residual strength test specimen consisted of two adjacent two-span deck panels connected to girders with shear studs and to each other with a tongue and groove connection. The experiments showed the UHPC deck system and its connections to easily achieve the target loads. The finite element (FE) model favorably predicted the behavior of the proposed deck system, as well.

3.1 Introduction

There is an urgent need to develop new techniques, durable materials, and systems for the rehabilitation and replacement of deteriorated bridge structures in the U.S. Moveable bridges are among those needing to be upgraded, as most are currently made of open grid steel decks. These decks have several problems including poor skid resistance and rideability, costly maintenance, high noise levels and susceptibility to vibrations (Mirmiran et al. 2009). In the context of addressing the aforementioned issues and to rehabilitate the structurally deficient bridges, development of innovative lightweight bridge deck systems is one of the active areas of research. Over the last decade, several researchers have carried out significant work to develop bridge decks using fiber reinforced polymers (FRPs), aluminum alloys and ultra high performance concrete (UHPC) (Robinson 2008; Alagusundaramoorthy 2006; Dobmeier 1999; Graybeal 2007).

UHPC is a relatively new structural material composed of high-strength cementitious matrix and steel fibers (Habel et al. 2007). It has a much better durability and a higher tensile strength than other cementitious materials (Habel 2006, Graybeal 2007). UHPC has around 4-8 times higher compressive strength than conventional concrete and its tensile strength ranges from 0.9 to 1.7 ksi (Graybeal and Hartmann 2003). The interaction of steel fibers at the microscopic level and their ability to sustain load after the onset of cracking are the major contributing factors to the high tensile strength and ductility of UHPC (Perry 2003, Harris and Roberts-Wollmann 2005). Curing of UHPC by submerging it in water at 194 °F for 48 hours considerably increases its compressive strength and modulus of elasticity, and almost eliminates any long-term

shrinkage (Graybeal 2006). UHPC also attains high flexural strengths ranging from 5.0 to 7.2 ksi based on standard flexural beam tests (Perry and Zakariassen 2003). In Australia, Japan, New Zealand, South Korea and the U.S., UHPC is being used in the construction of both the highway and pedestrian bridges (Blais 1999, Hajar 2003, Graybeal 2006). Previous researchers (Graybeal 2007, Perry 2007, and Toutlemonde 2007) have developed bridge decks with UHPC, but with higher self weights, than what may be suitable for moveable bridges.

The focus of this study is on the experimental (static and dynamic) and analytical evaluations of a new type of UHPC bridge deck with a solid riding surface and an acceptable self-weight ($\leq 25 \text{ lb/ft}^2$) for moveable bridge decks. UHPC used for this project is Ductal[®], which is developed from the joint research of three French companies; Bouygues, Lafarge, and Rhodia. The average compressive strength of UHPC achieved in the lab was 25.5 ksi. The high-strength steel (HSS) rebars that are used in the system are produced by MMFX Technologies of Irvine, CA. The deck has a low profile of only 5 in. depth, which is compatible with the open grid steel decks that typically span a 4 ft girder spacing. This paper presents the results of the testing on deck-to-girder connections; deck-to-deck connections; lateral load distribution; and full-scale fatigue and residual strength. Results of analytical evaluation using a general purpose finite element software ANSYS[®] are also presented.

This UHPC deck system is composed of primary and secondary ribs. Primary ribs are perpendicular to traffic, and span between the girders. The secondary ribs connect the primary ribs and run parallel to the direction of traffic. Based on the self-weight limit of 25 lb/ft^2 , a series of cross sections were developed and a sensitivity analysis was

performed to find out the most suitable option. Factors considered included reinforcement ratio, flange width and thickness, and rib depth and thickness in both directions. The overall depth was kept as 5 in. to be compatible with the current open grid steel decks. The section was designed as singly-reinforced, with one No. 7 rebar at a clear cover of $\frac{1}{2}$ in. The schematic of a single unit of the proposed deck is shown in Figure 3.1. This pattern of a single unit was repeated to build the multi-unit specimens.

3.2 Significance of Research

Development of more durable bridge deck systems is highly needed to upgrade the aging bridge infrastructure in the U.S. UHPC has a great potential to provide such solutions because of its higher strength and durability as compared to conventional concrete. Since no previous research is available on the development of lightweight UHPC bridge deck system for moveable bridges, this work can provide a foundation for future development in this area. Implementation of this system on moveable bridges will contribute to reduce the number of accidents and will also lower the maintenance cost.

3.3 Experimental Work

Table 3.1 shows the test matrix of this study. Deck-to-girder and deck-to-deck connections were tested individually before using them in the full-scale specimen, which was tested for fatigue and residual strength. All static and dynamic tests were conducted with the loading recommended by AASHTO LRFD (2005), using a prescribed footprint of an HS 20 truck dual-tire wheel (10 in. x 20. in). To simulate the tires, a 1 in. thick neoprene pad was placed under the steel loading plate. Strain gauges, string potentiometers, and displacement transducers were installed at strategic locations to acquire the strain and deflection data. All instruments were connected to a data

acquisition system with a sampling frequency of 1 Hz. The target live load for full scale test was 37.24 kips, including the dynamic impact factor and load factor, based on the AASHTO LRFD (2005) recommendations.

3.3.1 Shear Test for Connectors

This test was performed to investigate the ultimate shear capacity of the deck-to-girder connection, which is comprised of a 4 in. long, ½ in. diameter shear stud welded onto the top flange of the girder. Openings were left at appropriate locations in the deck specimens at the time of casting to be filled later with UHPC to fully encase the studs. Plastic sheets were used as bond breakers to avoid direct connection between deck and the girder, other than through the shear stud. This would ensure the worst case scenario. The welding of the studs onto girders was designed to take the shear developed by the braking force of an HS 20 truck in addition to the horizontal component of the wind loads. The factored design shear force, based on the recommendations of the AASHTO LRFD (2005) was calculated as 7.8 kips. In the case of an interior panel, the applied shear force will be resisted not only by the deck-to-girder connection, but also by the deck-to-deck connection between the adjacent panels. However, the last panel on the bridge deck will rely only on the deck-to-girder connection to resist the braking force. Therefore, it was deemed necessary to determine the shear capacity of the deck-to-girder connection alone. Figure 3.2 shows the test setup, the failure pattern, and the load-displacement response. Displacements were measured at top of both panels using a string potentiometer, while the load was measured using a load cell.

The ultimate shear strength of the connection was found as 15.3 kips, almost twice the required strength. The load-displacement curves in Figure 3.2 show that the two

deck portions exhibited similar behavior until the peak load, after which one of them cracked more than the other one, leading to a much higher displacement. The failure mode shown in Figure 3.2b implies that the portion of deck close to the load rotated about a horizontal axis. This rotation is caused by one big crack which started at the bottom and moved towards the top, all the while growing wider near the bottom. Such a failure is not expected in an actual bridge deck as several studs present in a line would resist the shear force, preventing such rotation. Since the purpose of this test was to establish the capacity of a single connection, only a portion of the deck was tested.

3.3.2 Uplift Test for Connectors

Uplift test characterizes the resistance of the deck-to-girder connection against uplift wind pressure. A portion of the deck with an opening to accommodate the stud was placed on the girder, after which the opening was filled with UHPC. Again, plastic sheets were used as bond breaker between the concrete and the flange to make sure that deck is connected to the girder only through the stud. Test was performed after 28 days of the filling of the opening. According to AASHTO LRFD (2005), the required ultimate strength of the connection is 2.2 kips. Figure 3.3 shows the test setup, mode of failure, and the load-deflection responses. Load was applied using two hydraulic jacks, one on each side of the connection. Deflections were measured at two locations, one at the center of the stud and another at the edge of the filled joint. With a peak load of more than 3.6 times the required strength, the connection proved to be more than adequate for the uplift. Failure occurred along the filled joint, with the deck lifted up while leaving the new UHPC joint and the stud intact and connected to the girder. The load-displacement

responses show that the old and new concrete experienced no relative slip before the failure took place.

3.3.3 Deck-to-Deck Connection Test

Strength of the deck-to-deck connection is important for the transfer of load from one panel to the other. Failure of this connection may lead to excessive deflection and potential delamination of the wearing surface. AASHTO LRFD (2005) suggests higher impact factor (1.75) for deck-to-deck connections, therefore target load for this test was 49 kips instead of 37.24 kips. Two simply-supported deck panels with 4 ft center-to-center spans were used to perform the test. Load was applied on the edge of the connection, representing the most critical condition. Four string potentiometers were installed, one under each rib, to monitor the deflections. Figure 3.4 shows the test setup, mode of failure, and the load-deflection responses. Shear cracks started appearing at 42.5 kips in the rib with the groove, which was directly under the load. As these cracks gradually grew wider, the rib with the tongue also began to crack in shear. The ribs on the edge showed some shear cracking, albeit insignificant, approaching the peak load. The test was stopped at about 0.8 in. displacement due to safety concerns. The load-deflection responses show a very small relative deflection between the two ribs. It is recommended to use epoxy grout in the field while placing the deck panels on the girders. The connection failed at 79 kips, which is more than twice the target load of 49 kips. The high strength of the deck-to-deck connection will ensure the development of panel action to effectively distribute the load in the lateral direction.

3.3.4 Lateral Distribution of Live Loads

Distribution factors (*DFs*) for this type of deck are not readily available in the AASHTO LRFD (2005), hence there was a need to determine the share of the load taken by each rib. For this purpose, simple-span and two-span flexural tests were performed on different specimens with different loading configurations. Details of the specimens are provided in Table 3.1. A displacement-control procedure was adopted at a displacement rate of 0.015 in./min.

DFs can either be calculated based on deflections of the ribs, or the strains in the steel rebars inside the ribs. In this study, the former method was chosen to avoid potential accuracy problems with strain readings. The *DF* for a specific rib was therefore calculated as

$$(DF)_i = \frac{(Deflection)_i}{\text{Sum of deflections for all ribs}} \quad (1)$$

where $(DF)_i$ and $(Deflection)_i$ represent *DF* and deflection for rib *i* at each load level, respectively. *DF* for each rib was averaged based on values calculated at every 10 kips and at the ultimate load. These average *DFs* for all specimens are presented in Figure 3.5. In Specimen 5T1S, the load was applied symmetrically, with two ribs on either side of the load. In this case, 79.5% of the total load was resisted by the rib directly under the load and its two adjacent ribs. In Specimen 4T1S, the load was applied asymmetrically. In this case, 89.1% of the total load was taken by the rib directly under the load and those next to it on either side. The farthest rib contributed only 10.9% of the total resistance, close to 10.3% in Specimen 5T1S. Comparing the first two specimens, if the load is applied directly on one of the ribs most of it will be taken by that rib and those

immediately next to it. However, this distribution changes when the load is applied in between the ribs. In Specimen 4T2S, the load was applied in between the ribs and the two ribs near the load took only 69.8 % of the total load, and those on the edges took the remainder. The slight variations point to the unintended asymmetry while placing the loading pad. Results of these three specimens show that the ribs under the load (or immediately next to it, when the load is applied between the two ribs) take 33% of total load at the target load of 37.24 kips and 34% of the total load when calculated based on the average from 10 kips to the ultimate load. The simple-span specimen with deck-to-deck connection, however, exhibited a different distribution than the single panel specimens. The load was applied on the edge of the connection on one of the two panels. The two ribs that together form the connection took a total of 64% of the total load, with 35% and 29% for the rib directly under the load and the one next to it, respectively. This difference of 6% between these two ribs should be minimized, if not eliminated altogether, for a better transfer of load from one panel to the other. It is anticipated that the epoxy grouting of the joint, as suggested earlier, may help to accomplish this objective.

Figure 3.6 shows the variation of the load share for each rib with the progression of loading. For all four specimens, it can be clearly seen that the share of the load for the rib directly under the load or immediately next to it, in case when load is applied between the ribs, increases at higher load levels. For Specimens 5T1S, 4T1S and 4T2S the share of the load taken by the ribs on the edges shows a decreasing trend with respect to the applied load. This implies that the area closest to the loading pad attracts more load as the test progresses. This phenomenon may also explain the ultimate punching failure

observed in these specimens. Abrupt changes in the slopes of the curves near the ultimate load may be attributed to the fact that when loading pad starts punching, the load concentration is increased at a faster rate around the pad. The specimen with the deck-to-deck connection also showed a similar behavior in terms of higher load concentrations at higher load levels. However, no sharp change is visible in the slopes of the curves, indicating the absence of punching, which is in agreement with the observation made during the test.

3.3.5 Fatigue and Residual Strength Tests

Figures 3.7 and 3.8 show the instrumentation plan, loading configuration, and deflection growth under the fatigue loading. In addition to the displacement transducers shown in Figure 3.7, strain gauges were applied on top and bottom steel rebars as well as concrete surfaces at the locations of maximum positive and negative moments. Two thermo couples were also mounted on the concrete surface, one at the top and the other at the bottom of one of the edge ribs in Span 2. The thermo couples recorded the variations in temperature throughout the fatigue test. Two loading pads were placed at the middle of each span at a center-to-center distance of 4 ft. which is more critical than 6 ft the wheel spacing of an HS 20 truck. Deck panels were subjected to two million cycles of design truck single axle sinusoidal load in the range of 0.5-16 kips in each span at a frequency of 4 Hz. The decision on the total number of cycles was based on the previously available literature (Vyas et al. 2009). The lower limit of 0.5 kip was set to prevent the pads from “walking”. The test was run continuously for about six (6) days. Load, displacement, strain and temperature data were recorded continuously for 16 sinusoidal cycles at all channels after every 1,000 cycles. During and after the test, the deck panels were

monitored for cracks in the panels or at connections. After the fatigue test, two static tests were performed on the panels to determine their residual strengths.

Before the application of fatigue loading the panels were subjected to static load to determine the initial stiffness of the system. The idea was to load each panel up to a maximum of 16 kips and then unload. However, at around 14.5 kips it was noticed that a shear crack began to develop in Panel 1 near the middle support. It was observed that in Span 1, the load was not being transferred to Panel 2. In fact, the groove was not engaging the tongue due to a slight gap in between that was the result of forming. Loading was stopped at this moment and it was decided to connect the tongue and groove using epoxy. All joints were sealed, and then epoxy was grouted from top of the connection. Pouring of epoxy was completed in three steps spanning over three days to make sure that it has filled all opening, as some epoxy was initially lost to leakage. The epoxy not only filled the deck-to-deck connection, but also sealed the shear crack which appeared in Panel 1. Epoxy was given 24 hrs from the last pour to fully cure. Then, the panels were reloaded to measure the initial stiffness, before fatigue loading began. The panels showed no sign of cracking or failure after 2 million cycles of fatigue loading. The sealed shear crack of Panel 1 was regularly monitored, and did not show any sign of growth. Figure 3.8 shows an increase in deflection at D6 after 20,000 cycles, which indicates that something happened at this moment. Although nothing unusual was observed, however there could be some cracking in the epoxy which would have affected the distribution of load in span-2 causing this growth of deflection. Change in response of D2 after 2,00,000 cycles can also be attributed towards cracking in epoxy. The absolute maximum deflection was observed in D6 which increased from 0.04 in. (L/1200) at cycle

1 to 0.15 (L/320) at cycles 2,000,000. Fatigue loading developed compressive stresses in concrete ranging from 2.5 to 4.9 ksi, and tensile stresses in steel ranging from 5.5 to 16.6 ksi at most critical locations, respectively the top fiber of concrete at mid-span and top steel rebar at interior support.

Figures 3.9 and 3.10 show the test setup, the load-deflection responses and cracking pattern for the two residual strength tests. In each test, only one span was loaded. In the first test (Test A), load was applied at the edge of the deck-to-deck connection, whereas in the second test (Test B) the load was centered on the connection itself. In Test A, the first shear crack appeared near the interior support at 40 kips, and the specimen achieved an ultimate load of 55 kips, which is 47% more than the target load of 37.24 kips. The shear crack kept on growing beyond 40 kips with smaller cracks appearing around the interior support. Approaching the ultimate load, longitudinal cracks appeared in the edge rib and within the rib with the tongue. It appears that the loading pad started punching close to the ultimate load, which developed tensile force between the flange and the edge rib leading to the longitudinal crack. The longitudinal crack in the rib with the tongue may have developed due to the shearing of the tongue. As the loading pad punched at ultimate load, the two ribs with tongue and groove took greater portion of the load, and the edge rib at the far end of the loading point experienced a relief in its load share. This is visible in the load-deflection responses.

In Test B, the first longitudinal crack in one of the edge ribs was seen at 60 kips and the first shear crack near the interior support appeared at 70 kips. The specimen achieved an ultimate load of 72.4 kips, which is 94% higher than the target load. The specimen maintained this ultimate load for some time and the deflection kept on

increasing, while more shear cracks appeared at both supports of the loaded span. These cracks travelled from the supports to the mid-span. Cracks appeared near the mid-span were smaller than those near the supports, and were closer to the web and flange junction. Punching of the loading pad was also observed at the time when load started dropping. The difference between the ultimate loads of Tests A and B shows that the load is more evenly distributed when it is applied directly on the connection as compared to the case when it is applied on its edge. The specimen also shows a more ductile behavior in Test B as compared to Test A. In the case of Test A, the difference between the load at the first shear crack and the ultimate load is 15 kips (or 27% of the ultimate load), whereas it is only 2.4 kips (or 3% of the ultimate load) in Test B. These observations suggest that the situation when the truck wheel is at the edge of the deck-to-deck connection is more critical, as compared to the case when wheel is directly on top of the connection.

3.4 Finite Element Analysis

In order to simulate the experimental results, a 3-D finite element (FE) analysis was conducted using a general purpose FE program ANSYS[®] 12.0 (2010). ANSYS[®] is a comprehensive FE package with special elements for modeling concrete. This section presents the technique used for modeling, elements used, and results of the analyses. There were two main components of the system. Concrete and steel rebars were modeled with SOLID65 and LINK8 elements, respectively. SOLID65 is an 8-noded solid element with 3 translational degrees of freedom (DOF) at each node; and possesses cracking, crushing, plastic deformation and creeping capabilities. The element is widely used for modeling concrete, and can incorporate steel rebars as smeared or discrete reinforcement. LINK8 is a 2-noded spar element with three translational DOFs at each node, and is

commonly used for modeling uniaxial tension and compression members. The element is capable of plasticity, creep, swelling, stress stiffening, and large deflections. A perfect bond was assumed between concrete and steel, therefore no bond modeling was required. The coinciding nodes of rebars and concrete were simply glued together. Because the loading and geometry were symmetrical, only a quarter of the deck was modeled to save computation time.

Since steel rebars were modeled as discrete reinforcement using LINK8 elements, the smeared reinforcement capability of SOLID65 was turned off. The cracking and crushing capabilities of SOLID65 were also turned off to avoid any potential convergence problem. The stress-strain relationships used for UHPC and steel rebar are shown in Figure 3.11. A multilinear isotropic hardening table was used to input stress-strain data. In addition to the nonlinear relationship, linear material properties were entered using the linear isotropic material properties table, including the modulus of elasticity (8,000 ksi for UHPC, and 29,000 ksi for steel) and the Poisson's ratio (0.2 for UHPC, and 0.3 for steel). Similar to the experiments, the analysis was conducted in displacement control. Figure 3.12 shows the comparison of experimental and analytical load-deflection responses for Specimen 4T2S, implying a favorable agreement, particularly in the elastic range. However, the model does not accurately predict the softening due to cracking or the load drop after the peak. This may be attributed to cracking and crushing features of the FE model that were not incorporated for the UHPC.

3.5 Conclusions

A proposed UHPC-HSS deck system was subjected to a series of component and system level tests. Based on the results, it can be concluded that this system is a feasible

alternative to open grid steel decks and is ready for implementation. Deck panels with its connections successfully endured two million cycles of fatigue loading and had a residual strength of at least 47% higher than the target load. Lack of load transfer across the tongue and groove connection during the initial static loading before the fatigue test demonstrated the need for using epoxy grout at the joint. The deck-to-girder connection and deck-to-deck connection proved to be more than adequate for the loading conditions expected from the HS 20 truck and wind forces. Testing for the determination of lateral distribution of live loads showed that when the load is applied directly on a rib most of it would be taken by that rib and the ribs immediately next to it on either side. The rib under the load, on average, takes 34% of the total load. It was further observed that with the increase in the applied load, the rib under the loading pad attracts more load, ultimately leading to punching failure. The FE analysis showed reasonable agreement with the experimental results. However, the FE model needs further refinement to accurately capture the cracking load and the load drop after the peak.

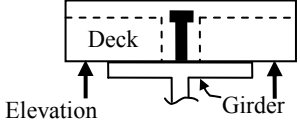
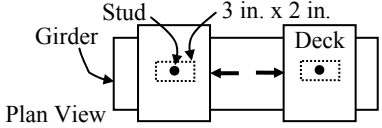
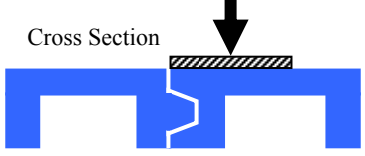
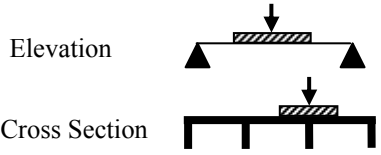
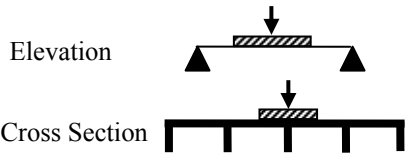
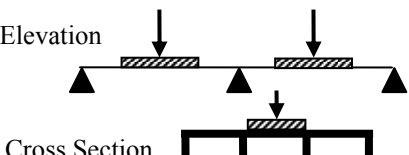
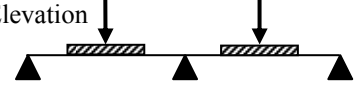

The proposed system is deemed ready for implementation, although the following issues may need further investigations. First, an evaluation is needed for the effectiveness of UHPC as wearing surface. Second, field monitoring of UHPC deck under ambient traffic and/or designated truck loading may also provide valuable information as to the durability and performance of the deck. Evaluation of deck-to-girder connection for the uplift force developed due to wind while the bridge is open is also recommended.

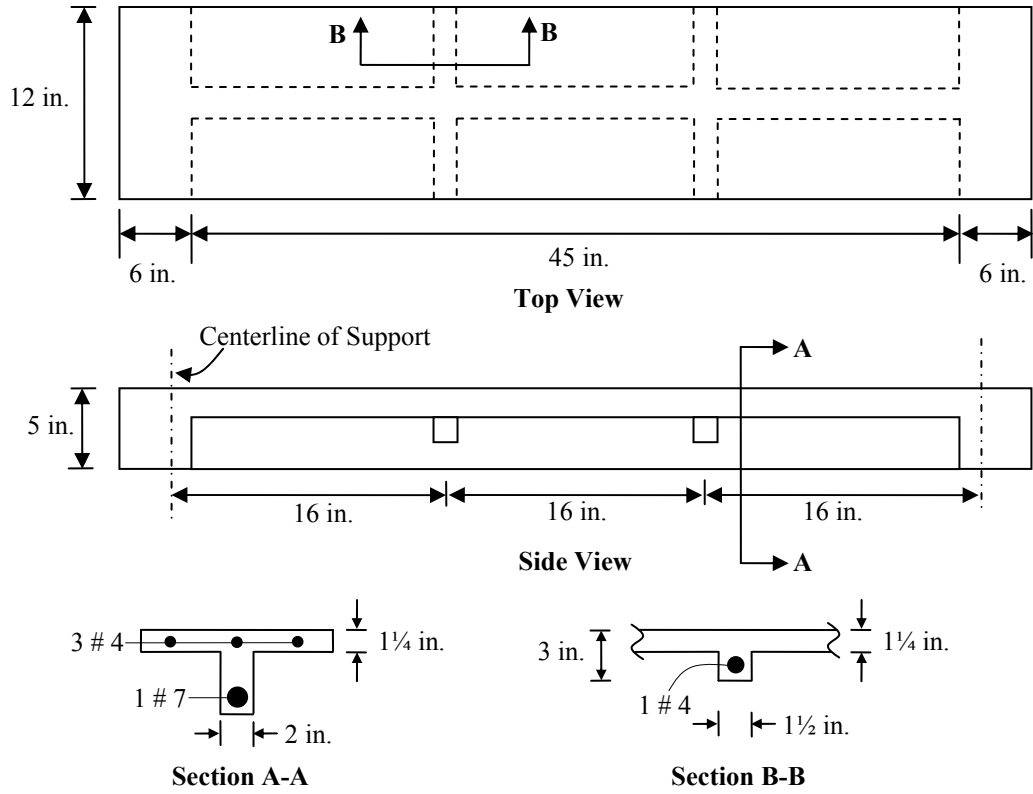
References

- AASHTO LRFD Bridge Design Specifications, 2005, American Association of State Highway and Transportation Officials, Washington, D.C.
- Alagusundaramoorthy, P., Harik, I., and Choo, C., 2006, "Structural Behavior of FRP Composite Bridge Deck Panels." *Journal of Bridge Engineering*, ASCE, Volume 11, Issue 4, pp. 384-393.
- ANSYS® Modeling and Meshing Guide, 2005, ANSYS Inc., Canonsburg, PA
- Blais, P.Y., and M. Couture, 1999, "Precast, Prestressed Pedestrian Bridge-World's First Reactive Powder Concrete Structure," *PCI Journal*, V. 44, No. 5, pp. 60-71
- Dobmeier, J. M., Barton, F. W., Gomez, J. P., Massarelli, P. J., and McKeel, W. T., 2001, "Failure Study of an Aluminum Bridge Deck Panel" *Journal of Performance of Constructed Facilities*, Volume 15, Issue 2, pp. 68-75
- Graybeal, B. A., 2006, "Structural Behavior of Ultra-High Performance Concrete Prestressed I-Girders," *Final Report*, Federal Highway Administration, McLean, VA.
- Graybeal, B. A., 2007, "Analysis of an Ultra-High Performance Concrete Two-Way Ribbed Bridge Deck Slab." Federal Highway Administration, Washington D.C.
- Graybeal, B. A., 2007, "Compressive Behavior of Ultra-High-Performance Fiber-Reinforced Concrete," *ACI Materials Journal*, V. 104, No. 2, pp. 146-152.
- Graybeal, B. A., and Hartmann, J.L., 2003, "Strength and Durability of Ultra-High Performance Concrete," *Proceedings of the 2003 PCI National Bridge Conference*, Orlando, FL, pp. 20.
- Habel, K., Denarié, E. and Brühwiler, E., 2007, "Experimental Investigation of Composite Ultra-High-Performance Fiber-Reinforced Concrete and Conventional Concrete Members," *ACI Structural Journal*, V. 104, No. 1, pp. 93-101.
- Habel, K., Viviani, M., Denarié, E. and Brühwiler, E., 2006, "Development of the Mechanical Properties of an Ultra-High Performance Fiber Reinforced Concrete (UHPRFC)," *Cement and Concrete Research*, V. 36, pp. 1362-1370.
- Hajar, Z., A. Simon, D. Lecointre, and Petitjean, J., 2003, "Construction of the First Road Bridges Made of Ultra-High-Performance Concrete," *Proceedings of 2003 International Symposium on High Performance Concrete*, Orlando, FL, pp. 18.

- Harris, D.K., and Roberts-Wollmann, C.L., 2005, "Characterization of the Punching Shear Capacity of Thin Ultra-High Performance Concrete Slabs," *Final Report*, Virginia Transportation Research Council, Charlottesville, VA.
- Mirmiran, A., Saleem, M.A., Mackie, K. and Xia, J., 2009, "Alternatives to Steel Grid Decks." *Final Report*, Florida International University, Miami, FL and University of Central Florida, Orlando, FL.
- Perry, V., 2003, "A Revolutionary New Material for New Solutions," *Technical Forum Presentation*, Lafarge North America.
- Perry, V., 2007, "Innovative Field Cast UHPC Joints for Precast Deck Panel Bridge Superstructures - CN Overhead Bridge at Rainy Lake, Ontario," *CSCE 2007 Annual General Meeting & Conference*, Canada.
- Perry, V.H., and Zakariassen, D., 2003, "Overview of UHPC Technology, Materials, Properties, Markets and Manufacturing," *Proceedings of the 2003 Concrete Bridge Conference*, Orlando, FL.
- Robinson, M.J., Koamatka, J.B., 2008, "Light-Weight Fiber-Reinforced Polymer Composite Deck Panels for Extreme Applications." *Journal of Composites for Construction*, Volume 12, Issue 3, pp. 344-354.
- Toutlemonde, F., 2007, "Fatigue Performance of UHPFRC Ribbed Slab Applied as a Road Bridge Deck Verified According to the Eurocodes," *Proceedings of 5th International Conference on Concrete under Severe Conditions*, France.
- Vyas, J. S., Zhao, L., Ansley, M. H. and Xia, J., 2009, "Characterization of a Low-Profile Fiber-Reinforced Polymer Deck System for Moveable Bridges." *Journal of Bridge Engineering*, Volume 14, Issue 1, pp. 55-65.

Table 3.1 Test Matrix

Serial No.	Description of Test	Schematics
1	Deck-to-Girder Connection	
	Uplift Test	
	Shear Test	
2	Deck-to-Deck Connection	
3	Lateral Distribution of Load	
	Simple-span specimen with four ribs (4T1S)	
	Simple-span specimen with five ribs (5T1S)	
	Two-span specimen with four ribs (4T2S)	
4	Full-Scale Specimen	
	Fatigue Test	
	Residual Strength Test	

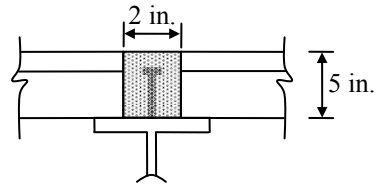


Note: 1 in. = 25.4 mm

Figure 3.1 Schematics of Single-Unit Deck Panel



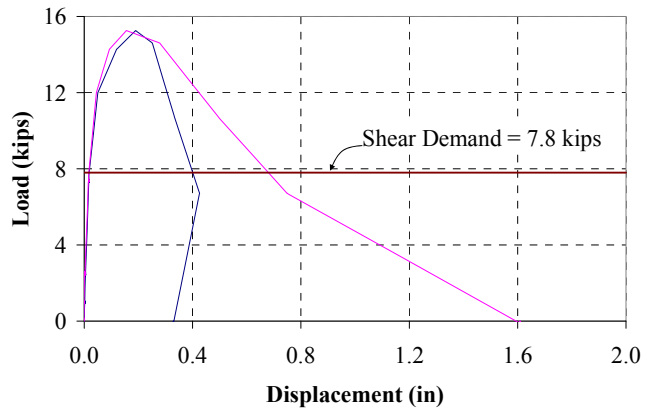
(a)



(c)



(b)

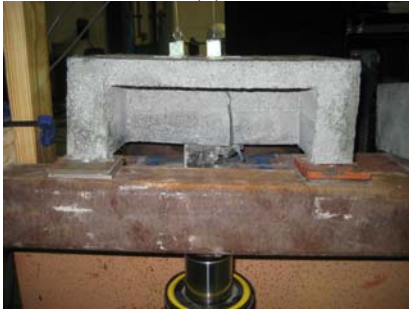


(d)

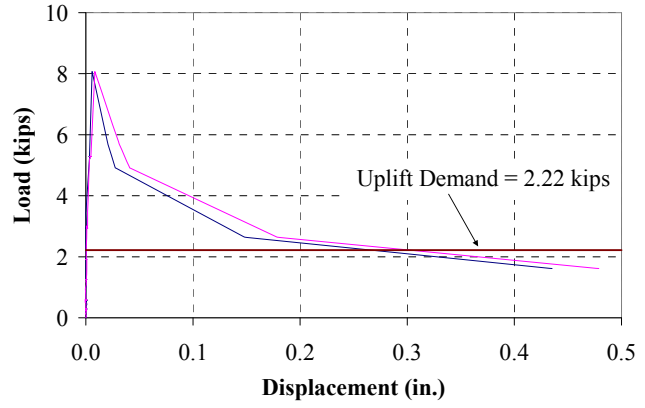
Figure 3.2 Testing of Deck-to-Girder Connection for Shear: (a) Test Setup; (b) Mode of Failure; (c) Schematics of Connection; and (d) Load-Displacement Responses



(a)



(b)

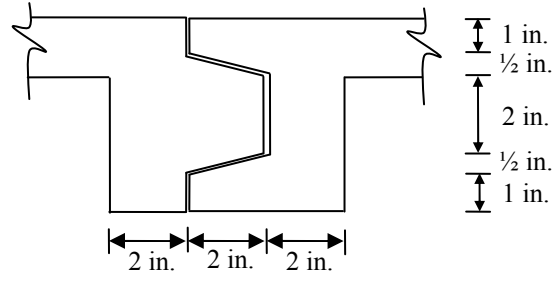


(c)

Figure 3.3 Testing of Deck-to-Girder Connection for Uplift: (a) Test Setup; (b) Mode of Failure; and (c) Load-Displacement Responses



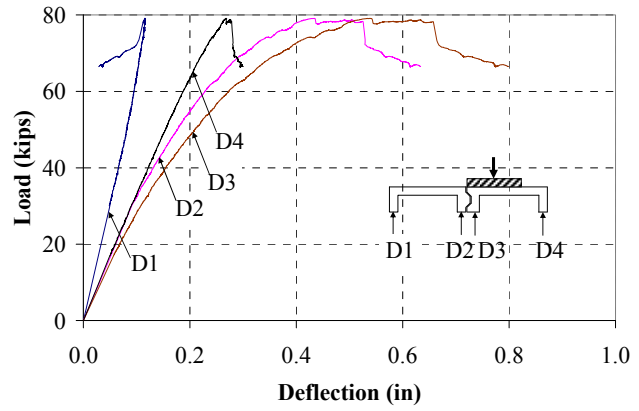
(a)



(c)



(b)



(d)

Figure 3.4 Testing of Deck-to-Deck Connection: (a) Test Setup; (b) Mode of Failure; (c) Schematics of the Connection; and (d) Load-Deflection Responses

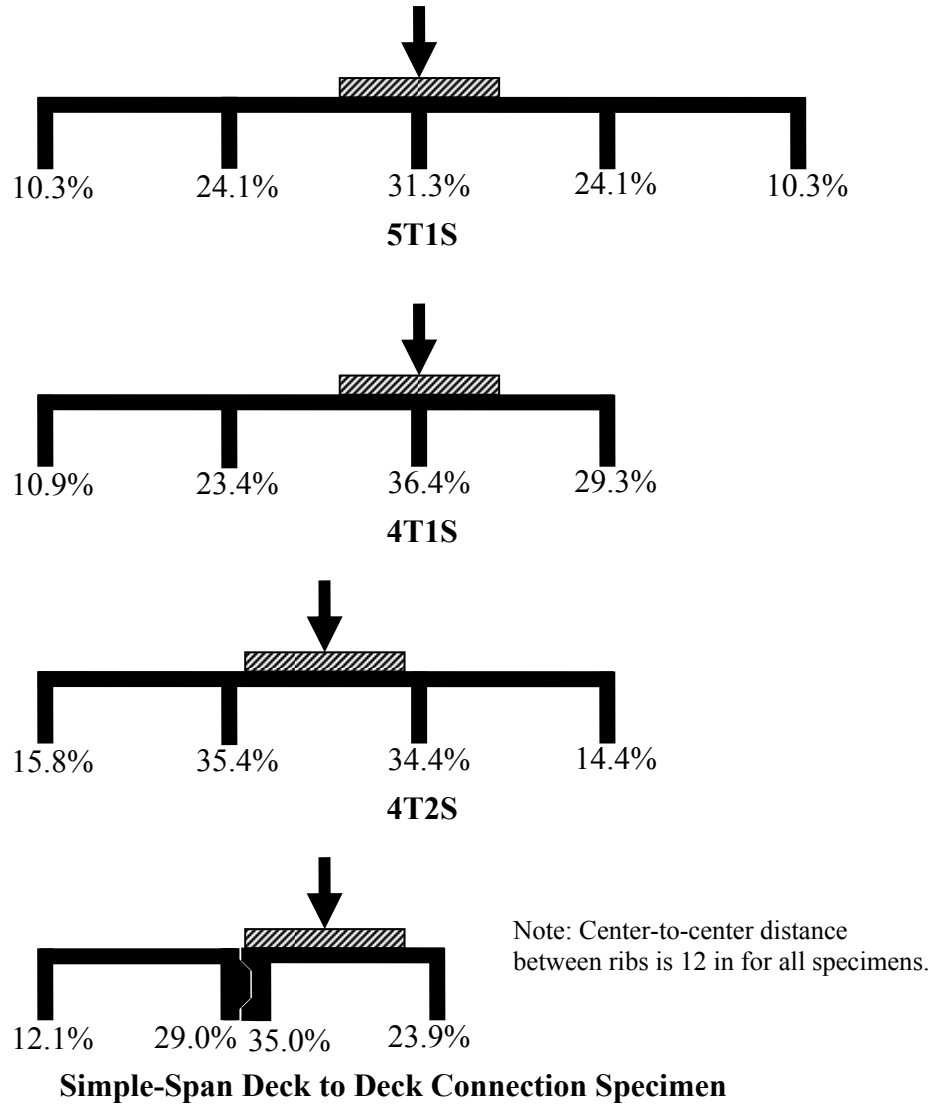


Figure 3.5 Average Distribution Factors for Various Specimens

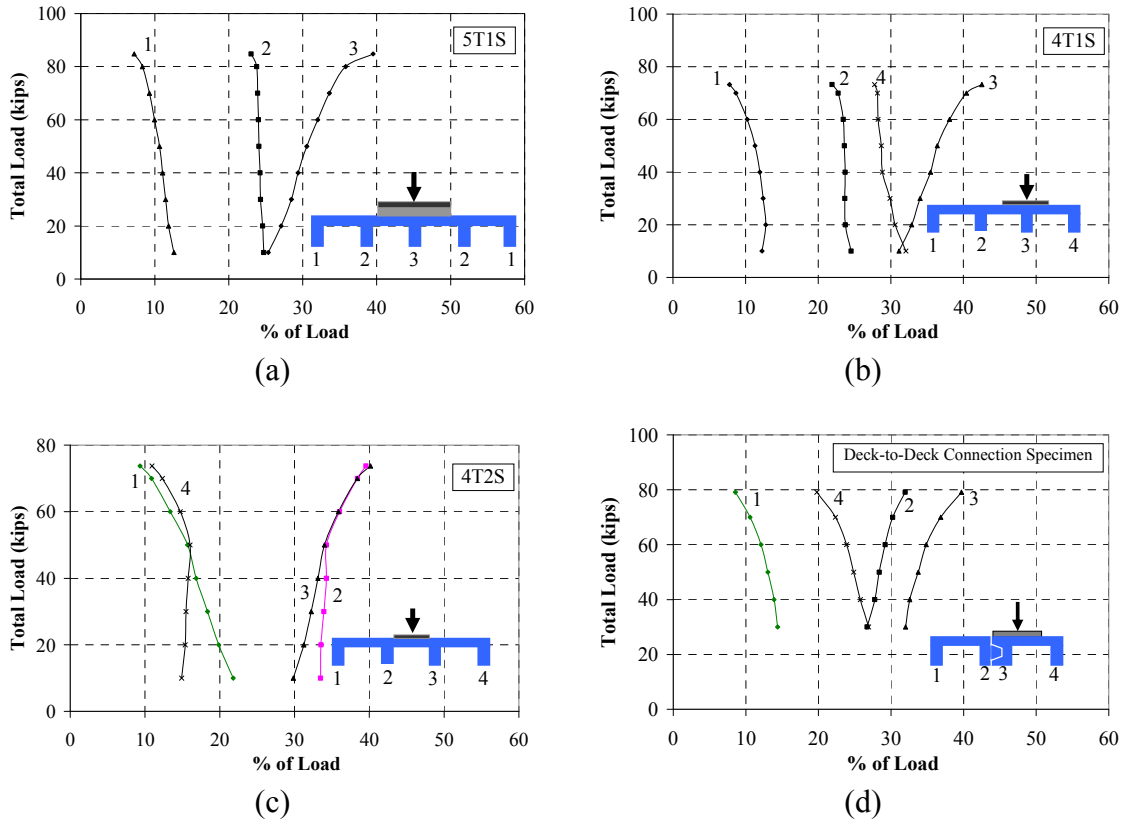


Figure 3.6 Lateral Distribution of Load: (a) 5T1S; (b) 4T1S; (c) 4T2S; and (d) Deck-to-Deck Connection Specimen

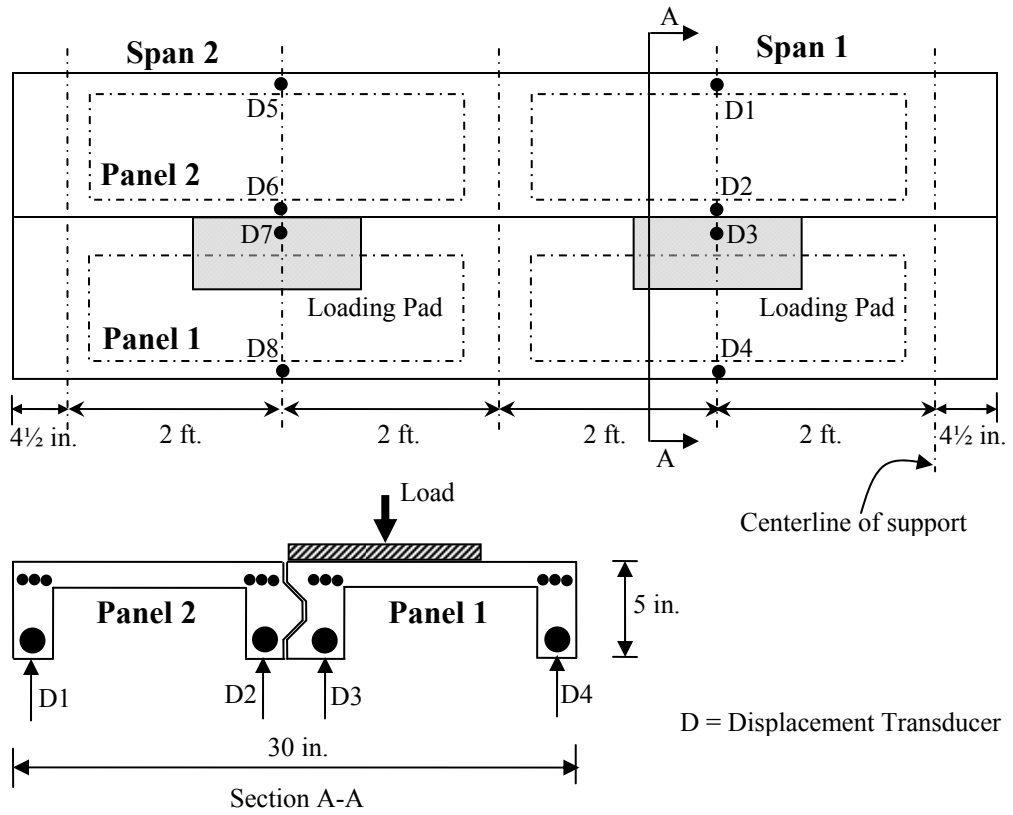
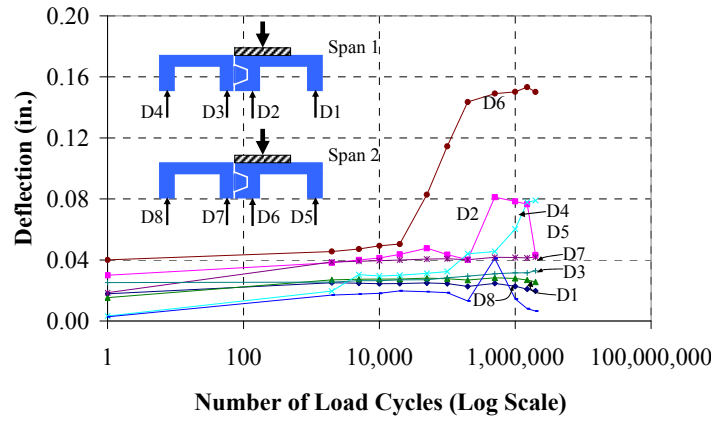


Figure 3.7 Loading Configuration and Instrumentation Plan for the Fatigue Test



(a)



(c)

Figure 3.8 Fatigue Test: (a) Test Setup; and (b) Growth of Deflection under Fatigue Loading (Performed at FDOT Marcus Ansley Structures Research Laboratory)



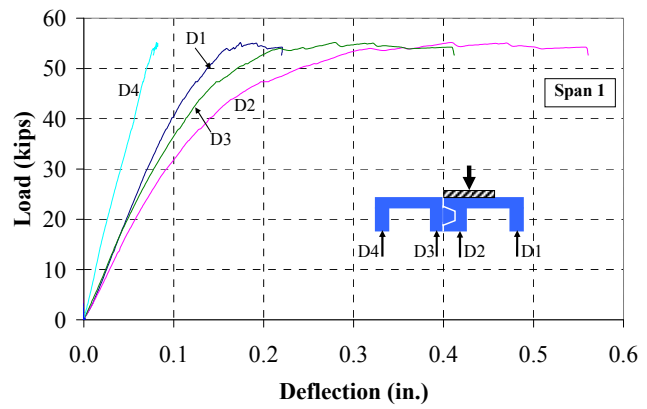
(a)



(c)



(b)

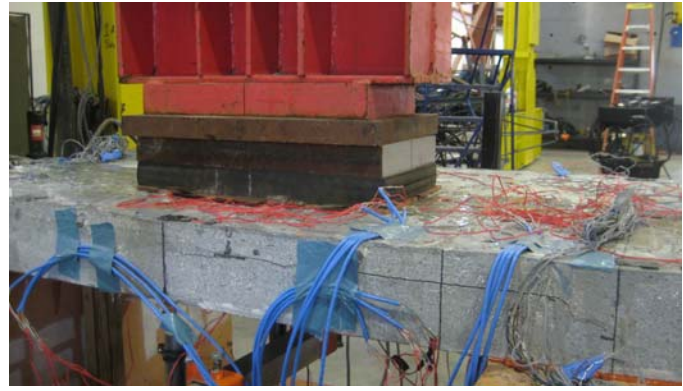


(d)

Figure 3.9 Residual Strength Test A with Load on Edge of Deck-to-Deck Connection:
 (a) Test Setup; (b) Shear Cracks; (c) Longitudinal Cracks; and (d) Load-Deflection Responses (Performed at FDOT Marcus Ansley Structures Research Laboratory)



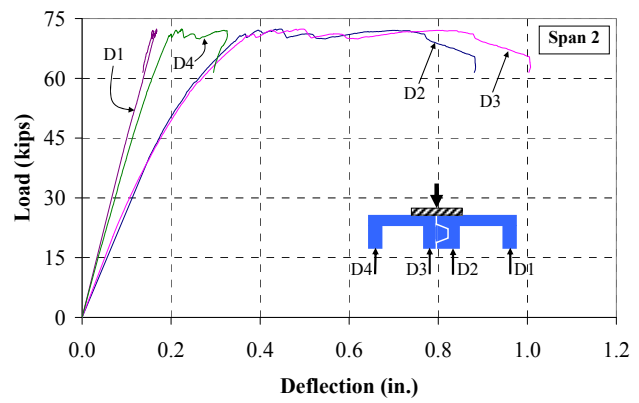
(a)



(c)

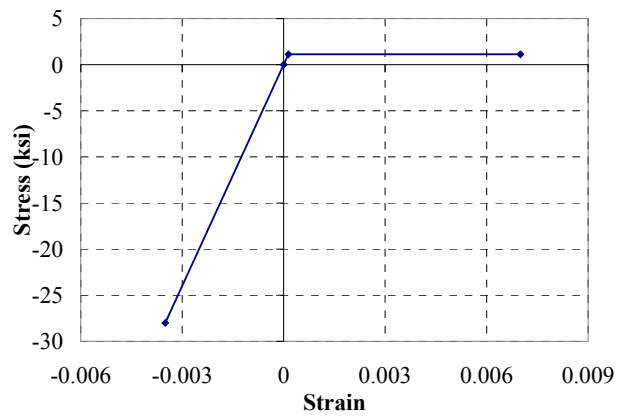


(b)

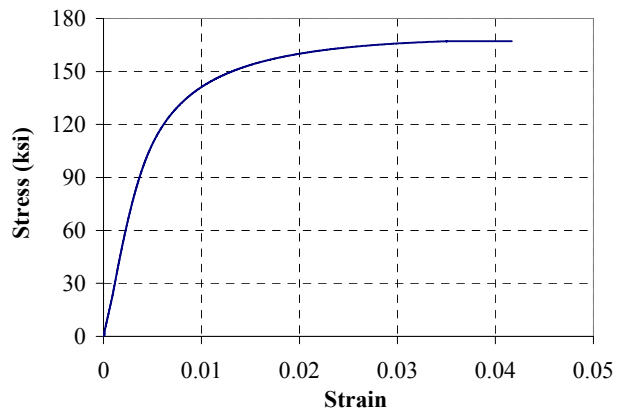


(d)

Figure 3.10 Residual Strength Test B with Load on Top of Deck-to-Deck Connection:
 (a) Test Setup; (b) Shear Cracks; (c) Longitudinal Cracks; and (d) Load-Deflection Responses (Performed at FDOT Marcus Ansley Structures Research Laboratory)

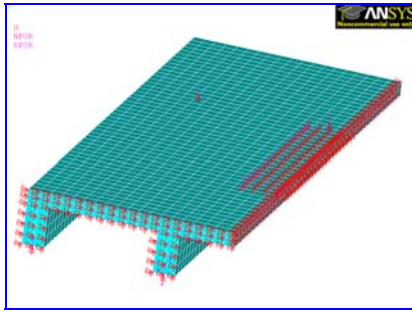


(a)

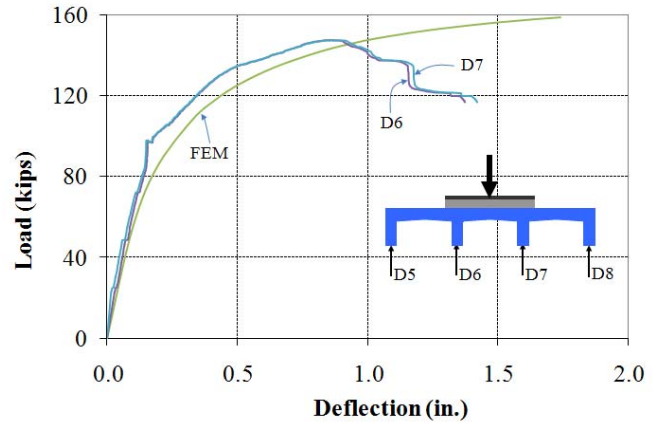


(b)

Figure 3.11 Stress-Strain Relationships for: (a) UHPC; and (b) MMFX Steel



(a)



(b)

Figure 3.12 FE Analysis of Specimen 4T2S: (a) FE model; and (b) Comparison of Experimental and Analytical Results

4. DEVELOPMENT LENGTH OF HIGH STRENGTH STEEL REBARS IN ULTRA-HIGH PERFORMANCE CONCRETE

Muhammad Azhar Saleem¹, Amir Mirmiran², Jun Xia³, and Kevin Mackie⁴

A Paper Prepared for ASCE Journal of Materials in Civil Engineering

Abstract

Ultra-high performance concrete (UHPC) is increasingly making its way into the civil engineering market. Characterization of UHPC has therefore become an active area of research. Since this type of concrete has recently been developed, its behavior is not yet fully understood and investigated. That includes its bond and development characteristics with high-strength steel reinforcement. This paper presents the experimental results of the pullout and beam tests conducted with high-strength steel and UHPC. This work is a part of a larger project related to the development of UHPC bridge decks. Since the bridge deck has been developed with #3 and #7 rebars, only these two rebar sizes were used in the experiments. Firstly, pullout specimens were tested with three different embedment lengths of 8, 10 and 12 times the rebar diameter. Then, based on the results of pullout specimens, beam specimens were tested with embedment lengths of 10, 12, 14 and 48 times the bar diameter for #3 rebars and 14, 16, 18 and 21 times the bar diameter for #7 rebars. The size of the T-section beam specimens was derived from the size of the rib in the proposed deck system to simulate the actual conditions. The study shows that #3 and #7 rebars develop at embedment lengths of 12 and 18 the rebar diameter, respectively. The paper also presents a comparison between experimental

¹ PhD Candidate, Dept. of Civil & Environ. Engrg., Florida Int'l. Univ., Miami, FL 33174, msale005@fiu.edu

² Prof. & Dean, College of Engrg. & Computing, Florida International Univ., Miami, FL 33174, mirmiran@fiu.edu

³ PhD Candidate, Dept. Civil Env. & Constr. Engrg., Univ. of Central Fla., Orlando, FL 32816, junxia@mail.ucf.edu

⁴ Asst. Prof., Dept. Civil Envir. & Constr. Engrg., Univ. of Central Fla., Orlando, FL 32816, kmackie@mail.ucf.edu

results and the recommendations of ACI 318-08 and ACI 408R-03 for the development lengths. It was found that ACI 408R-03 compares more favorably with the findings of this study.

CE Database Subject Headings

Bond; Development length; High-strength steel; Pullout; UHPC

4.1 Introduction

During the last two decades, number of studies have been carried out on bond and development characteristics of normal and high-strength concretes with steel and fiber reinforced polymer (FRP) rebars (Holschemacher et al. 2005; Azizinamini et al. 1993 and 1995; Harajli 2004; Hamad and Itani 1998; Firas et al. 2010; Esfahani and Kianoush 2005). Since high-strength and high performance concretes are becoming increasingly popular, they have attracted the focus of research in recent years (Chao et al. 2009). Researchers have also investigated the bond characteristics of fiber reinforced concrete with mild steel rebars (Horiguchi et al. 1988; Harajli et al. 2002; Chao et al. 2009). No previous research is available on the bond and development characterization of high-strength steel (HSS) in ultra-high performance concrete (UHPC). This study is focused on establishing the development length of MMFX steel rebars in UHPC when concrete cover is limited. MMFX steel is high-strength reinforcement with a yield strength of 100 ksi, which satisfies the requirement of ASTM A1035. Unlike mild steel, MMFX rebars do not show a yielding plateau in its stress-strain response. Yield strength is therefore determined using the 0.2% offset method (Seliem et al. 2009).

Force transfer between steel and concrete is due to three phenomena; adhesion; surface friction; and mechanical interlock (Valcuende and Parra 2009). In case of

deformed rebars inside normal strength concrete (NSC), all three actions are available for force transfer. However, mechanical interlocking is not present in plain rebars, hence leading to smaller bond strength than deformed rebars. Adhesion bond fails at a very small amount of slip (Chao et al. 2009), and therefore only the surface friction provides the bond strength in case of plain rebars. Mo and Chen (1996) conducted pullout tests on NSC using plain and deformed steel rebars. They concluded that bond strength of plain rebars is only 29 % of that of deformed rebars. They also observed that plain rebars have greater slip at failure than that of deformed rebars. In some cases, surface friction may also be smaller, leading to smaller bond strength. For instance, self compacting concrete (SCC) fails through rebar pullout due to the fines content leading to a smoother failure surface (Schiessl and Zilch 2001; Valcuende and Parra 2009). The mean and ultimate bond strength, however, are greater in SCC, as compared to normally vibrated concrete (Valcuende and Parra 2009).

Khandaker (2008) performed pullout tests on light-weight and normal-weight concretes. He observed that for plain rebars bond strength is not affected by the compressive strength or type of concrete. However, for deformed rebars, bond strength increases with the increase in the compressive strength of concrete. He also concluded that bond strength decreases with the increase in embedment length, both for normal- and light-weight concrete.

In the case of fiber reinforced concrete (FRC), fibers help in limiting the crack width through bridging and confinement which results in higher bond resistance (Chao et al. 2009) and more ductile bond failure as compared to plain concrete. Since UHPC includes fibers, its development length may be significantly reduced (Chao et al. 2009).

Holschemacher et al. (2005) suggested that ultra high-strength concrete shows very high bond strength and stiffness due to its high compressive strength and modulus of elasticity. Azizinamini et al. (1993) had similar observation for high-strength concrete. Harajli and Salloukh (1997) concluded that by adding hooked fibers up to 2% by volume fraction, the bond strength may increase up to 55%, as compared to plain concrete. Horiguchi et al. (1988) performed pullout tests on FRC and found out that by adding 2.5% fibers by volume the bond strength increases by 60%. UHPC used in this study has steel fibers which help in increasing the bond strength and reducing the development length. On the other hand, it also has silica fume which decrease the bond strength. Hamad and Itani (1998) found that replacing 5 to 20% of cement by an equal amount of silica fume could result in 10% reduction of bond strength. The reduction in bond strength due to silica fume is however offset by the fibers and the overall impact of fibers and silica fume results in a net increase in bond strength.

Pullout and beam tests are the two common types of tests for bond and development characterization. Some researchers have raised questions as to the accuracy of pullout tests. Harajli et al. (2002) concluded that pullout specimens underestimate the bond strength of rebars in tension. Therefore, he performed beams tests to obtain more accurate results. Mo and Chen (1996) made similar observation on pullout tests. Howell and Higgins (2007) concluded that for round reinforcing rebars, beam tests exhibit lower average stresses than the pullout tests. Using beam tests, Harajli et al. (2004) further reported that for small development lengths, confining concrete with transverse steel increases the bond strength only slightly, however it enhances the ductility considerably. Tastani and Pantazopoulou (2010) reported that the transverse reinforcement or thick

cover both may prevent or delay the splitting failure. Seliem et al. (2009) performed beam tests with spliced MMFX rebars, and showed that confinement with shear stirrups in the spliced region significantly improves the ductility. However, confinement does not affect the initiation of splitting cracks. Earlier, Darwin et al. (1996) had reported that the yield strength of transverse reinforcement plays no significant role in its effectiveness for improving the bond strength. Based on these conclusions, it was decided for the current study to use shear reinforcement in the beam specimens to help avoiding splitting and shear failure.

This study was part of a larger research project to develop alternatives to open grid steel bridge decks. A UHPC bridge deck system has been proposed through this research, which uses high-strength steel (MMFX). The motivation for this study comes from the fact that no previous research could be found on the bond and development of HSS rebars in UHPC. Figure 4.1 shows the schematics of the proposed deck system.

4.2 Experimental Program

The primary objective of experimental program was to investigate the development length of HSS rebars in UHPC. UHPC used for this project was Ductal[®], which was developed from the joint research of three French companies; Bouygues, Lafarge, and Rhodia. Table 4.1 shows the constituent materials in UHPC. The stress-strain response curves of UHPC and MMFX rebars are shown in Figure 4.2. A comprehensive test matrix was developed using both pullout and beam tests. Since the proposed deck system included #3 and #7 rebars as main reinforcement, only these two rebar sizes were used in the experiments. While deciding the sizes and shapes of specimens, it was kept in mind that the specimens should mimic the actual conditions in

the proposed bridge deck. The primary rib of the proposed deck is 2 in. wide. Therefore, all pullout specimens were prepared with 2 in. width. Also, the clear cover at the bottom of the main reinforcement in the deck is $\frac{1}{2}$ in. Therefore, top and bottom covers in the pullout specimens were both kept as $\frac{1}{2}$ in. Figure 4.3 shows the schematics of the pullout specimens. All pullout specimens were 12 in. long except the three specimens of #7 rebar with $18d_b$ embedment length which were 18 in. long. Polyvinyl chloride (PVC) tubes were used to debond the rebars from the concrete. PVC tubes were sealed with silicon to avoid any concrete infiltration. The beam specimens had a T shape cross-section, similar to the single unit of the deck system. The width of the web was kept as 2 in. for both #3 and #7 rebars with a clear cover of $\frac{1}{2}$ in. at the bottom. End blocks were added to avoid twisting of the specimen due to unintentional eccentricity during loading. Figure 4.4 shows the schematics of the beam specimens.

4.2.1 Loading and Instrumentation

Three quantities were measured during the pullout tests: load, slip of rebar relative to concrete, and the strain in rebar. Load was applied through a universal testing machine at a rate of 25 lbs/sec. Slip was measured using a string potentiometer, and strain using a surface mounted post- yield strain gauge. All instrumentation was connected to a high-speed data acquisition system, which recorded the data at a frequency of 1 Hz. In the case of beam specimens the quantities measured included total load; deflection at mid span; strain in steel rebar at mid-span, under one of the two point loads, and at the middle of the embedment length; and slip of steel rebar relative to concrete. Two string pots were used one for deflection and the other for slip measurement. A 50-kip load cell was used to measure the load, which was applied using a hydraulic jack operated through

an electric pump. Four point bending was used for the beam test, which provided a region of uniform bending moment. Distance between the two point loads was kept as 12 in. for all beam specimens. Specimens were constantly observed during the test to note any sign of distress. Excessive cracking or displacement and significant load drop were considered as failure and an indication to stop the test. The embedment length was measured from the location of point load towards the edge of the specimen.

4.2.2 Embedment length

The embedment lengths used for pullout specimens were initially selected as $8d_b$, $10d_b$ and $12d_b$, based on the flexural tests of the deck specimens and data from previous studies (Harajli et al. 2002). Both #3 and #7 rebar specimens were cast with the same normalized embedment lengths. Based on the results of these specimens, three (3) more specimens of #7 rebar with an embedment length of $18d_b$ were cast and tested. Previous researchers (Harajli et al. 2002; Mo and Chen 1996) had concluded that the pullout test underestimate the bond strength. This observation was the main motivation behind performing the beam tests. There was, however, a challenge with the beam specimens, which other researcher did not encounter, and that was the small concrete cover of only $\frac{1}{2}$ in. This small cover could not only cause premature failure but also made it difficult to provide shear stirrups, which were found necessary to avoid splitting and shear failure. Because of space limitation, plain #2 Grade 60 steel rebars were used as shear reinforcement at an average spacing of 1.5 in. on center, which is slightly greater than the maximum spacing of 1.3 and 1.4 in. for the #3 and #7 rebar specimens, recommended by ACI 318-08. Spacing smaller than 1.5 in. would have created issues in placing the UHPC and tying the shear reinforcement to the flexural reinforcement. Also, several researchers

(Harajli 2004; Azizinamini et al. 1993; Seliem et al. 2009) have performed beam tests with spliced rebars to evaluate the bond and development behavior. However, the traditionally performed beam tests with spliced rebars could not be performed in the current research because of the limitation of the rib size. In light of the results of pullout tests, it was decided to use $10d_b$, $12d_b$ and $14d_b$ for #3 and $14d_b$, $16d_b$ and $18d_b$ for #7 rebars beam specimens. Two beam specimens, each of #3 and #7 rebar were cast without any PVC tube leading to embedment lengths of $48d_b$ and $21d_b$ for the # 3 and #7 rebars respectively. Table 4.2 shows the complete test matrix of the experimental program.

4.3 Test Results and Discussions

4.3.1 Pullout Tests

Figure 4.5 shows typical load-slip responses for #3 rebar specimens with $8d_b$, $10d_b$ and $12d_b$ embedment lengths. Because plotting all the responses together would make it difficult to differentiate among them, only a typical response is plotted from each group of embedment lengths. A complete summary of ultimate strains and ultimate slips is, however, provided in Table 4.3. The failure load consistently increased with the increase in the embedment length. However, the variation of slip is not consistent. For instance, in Figure 4.5 the specimen with $12d_b$ embedment length showed higher slippage than the specimens with $8d_b$ and $10d_b$ embedment lengths. One reason could be the local failure of concrete key near one of the transverse ribs of steel rebar at around 5.2 kips of load, when a change of stiffness is noted. Such local failure may be attributed to voids in the concrete due to entrapped air. Variations in the ultimate strains of steel and the slips of rebars among specimens with similar embedment lengths can be observed in Table 4.3. There could be several reasons for these variations, including difference in concrete

cover due to human error in the preparation of formwork or placing of rebar, imperfect alignment of specimen in the machine, and variations among the load bearing surfaces of various specimens. All or few of these factors contribute towards inconsistency in the results. However, a general rising trend of ultimate strain can be observed in the #3 rebar specimens from $8d_b$ to $12d_b$ embedment lengths.

Figure 4.6 shows typical load-strain responses of #3 rebar specimens. Two out of three #3 rebar specimens with $12d_b$ embedment length crossed the yield strain (0.004) with a magnitude of 0.0067 and 0.0049. This gives an indication that the development length for #3 rebar could be around $12d_b$.

Figure 4.7 presents the typical load-slip responses for #7 pullout specimens. Initially, the specimens with $8d_b$, $10d_b$ and $12d_b$ embedment lengths were tested and then based on the trend of the strains, it was predicted that yield strain could be achieved with an $18d_b$ embedment length. Therefore, three specimens with $18d_b$ embedment length were cast and tested in the second phase along with the beam specimens. Specimens with $8d_b$, $10d_b$ and $12d_b$ embedment length show consistent behaviors, however, the ones with $18d_b$ depicted very different responses. Previous researchers (Khandaker 2008) concluded that bond strength decreases with the increase in embedment length. The behavior of $18d_b$ specimen seems consistent with this observation. Azizinamini et al. (1993) also made a similar argument that increasing the development length is not an efficient way to enhance the bond strength in case of high-strength concrete, especially when cover is small. It appears that bond strength increases with the increase in embedment length up to a certain limit, and then bond strength decreases with further increase in embedment length. For the specimens of the present study such a threshold appears to exist

somewhere between $12d_b$ and $18d_b$. With the increase in the embedment length, more and more transverse ribs are available to resist the applied force, which causes stress concentration in the region around the load bearing area, resulting in premature failure. Azizinamini et al. (1993) argued that in comparison with NSC specimens, HSC specimens have stronger concrete keys in front of transverse ribs, which have higher resistance against crushing and slippage leading to the concentration of bond force in few ribs at the loaded end. Either the concrete keys are strong or more ribs are available to resist the force, both can cause stress concentration at the loaded end. In the present study UHPC is used which means the concrete keys are quite strong and when the embedment length is increased it further helps in resisting the force and chances of stress concentration are increased making the premature failure more likely to happen.

None of the pullout specimens with #7 rebars could reach the yielding strain. Figure 4.8 shows the typical load-strain responses of #7 specimens. All specimens show linear behavior, and fail way before reaching the yielding strain, indicating that the steel rebars could not be fully mobilized. Figure 4.9 shows the modes of failure of all specimens. Most of the #3 specimens showed one distinct crack which runs from the loaded end up to the full embedment length. However, Specimens #3- $12d_b$ -1 and #3- $12d_b$ -2 showed some local cracks near the loaded end. All #7 pullout specimens showed significant local cracks pointing towards stress concentration in the load bearing region. Another reason for local cracks could be the smaller cover on one side of #7 rebars, as compared to the #3 specimens. In fact, smaller concrete cover, in addition to stress concentration, is an important factor which prevents full mobilization of stress in rebars and causes local failure. Concrete cover could not have been increased in this study

because the size of the specimens was taken from the size of the web of the proposed deck system. It may be concluded that the pullout test may not provide appropriate results for large rebar size when small concrete cover is provided. Figure 4.10 reinforces this argument, showing crack lengths of #7 specimens with a decreasing trend as opposed to the #3 specimens. This implies local failure when higher embedment lengths are provided for larger rebar sizes with small concrete cover.

4.3.2 Beam tests

Since the pullout specimens with #7 rebars could not provide conclusive results for the development length, it was decided to perform beam tests. Table 4.4 provides the summary of test results for all beams specimens. Figure 4.11 shows the typical load-deflection responses for the beam specimens with various embedment lengths. It can be seen that the #3 rebar specimens with $10d_b$, $12d_b$ and $14d_b$ embedment lengths all failed at a very early stage. These six specimens cracked at the location where debonding of bottom rebar began. These were all premature failures, and the steel rebars could not be fully mobilized. The ultimate steel strain in all #3 beam specimens could only reach a maximum of 20% of yield strain, except for the specimens without debonding which corresponded to the embedment length of $48d_b$.

Figure 4.12 shows the modes of failures of all beam specimens. The length of unbonded part of the rebar played a significant role in determining the way a particular specimen would fail. Figure 4.13 shows a variation of the unbonded lengths of rebars with respect to their embedment lengths. The trend line for #3 beam specimens is much higher than the one for #7 beam specimens, indicating that the higher the magnitude of unbonded length the greater would be the chances of a premature failure. Such a

premature failure may have been avoided by using a shorter beam for #3 rebars as compared to #7 beam specimens. The load-deflection responses in Figure 4.11 indicate that the initial stiffnesses of all specimens are comparable and the ultimate load increases with the increase in the embedment length. The specimens with $14d_b$ and $16d_b$ embedment lengths failed in a similar way as those of #3 beam specimens. However, #7 rebar specimens achieved higher strains than their #3 counterparts. One of the two specimens each with $18d_b$ and $21d_b$ embedment lengths crossed the yield strain and failed in flexure at the mid-span in the zero shear force zone.

4.4 Comparisons with ACI 318-08 and ACI 408R-03

Both ACI 318-08 and 408R-03 provide equations for calculating the development length for steel rebars embedded in concrete. ACI 318-08 limits its applicability to concretes with compressive strength lower than 10,000 psi. Azizinamini et al. (1995), however, suggested that the above limit may be removed with a condition of providing shear reinforcement throughout the development and splice lengths. Hamad and Itani (1998) also called this limit as unnecessary and unwarranted. Darwin et al. (1996) concluded that $\sqrt{f'_c}$ does not provide an accurate representation of the effect of concrete compressive strength on the bond strength. His suggestion of instead using $\sqrt[4]{f'_c}$ for concretes with compressive strengths between 2,500 and 16,000 psi. is adopted in ACI 408R-03. Canbay and Frosch (2006) proposed an expression, which they claimed to be applicable for concretes with compressive strength up to 16,000 psi.

From the test results of this study, it appears that the restriction of 10,000 psi compressive strength is valid for HSS embedded in UHPC. Figure 4.14 provides a

comparison of the development lengths suggested by the present study and those calculated from the formulae of the ACI 318-08 and ACI 408R-03. The values of f_c' and f_y used for calculating the development lengths were 25,000 psi and 100,000 psi respectively. It can be clearly seen that the ACI 318-08 leads to very high values of the development length for both #3 and #7 rebars. However, the values calculated from the ACI 408R-03 are very close to the ones recommended based on the present study. According to the ACI 408R-03 the development lengths for #3 and #7 rebars are $15d_b$ and $20d_b$, respectively, versus $12d_b$ and $18d_b$ suggested by the present study. This study also confirms the conclusion of Seliem et al. (2009) that for HSS rebars the equations of ACI 408R-03 provide a reasonable development length.

4.5 Summary and Conclusions

This study focused on the experimental investigation of development length of HSS rebars of two different sizes (# 3 and #7) embedded in UHPC. Both pullout and beam tests were performed. The results were also compared with the recommended values from the ACI 318-08 and 408R-03. Following are the conclusions drawn from this study:

1. Development lengths for #3 and #7 HSS rebars embedded in UHPC are found as $12d_b$ and $18d_b$, respectively. These values should be considered as an estimate and may require further verification.
2. Development lengths calculated based on the equations provided by the ACI-408R-03 reasonably agree with the values suggested by the present study. On the other hand, ACI 318-08 greatly overestimates the development length for HSS rebars embedded in UHPC.

3. Pullout tests provide reasonable results for smaller rebar sizes but not for the large rebar, especially when concrete cover is small. Beams tests are recommended for such cases. However, the configurations of the specimens, test setup and method of loading should be carefully selected to avoid premature failure.
4. Finding of the previous researchers (Khandaker 2008) that the bond strength decreases with the increase in the embedment length is confirmed for HSS rebars embedded in UHPC.

It is recommended to perform a set of pullout and beams tests with other rebar sizes to develop a database, which could then be used to propose an equation for calculating development length for HSS rebars embedded in UHPC. This database could also be used to propose modifications to the ACI 408R-03 equation. Traditionally performed beam tests with spliced rebars may also provide helpful data for this purpose.

References

- AASHTO LRFD Bridge Design Specifications, 2005, Interim Revisions, American Association of State Highway and Transportation Officials, Washington, D.C.
- ACI Committee 318, "Building Code Requirements for Structural Concrete (ACI 318-05)." American Concrete Institute, Farmington Hills, MI.
- ACI Committee 408, 2003, "Bond and Development of Straight Reinforcing Bars in Tension (ACI 408R-03)." American Concrete Institute, Farmington Hills, MI.
- ASTM A 1035/A 1035M, 2006, "Standard Specification for Deformed and Plain, Low-Carbon, Chromium, Steel Bars for Concrete Reinforcement." ASTM International, West Conshohocken, PA.
- Azizinamini, A., Chisala, M., and Ghosh, S. K., 1995, "Tension Development Length of Reinforcing Bars Embedded in High-Strength Concrete," *Engineering Structures*, V. 17, No. 7, pp. 512-522.
- Azizinamini, A., Stark, M., Roller, J. J., and Ghosh, S. K., 1993, "Bond Performance of Reinforcing Bars Embedded in High-Strength Concrete," *ACI Structural Journal*, V. 90, No. 5, pp. 554-561.
- Canbay, E., and Frosch, R. J., 2006, "Design of Lap-Spliced Bars: Is Simplification Possible?," *ACI Structural Journal*, V. 103, No. 3, pp. 444-451.
- Chao, S. H., Naaman, A. E., and Parra-Montesinos, G. J., 2009, "Bond Behavior of Reinforcing Bars in Tensile Strain-Hardening Fiber-Reinforced Cement Composites," *ACI Structural Journal*, V. 106, No. 6, pp. 897-906.
- Darwin, D., Zuo, J., Tholen, M. L., and Idun, E. K., 1996, "Development Length Criteria for Conventional and High Relative Rib Area Reinforcing Bars," *ACI Structural Journal*, V. 93, No. 3, pp. 1-13.
- Esfahani, M. R., and Kianoush, M. R., 2005, "Development/Splice Length of Reinforcing Bars," *ACI Structural Journal*, V. 102, No. 1, pp. 22-30.
- Firas, S. A., Foret Gilles, F., and Robert, L. R., 2010, "Bond between Carbon Fibre-Reinforced Polymer (CFRP) Bars and Ultra High Performance Fibre Reinforced Concrete (UHPC): Experimental Study," *Construction and Building Materials*, doi:10.1016/j.conbuildmat.2010.02.006.
- Hamad, B. S., and Itani, M. S., 1998, "Bond Strength of Reinforcement in High-Performance Concrete: The Role of Silica Fume, Casting Position, and Superplasticizer Dosage," *ACI Materials Journal*, Vol. 95, No. 5, pp. 499-511.

- Harajli, M. H., 2004, "Comparison of Bond Strength of Steel Bars in Normal and High-Strength Concrete," *Journal of Materials in Civil Engineering*, Vol. 16, No. 4, pp. 365-374.
- Harajli, M. H., and Salloukh, K. A., 1997, "Effect of Fibers on Development/Splice Strength of Reinforcing Bars in Tension," *ACI Materials Journal*, V. 94, No. 4, pp. 317-324.
- Harajli, M. H., Hamad, B.S., and Rteil, A. A., 2004, "Effect of Confinement on Bond Strength between Steel Bars and Concrete," *ACI Structural Journal*, V. 101, No. 5, pp. 595-603.
- Harajli, M., Hamad, B., and Karam, K., 2002, "Bond-slip Response of Reinforcing Bars Embedded in Plain and Fiber Concrete," *Journal of Materials in Civil Engineering*, V. 14, No. 6, pp. 503-511.
- Holschemacher, K., Weibe, D., and Klotz, S., 2005, "Bond of Reinforcement in Ultra High-Strength Concrete," *SP-228-34*, American Concrete Institute, Farmington Hills, MI
- Horiguchi, T., Saeki, H., and Fujita, Y., March-April 1988, "Evaluation of Pullout Test for Estimating Shear, Flexural, and Compressive Strength of Fiber Reinforced Silica Fume Concrete," *ACI Materials Journal*, pp. 126-132.
- Howell, D. A., and Higgins, C., 2007, "Bond and Development of Deformed Square Reinforcing Bars," *ACI Structural Journal*, V. 104, No. 3, pp. 333-343
- Khandaker, M., and Hossain, A., 2008, "Bond Characteristics of plain and deformed bars in lightweight pumice concrete," *Construction and Building Materials*, 22(2009), pp. 1491-1499.
- Mo, Y. L., and Chan, J., 1996, "Bond and Slip of Plain Rebars in Concrete," *Journal of Materials in Civil Engineering*, V. 8, No. 4, pp. 208-211.
- Schiessl A, Zilch K., 2001, "The effects of the modified composition of SCC on shear and bond behaviour," *Proceedings of second international RILEM symposium on self compacting concrete*, Tokyo, Japan, pp. 501-506.
- Seliem, H. M., Hosny, A., Rizkalla, S., Zia, P., Briggs, M., Miller, S., Darwin, D., Browning, J., Glass, G. M., Hoyt, K., Donnelly, K., and Jirsa, J. O., 2009, "Bond Characteristics of ASTM A1035 Steel Reinforcing Bars," *ACI Structural Journal*, V. 106, No. 4, pp. 530-539

Tastani, S. P., and Pantazopoulou, S. J., 2010, "Direct Tension Pullout Bond Test: Experimental Results," *Journal of Structural Engineering*, V. 136, No. 6. pp. 731-743.

Valcuende, M. and Parra, C., 2009, "Bond behaviour of reinforcement in self-compacting concretes," *Construction and Building Materials*, 23(2009), pp. 162-170.

Table 4.1 Proportions of UHPC Constituent Materials*

Constituent Materials	Percentage by Weight (%)	Weight Relative to Cement
Cement	28.6	1.00
Silica Fume	9.3	0.33
Ground Quartz	8.5	0.30
Fine Sand	41.1	1.44
Steel Fibers	6.4	0.22
Superplasticizer	0.5	0.02
Water	5.6	0.20
Total	100	

* Source: <http://www.lafargenorthamerica.com> (May 1, 2008)

Table 4.2 Test Matrix

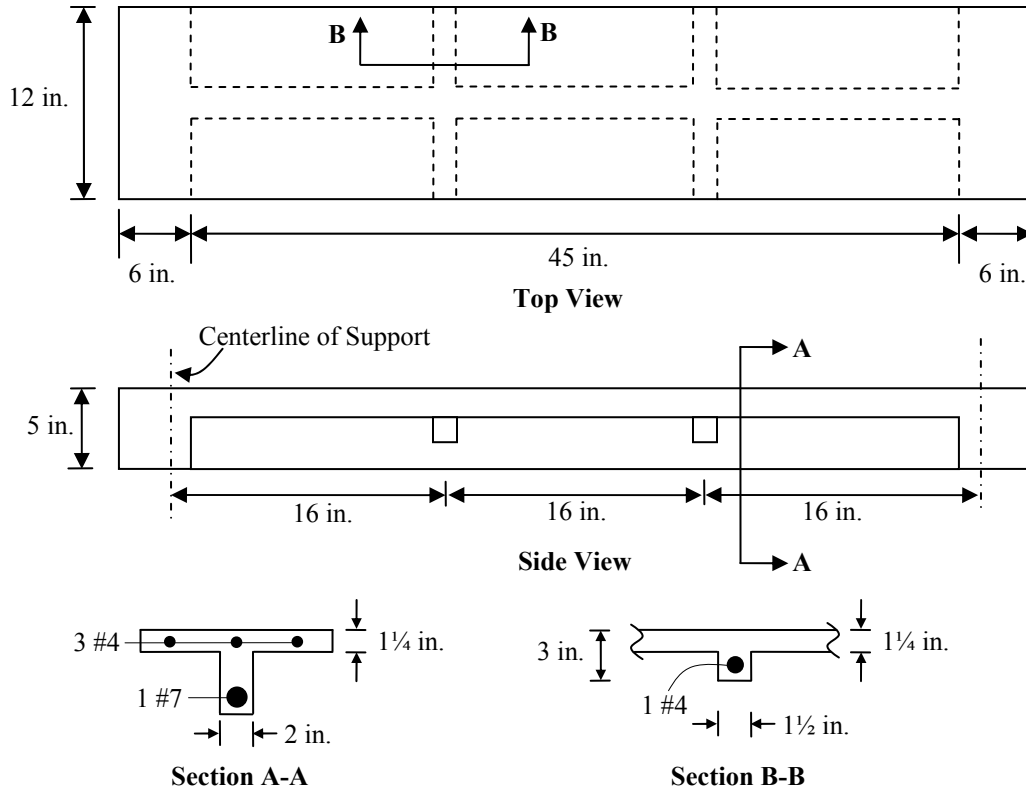
Type of Test	Bar Size	Embedment Length	Number of Specimens	
		(in.)		
Pullout	#3	8d _b	3	3
	#3	10d _b	3.75	3
	#3	12d _b	4.5	3
	#7	8d _b	7	3
	#7	10d _b	8.75	3
	#7	12d _b	10.5	3
	#7	18d _b	15.75	3
Beam	#3	10d _b	3.75	2
	#3	12d _b	4.5	2
	#3	14d _b	5.25	2
	#3	48d _b	18	2
	#7	14d _b	12.25	2
	#7	16d _b	14	2
	#7	18d _b	15.75	2
	#7	21d _b	18.38	2

Table 4.3 Summary of Pullout Test Results

Specimen Name	28-day Compressive Strength (ksi)	Rebar Strain at Ultimate Load (ϵ_u)	Strain Ratio (ϵ_u / ϵ_v)	Slip at Ultimate Load (in.)
#3-8d _b -1	24.0	0.0025	0.63	0.115
#3-8d _b -2	24.0	0.0021	0.53	0.070
#3-8d _b -3	24.0	0.0028	0.70	0.062
#3-10d _b -1	24.0	0.0040	1.0	0.037
#3-10d _b -2	24.0	0.0033	0.83	0.048
#3-10d _b -3	24.0	0.0025	0.63	0.080
#3-12d _b -1	24.0	0.0067	1.68	0.101
#3-12d _b -2	24.0	0.0035	0.88	0.039
#3-12d _b -3	24.0	0.0049	1.23	0.053
#7-8d _b -1	24.0	0.0016	0.40	0.051
#7-8d _b -2	24.0	0.0011	0.28	0.025
#7-8d _b -3	24.0	0.0024	0.60	0.031
#7-10d _b -1	24.0	0.0021	0.53	0.051
#7-10d _b -2	24.0	0.0020	0.50	0.077
#7-10d _b -3	24.0	0.0022	0.55	0.086
#7-12d _b -1	24.0	0.0025	0.63	0.055
#7-12d _b -2	24.0	0.0019	0.48	0.064
#7-12d _b -3	24.0	0.0024	0.60	0.061
#7-18d _b -1	25.2	0.0017	0.43	0.209
#7-18d _b -2	25.2	0.0017	0.43	0.115
#7-18d _b -3	25.2	0.0009	0.23	0.127

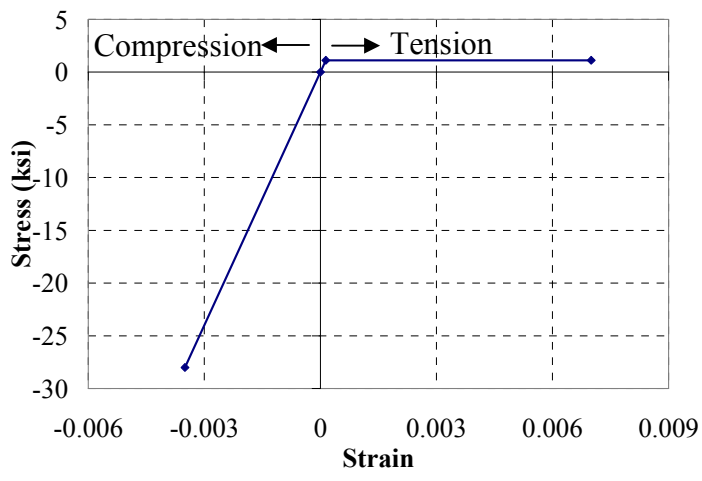
Table 4.4 Summary of Beam Test Results

Specimen Name	28 Days Compressive Strength (ksi)	Ultimate Strain in Rebar (ϵ_u)	ϵ_u / ϵ_y	Slip at Ultimate Load (in.)
#3-10d _b -1	24.4	0.0007	0.18	0.039
#3-10d _b -2	22.6	0.0006	0.15	0.033
#3-12d _b -1	25.0	0.0006	0.15	0.0037
#3-12d _b -2	25.4	Strain gauge damaged.		
#3-14d _b -1	25.8	0.0007	0.18	0.0037
#3-14d _b -2	25.5	0.0008	0.20	0.018
#3-48d _b -1	26.2	0.0218	5.45	No Slip
#3-48d _b -2	24.9	0.0109	2.73	No Slip
#7-14d _b -1	24.3	0.0026	0.65	0.306
#7-14d _b -2	25.3	0.0024	0.60	0.304
#7-16d _b -1	23.6	0.0020	0.50	0.118
#7-16d _b -2	25.0	0.0019	0.48	0.185
#7-18d _b -1	25.8	0.0071	1.78	0.077
#7-18d _b -2	24.3	0.0035	0.88	0.030
#7-21d _b -1	24.6	0.0054	1.35	No Slip
#7-21d _b -2	25.1	0.0035	0.88	No Slip

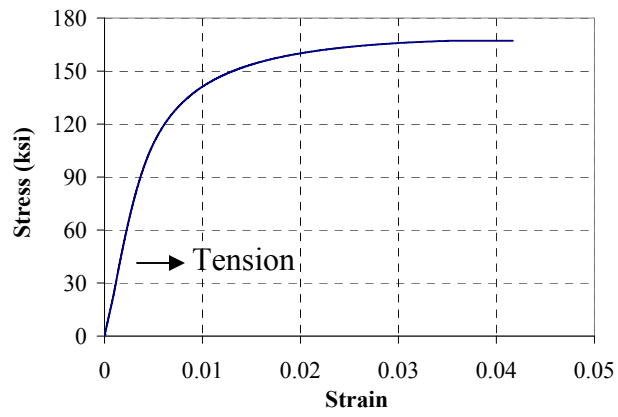


Note: 1 in. = 25.4 mm

Figure 4.1 Schematics of the Proposed UHPC-HSS Deck System

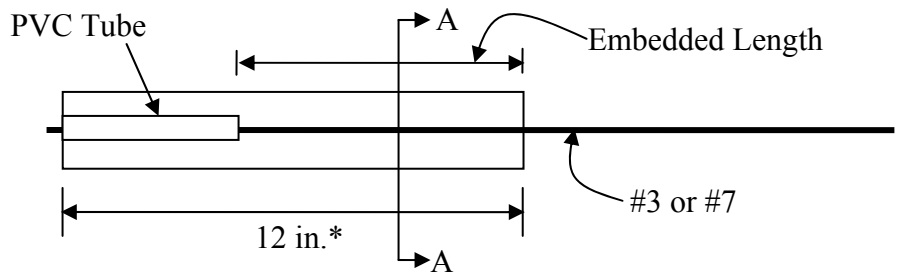


(a)

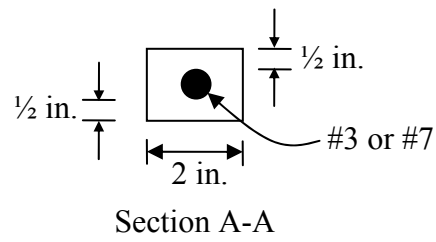


(b)

Figure 4.2 Stress-Strain Relationships for: (a) UHPC; and (b) MMFX Steel



*18 in. for #7-18d_b Specimens



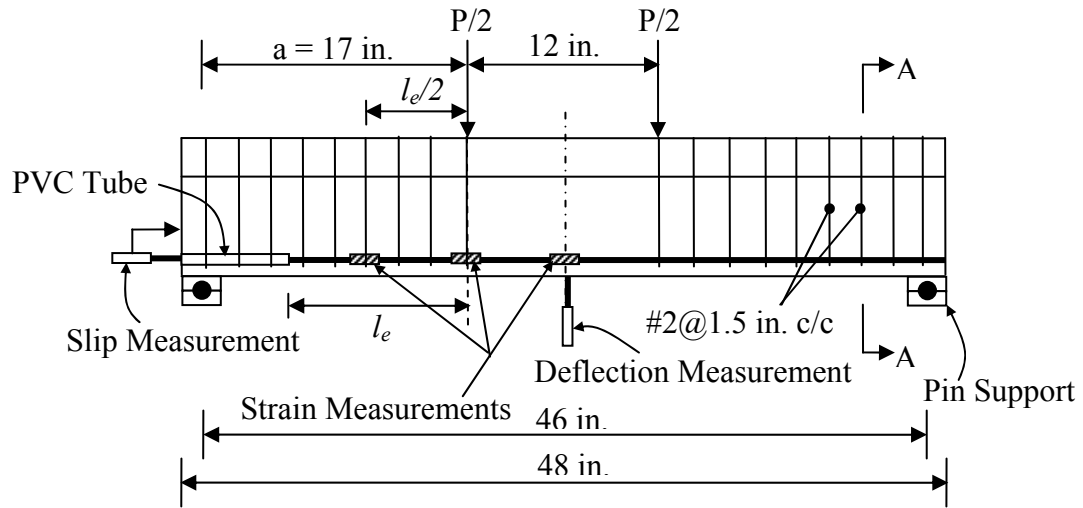
Section A-A

(a)



(b)

Figure 4.3 Pullout Test: (a) Schematics of Specimens; and (b) Specimens Ready for Casting



Instrumentation Plan

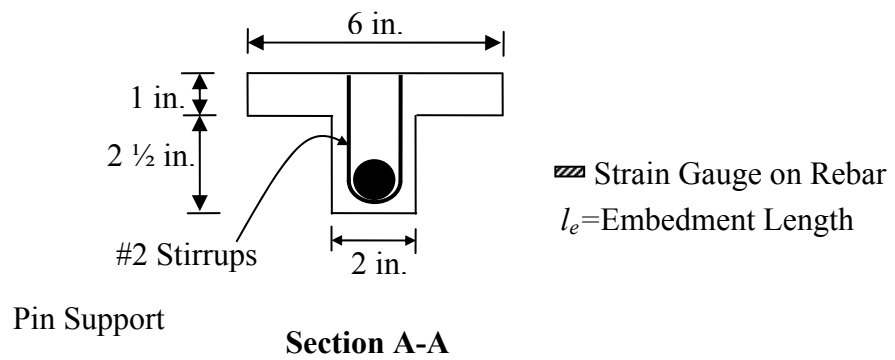


Figure 4.4 Schematics of Beam Specimens with Instrumentation

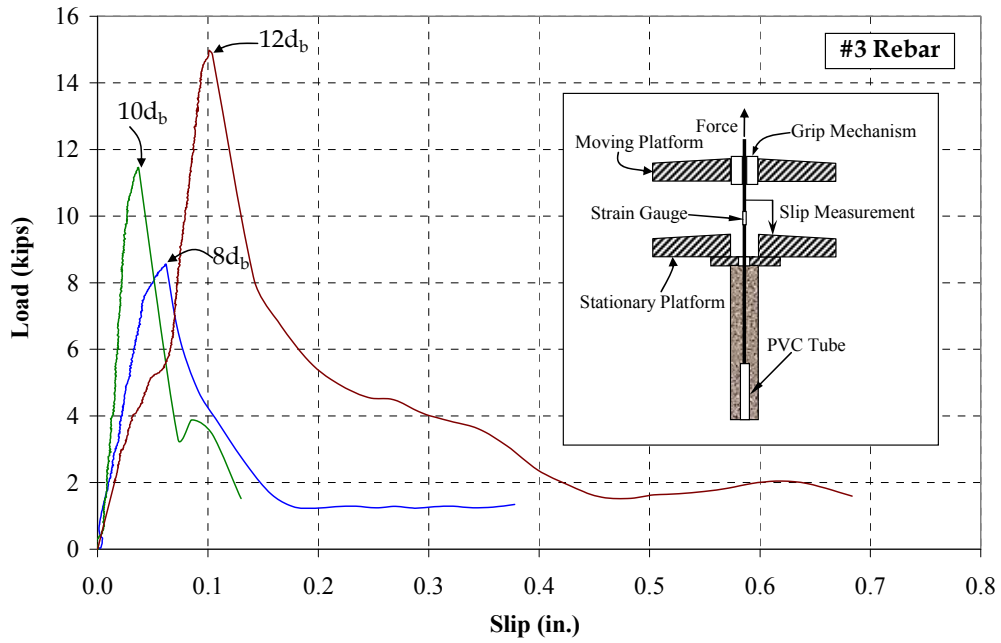


Figure 4.5 Typical Load-Slip Responses for #3 Rebar Pullout Specimens

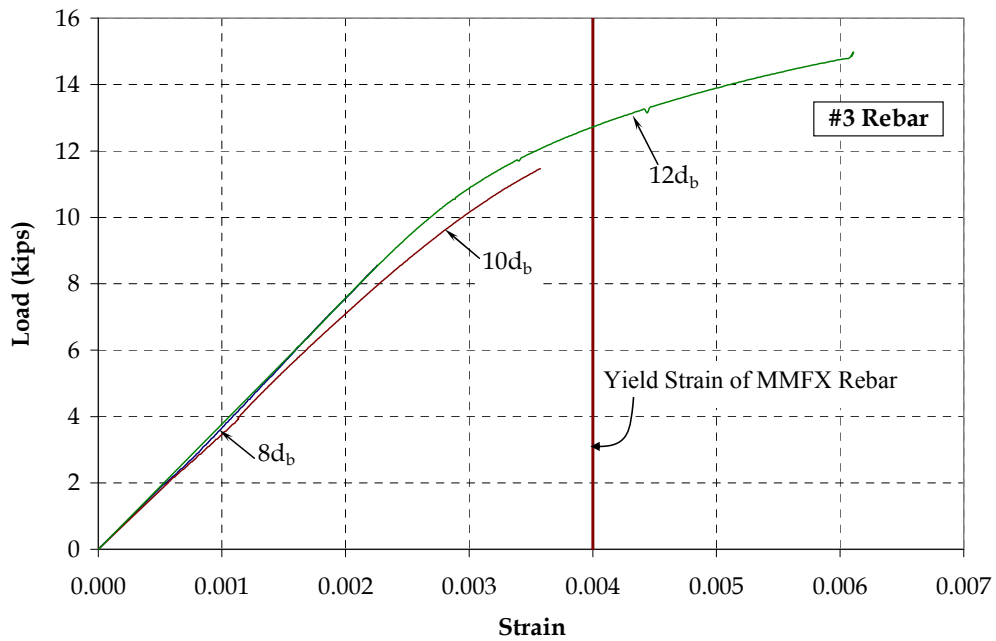


Figure 4.6 Typical Load-Strain Responses for #3 Rebar Pullout Specimens

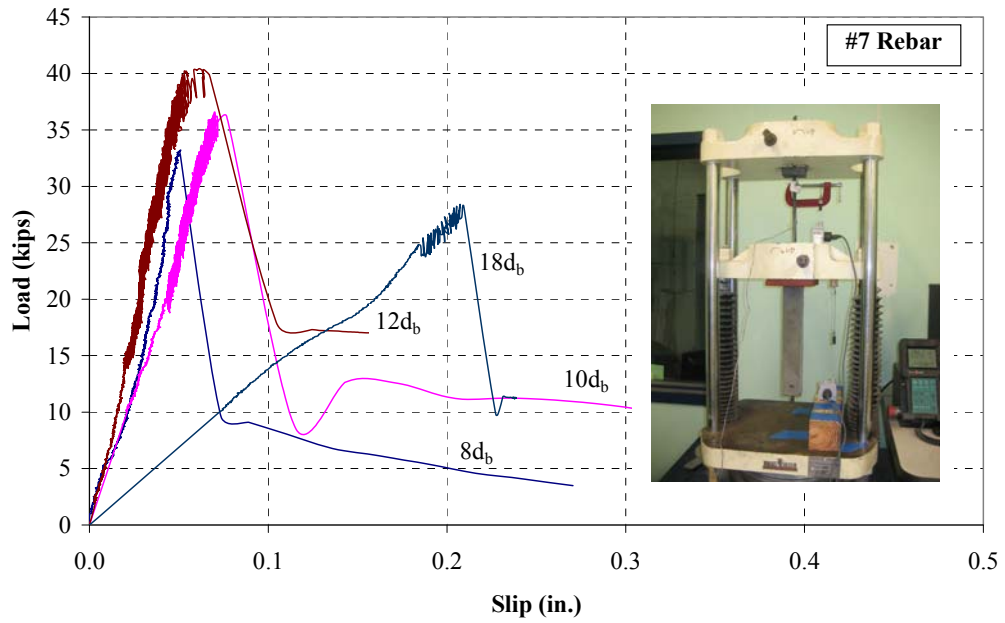


Figure 4.7 Typical Load-Slip Responses for #7 Rebar Pullout Specimens

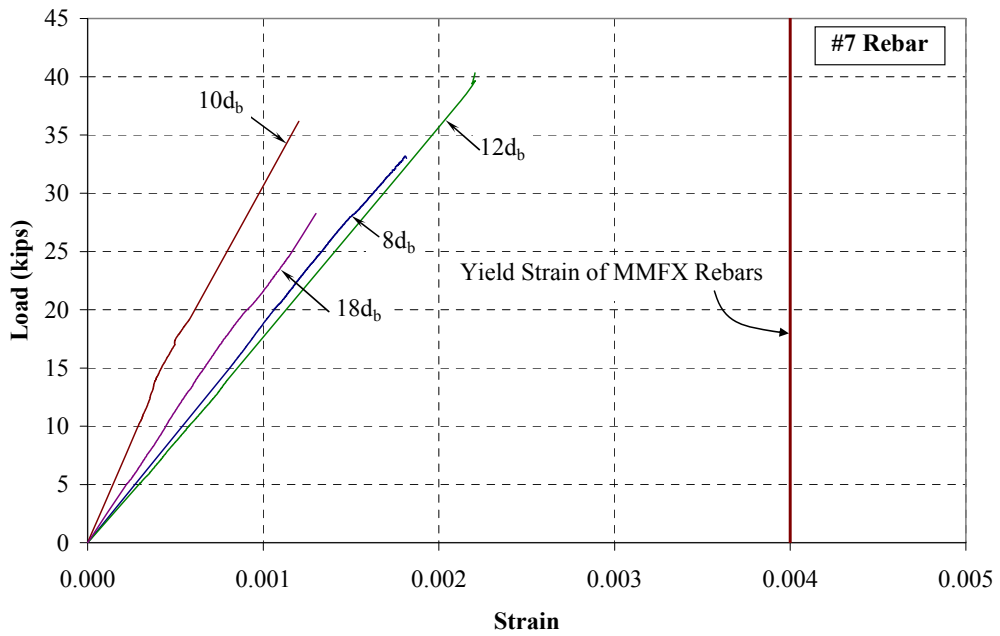


Figure 4.8 Typical Load-Strain Responses for #7 Rebar Pullout Specimens

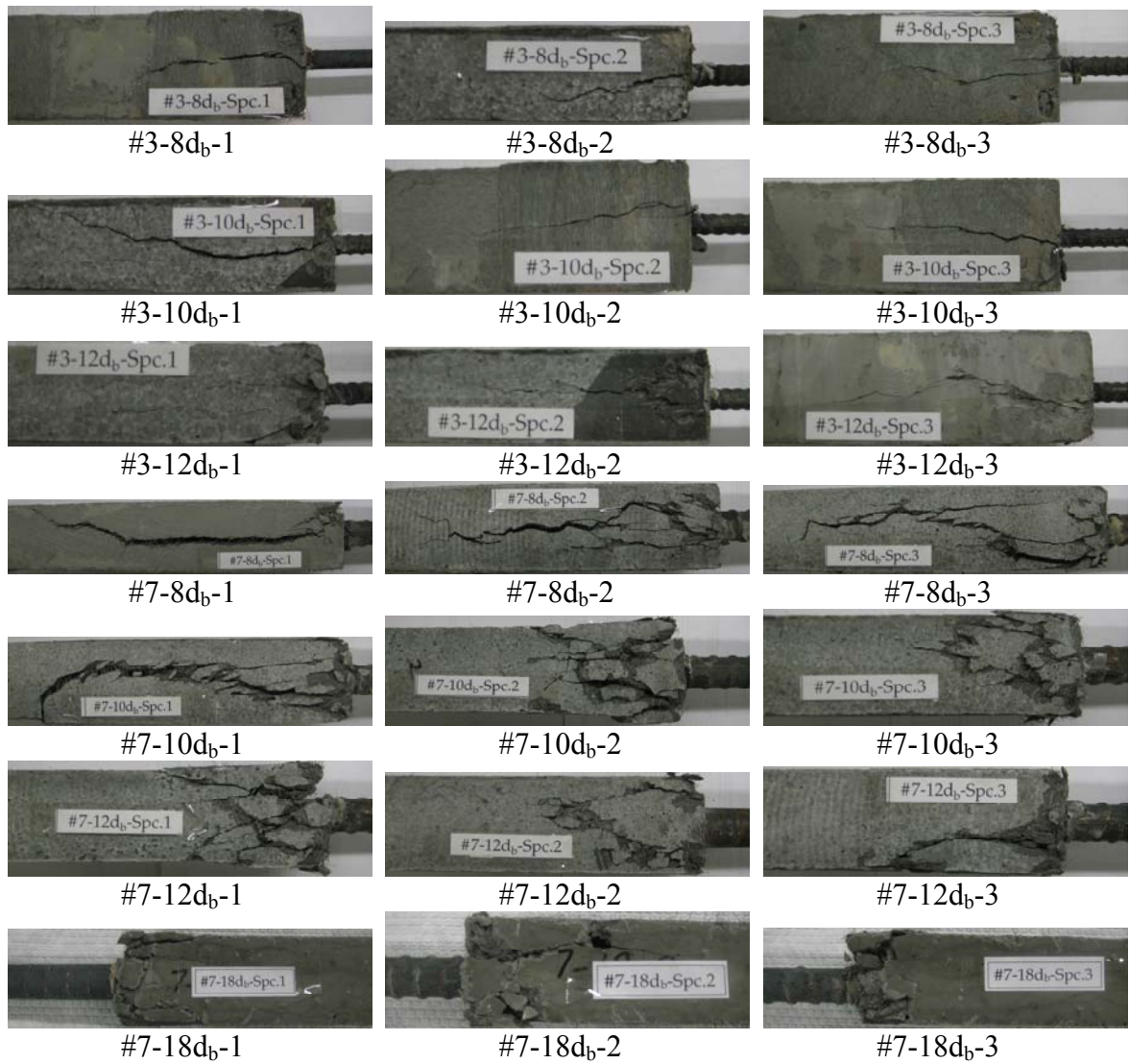


Figure 4.9 Modes of Failure in Pullout Specimens

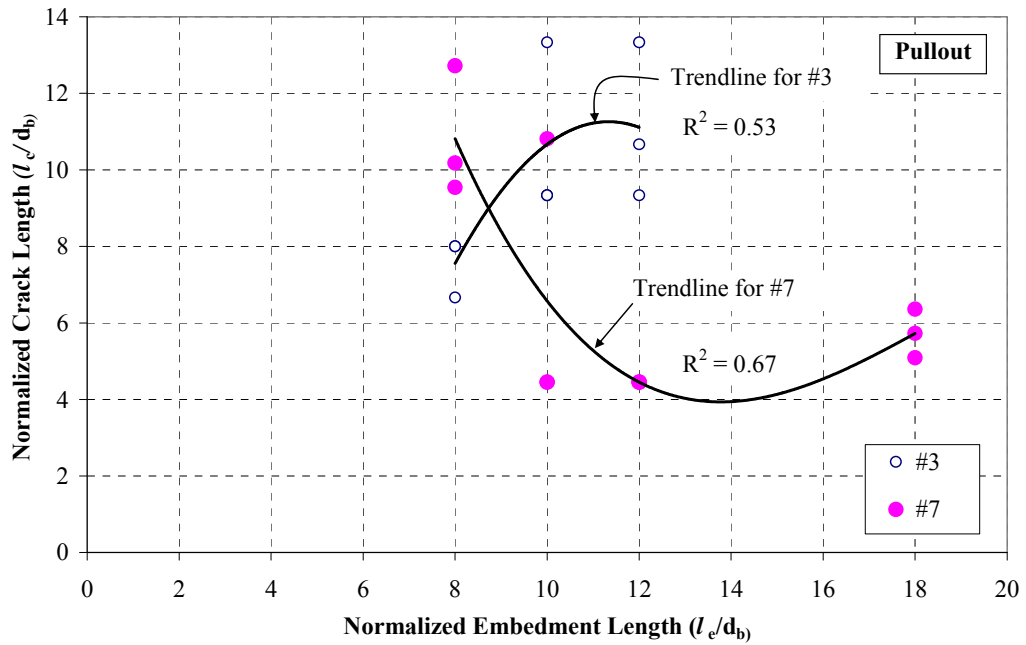


Figure 4.10 Variation of Crack Lengths in Pullout Specimens with respect to Embedment Lengths

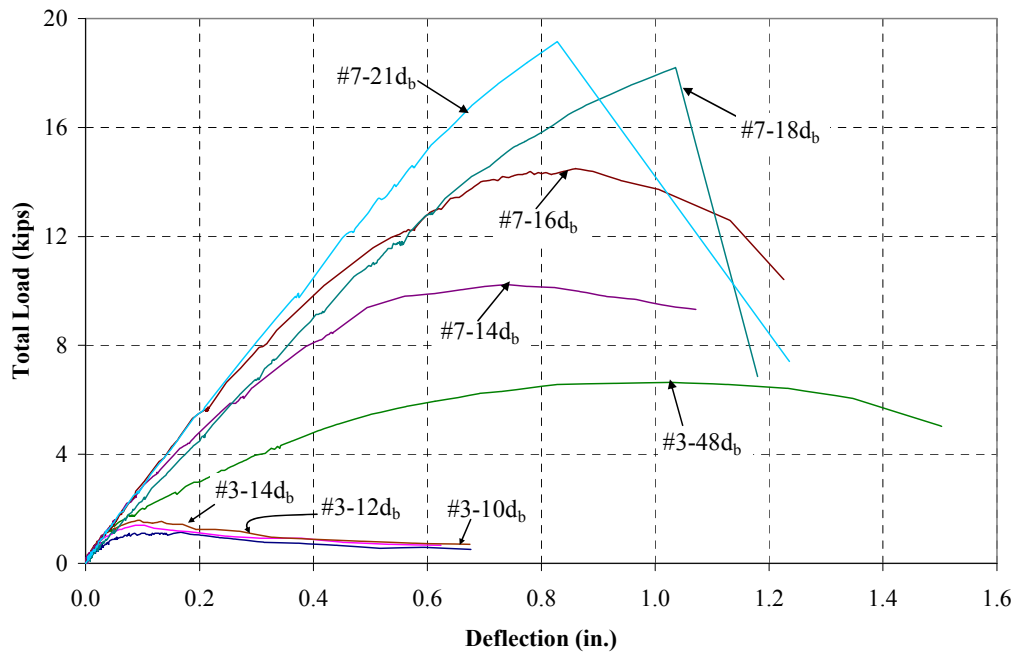


Figure 4.11 Typical Load-Deflection Responses of Beam Specimens

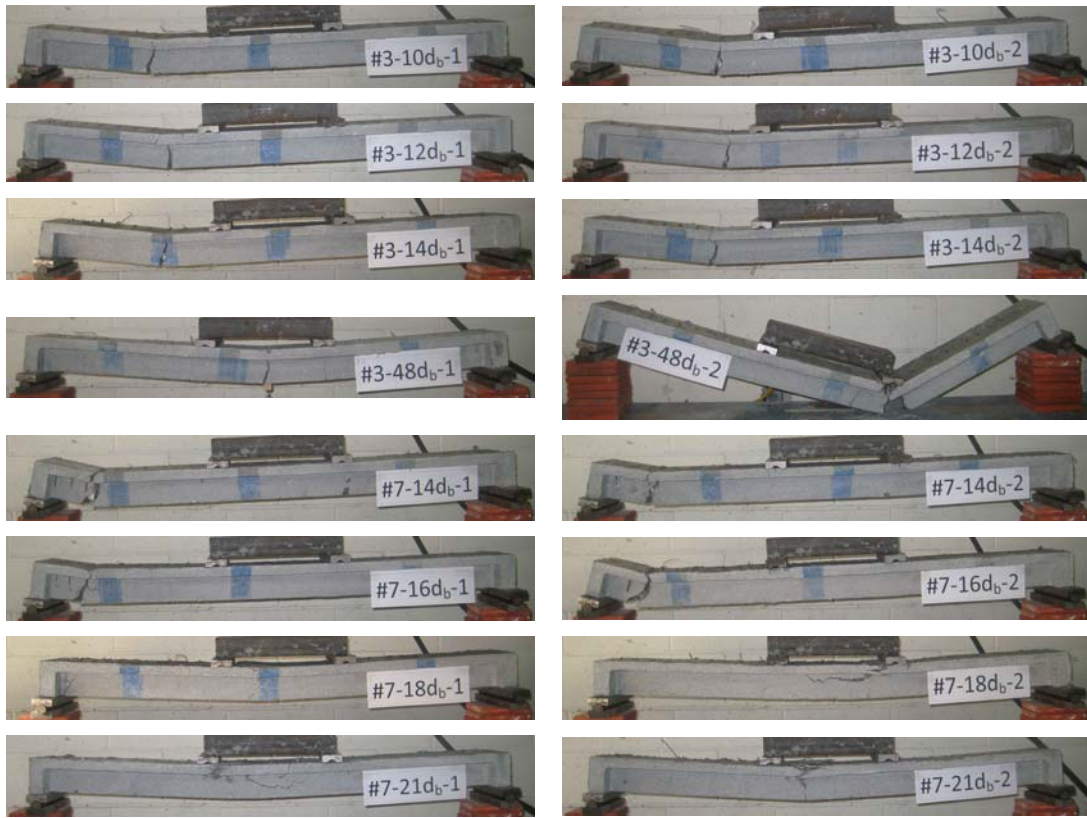


Figure 4.12 Modes of Failure in Beams Specimens

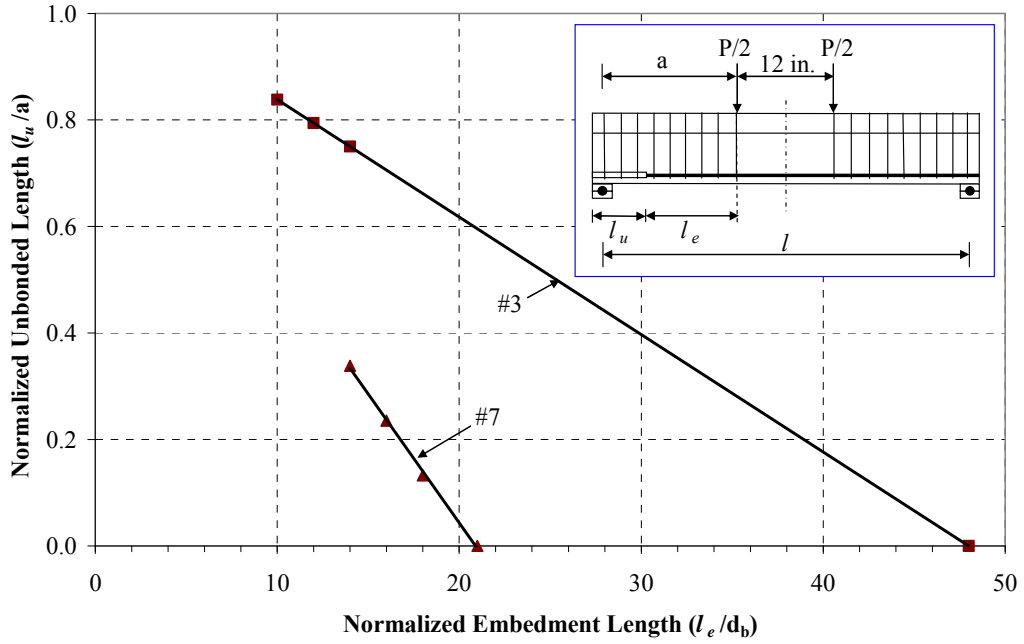


Figure 4.13 Variation of Unbonded Lengths of Rebars with respect to Embedment Lengths in Beam Specimens

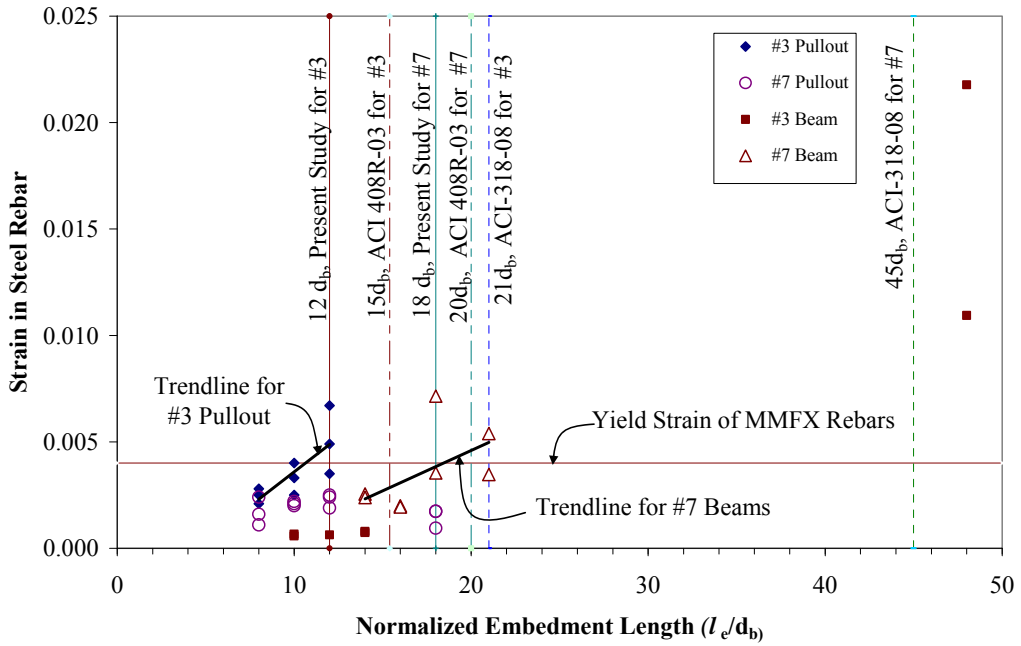


Figure 4.14 Comparisons of Test Data from Present Study with ACI 318-08 and ACI 408R-03

5. EXPERIMENTAL EVALUATION OF ALUMINUM BRIDGE DECK SYSTEM

Muhammad A. Saleem¹, Amir Mirmiran², Jun Xia³, and Kevin Mackie⁴

Accepted for publication in the ASCE Journal of Bridge Engineering

Abstract

Most of the moveable bridges in the U.S. have open grid steel decks, mainly because they are factory assembled, lightweight, and easy to install. Open grid steel decks, however, are not as skid resistant as solid decks. Costly maintenance, high noise levels, poor riding comfort, and susceptibility to vibrations are among the other disadvantages of these decks. The objective of the research presented in this paper is to evaluate an alternative lightweight extruded aluminum deck system that has a solid surface and meets the loading requirements as well as weight and thickness limits for moveable bridge decks. These aluminum deck panels with their tongue and groove connections have previously been used in Europe, mainly Sweden. A detailed experimental evaluation of the aluminum deck system has been carried out, including static and fatigue load testing on the deck panels, as well as ancillary tests on the connections with the girders. Based on the in-depth experimental evaluation and the subsequent finite element modeling and predictions, the extruded aluminum deck is shown to be a feasible alternative to open grid steel deck and ready for implementation on moveable bridges as well as bridges that require a lightweight deck.

CE Database Subject Headings

Aluminum; Bridge; Deck, Fatigue; Lightweight; Moveable; Open grid; Steel.

¹ PhD Candidate, Dept. of Civil & Environ. Engrg., Florida Int'l. Univ., Miami, FL 33174, msale005@fiu.edu

² Prof. & Dean, College of Engrg. & Computing, Florida International Univ., Miami, FL 33174, mirmiran@fiu.edu

³ PhD Candidate, Dept. Civil Env. & Constr. Engrg., Univ. of Central Fla., Orlando, FL 32816, junxia@mail.ucf.edu

⁴ Asst. Prof., Dept. Civil Envir. & Constr. Engrg., Univ. of Central Fla., Orlando, FL 32816, kmackie@mail.ucf.edu

5.1 Introduction

Open grid steel decks are commonly used on moveable bridges throughout the U.S. There are currently a total of 856 moveable bridges in the U.S., of which 54% are bascule, 25% swing and 21% lift bridges (National Bridge Inventory 2008). Three types of open grid steel decks are in use: unfilled system, concrete-filled system, and unfilled composite system (Exodermic™ 2008). Unfilled system is used with or without roughened surface. Filled system includes concrete within either the full or partial depth of the grid (ASTM D 5484-99). Unfilled composite system consists of reinforced concrete slab composite with an unfilled grid (Exodermic™ 2008). On average, unfilled grid decks weigh less than 25 lb/ft²; while some can weigh as little as 14 lb/ft². These decks are factory assembled and quite easy to install. Also, deck crowning, scuppers, and drains are not required, because rain water drains through the openings in the deck. Open grid decks, however, have rideability, maintenance, and environmental issues. These bridge decks are not as skid resistant as decks with a solid riding surface and can also polish over time, leading to poor rideability. Noise is another potential concern in some urban areas. Baseline acoustic testing by Takkasila and Reddy (1996) measured the noise radiating from these bridge decks at levels that may cause public concern in urban areas. Due to the safety, maintenance, and environmental concerns pertaining to open grid steel decks, research is needed into alternative deck systems that can address the rideability issues, while meeting the strict self-weight limit of 25 lb/ft² on these types of bridges.

As a lightweight material, aluminum provides one such alternative. Several aluminum systems were found in the literature. After careful evaluation of five different systems from five different countries, the research team identified off-the-shelf profiles

made by SAPA Group of Sweden as suitable for such bridge applications. This lightweight aluminum bridge deck system is made up of five voided extrusions that are attached to each other using tongue and groove connections, and are mechanically fastened to steel girders. These deck panels are available in two sizes, 11 and 12 in. wide; both 4 in. deep. The extruded panel weighs 14 lb/ft², which more than satisfies the self-weight requirement for replacing an open grid steel deck. Although this system has been used in Europe, mainly Sweden, it has not seen any application in the U.S. Acrylic-based material (Acrydur[®]) and hot asphalt mix are the most commonly used wearing surfaces with these decks, although other wear surfaces may be selected as appropriate. Figure 5.1 shows the shape and size of a single deck panel and its connections with steel girders.

5.2 Review of Previous Work

Applications of aluminum in bridges can be traced back to 1933, when the timber and steel floor system in the Smithfield Street Bridge in Pittsburg, PA, was replaced with an aluminum deck in order to increase the load-carrying capacity (Growdon et al. 1934; and Arrien et al. 2001). The first aluminum railway bridge in the U.S. was constructed over the Grasse River near Massena, NY, in 1946 (Arrien et al. 2001). The first aluminum highway bridge in North America was erected in Arvida, Canada, over the Saguenay River in 1950 (Das and Kaufman 2007).

There are four principal concerns for the adoption of an aluminum alloy in bridge deck applications. They include potential for electrochemical corrosion, fatigue degradation, galvanic corrosion, and a durable wearing surface that adheres to the extruded shapes. While sometimes viewed to have poor corrosion resistance, researchers have performed laboratory-scale tests and concluded that aluminum has excellent

corrosion resistance, and that it does not need any protection in this regard (Siwowski 2009; and Mazzolani 2006). Hoglund and Nilsson (2006) have reported that the 6000 series aluminum alloy exhibits optimal mechanical and anti-corrosive properties, which could be of great benefit for bridge applications.

Fatigue is another issue that needs to be addressed for aluminum bridge decks. In a detailed study, Wright (1997) reported that the aluminum deck of Smithfield Street Bridge showed very little degradation due to fatigue and corrosion after 27 years of service. Soetens and Straalen (2003) and Siwowski and Zoltowski (2003), on the other hand, reported that welded connections in aluminum bridge decks are susceptible to fatigue. Strength in the heat-affected zones is significantly reduced by the heat of welding (Dobmeier et al. 2001), and fatigue fracture may occur even at service load levels. Epoxy-based or bolted connections are potential solutions to mitigate such fatigue concerns.

Galvanic corrosion is another concern in bridges with dissimilar metals. Aluminum decks, when used with steel girders, can experience galvanic corrosion, unless the deck is kept separate from steel girders. A layer of stainless steel, if attached to the top flanges of steel girders, can prevent galvanic corrosion. This solution was adopted for the Aselva Bridge in 1958 (Siwowski and Zoltowski 2003). Aluminum haunches constructed on the girder top flange is another solution to this problem.

Decision on the type of wear surface is important because aluminum decks have a very smooth surface that may cause delamination of the wear surface. Various types of wear surfaces have been suggested in the literature, including asphalt, polyester and sand, and acrylic-based courses. In 1933, the Smithfield Street Bridge was rehabilitated using

aluminum deck with an asphalt wear course. In 1967, a new lighter-weight aluminum orthotropic deck with a polyester and sand wear course was assembled on the existing aluminum deck. In the U.K. and Germany, aluminum plates have been used as decks with an asphalt wear course (Siwowski and Zoltowski 2003). Hoglund and Nilsson (2006) reported on an acrylic-based material (Acrydur[®]) that has shown very high resistance to wear in existing bridges over long term. The Federal Highway Administration (FHWA) has funded research on a variety of polymer-sand aggregate surface materials that are designed to bond with aluminum and to prevent skidding (Wright 1997).

5.3 Loading Requirements

AASHTO LRFD (2005) recommends a live load model for the design of highway bridges which consists of a combination of design truck or design tandem and design lane load. However, for the design of decks spanning in transverse direction, lane load can be ignored (AASHTO 3.6.1.3.3). Since the design truck (HS 20) is more critical than the design tandem therefore, target load is calculated considering design truck only. Live load calculation is based on the following design philosophy:

$$\phi R_n \geq \sum_i \eta_i \gamma_i Q_i \quad (1)$$

where ϕ is the strength reduction factor, R_n is the nominal resistance, η_i is the i^{th} modification factor, γ_i is the i^{th} load factor, and Q_i is the i^{th} load in the load combination. From AASHTO LRFD (2005), one can infer that $\gamma = 1.75$, $\phi = 0.9$, and $\eta = 1.0$. Also, typically, the impact factor is 1.33. For the wheel load of an HS 20 truck, which is 16 kips, one can then derive the ultimate load P_u as 37.24 kips, which is also the target load for the experiments.

5.4 Experimental Work

The primary objective of testing aluminum bridge deck panels was to establish the ultimate load capacity, mode of failure, and long-term fatigue performance. To fulfill these objectives, a comprehensive test matrix was developed, as presented in Table 5.1 (Mirmiran et al. 2009).

Both flexural and fatigue tests were conducted with the AASHTO prescribed footprint of an HS 20 truck dual-tire wheel (20 x 10 in.). The panels were oriented with extrusions perpendicular to the girders and the direction of traffic. Strain gauges, linear potentiometers, and string potentiometers were installed at strategic locations to acquire the strain and deflection data. All instruments were connected to a Vishay[®] data acquisition system with a sampling frequency of 1 Hz. Six deck panels were obtained and cut to size to perform various tests.

5.4.1 Flexural Tests

Both simple span and two-span continuous deck specimens were tested (Figure 5.2). The simple-span specimens were subjected to a single load at mid-span, whereas the two-span specimens were loaded with one load at the middle of each span. Both the panel and beam actions were examined at service and ultimate load levels. A displacement-control procedure was adopted with a displacement rate of 0.015 in./min. Deck panels were first loaded up to yielding, and were then fully unloaded and reloaded to failure. Excessive deflection of the deck panel or local buckling of plate elements was considered as the failure point and an indicator to stop the test.

For the simple-span and the simple-span inverted panel tests, a 6 ft and a 8 ft long piece, respectively, were cut from two full panels. The left-over pieces were later used for

the ancillary tests. For the two-span continuous test, a complete deck panel was used. To simulate the wheel load, a 1 in. thick neoprene pad was used under the steel loading plate.

For the simple-span and inverted panel tests, three strain gauges were installed at the mid-span on the tension side (bottom face) of the section, one at the middle of the section and one at each edge. For the two-span deck, strain gauges were applied at the bottom in the mid-span and on the top face at the interior support. String potentiometers with 12 in. range were used to monitor deflections. Three string potentiometers were used in each of the three flexural tests, one at the middle of the section and one at each edge.

Figure 5.3 shows the load-deflection response, finite element prediction (as discussed later) and the deflected shape of the simple-span deck near ultimate load. It also shows M/M_y ratio on the secondary y-axis. Where M is the maximum moment at the mid-span and M_y is the moment at the first yield in the section. Since M_y (24.7 kip-ft) for the bottom fiber is lesser than the M_y (30.0 kip-ft) for top fiber, therefore M_y for the bottom fiber is used for all graphs. The deck panel exhibited a stiffness of 90.1 kip/in. up to a load of 45.0 kips, and then began softening gradually. The unloading began at a load of 63.0 kips, which turned out to be above the first yield point, but before developing the full plastic hinge. The deck panel had a residual tensile strain of around 0.009 at mid-span when fully unloaded. The ultimate load of 70.1 kips was 87% higher than the required ultimate load of 37.24 kips. The deck panel was still able to sustain further deflection, but the test was stopped due to safety reasons.

The two-span continuous panel was tested to observe the behavior of the deck under a negative moment. Because the cross section of the deck is asymmetrical about its bending axis, it behaved quite differently in the positive and negative moment regions.

Figure 5.4 shows the experimental and analytical load-deflection responses and the deformed shape. Moment (M) used to calculate the M/M_y ratio is the moment at the middle support since it is larger than the mid-span moment. The loading, unloading, and reloading curves are almost parallel indicating minimal stiffness degradation. The initial stiffness is 205 kip/in, which is 128% higher than that of the simple-span specimen. The total ultimate load is 168 kips or 84 kips for each span, approximately 20% higher than that in the simple-span panel. The major difference between the simple-span and the two-span panels is in the stiffness, due to the redundancy of the system.

The inverted panel test simulated the deck overhang with a hogging moment. The load was applied at the third point of a 8 ft simple-span to simulate an overhang length of 6 ft. The deck had an initial stiffness of 37.7 kip/in and an ultimate load of 35.1 kips (Figure 5.5). The figure inset shows signs of local buckling in the top and side plates near the ultimate load.

5.4.2 Shear Test for Connectors

This test was performed to determine the ultimate shear capacity of the deck-to-girder connection, which consists of a clamp that holds down the deck with the help of a 2¼ in. long stainless steel screw. This clamped connection will be subjected to a horizontal shear force in the field due to braking of the moving vehicles. In the case of an interior panel, the braking force will be resisted in two ways, firstly by the tongue and groove connection that will transfer the force to the adjacent panel, and secondly by the clamped connection that will transfer the force to the girder. For the last panel on the bridge deck, the braking force will be resisted by the clamped connections only. Therefore, it is imperative to determine the shear capacity of the clamped connection

alone. According to AASHTO LRFD (2005), the braking force is 25% of the axle weights (72 kips) of design truck. With multi presence factor of 1.2 and a load factor of 1.75 the factored braking force becomes 37.8 kips. Total distance between axels of an HS 20 truck is 28 ft, which can accommodate 30 deck panels. These 30 panels will mostly contribute to resist the braking force. Each deck panel rests on three girders and has two clamped connections on each girder. Therefore the required shear force for each clamp becomes $37.8/(30 \times 3 \times 2) = 0.21$ kip. In the test setup, two clamps resist the shear force on each panel therefore shear demand becomes 0.42 kip. Figure 5.6 shows the schematic diagram of the test setup, the failure pattern, and the load-displacement response. Displacement was measured at top of the panel using a linear potentiometer, and the load was measured using a load cell.

The ultimate shear strength of the connection proved to be more than 2.7 times the required strength. The load-displacement curve in Figure 5.6 shows two peaks. The sudden load drop after the first peak represents the failure of the first clamp along with a portion of the deck edge, which was chipped off the deck. After the failure of the first clamp, the entire load was taken by the second clamp, which also failed suddenly at a later stage. In case a clamp of an in-service deck fails due to unexpected loading, it can be easily replaced. However, if the deck edge is also chipped off then the entire panel needs to be replaced. Failure of one clamp on a deck will not be catastrophic, as there will always be other clamps to take the load. A routine inspection of the deck is recommended to check whether all clamps are intact.

5.4.3 Uplift Test for Connectors

This test characterizes the resistance of the clamped connection against uplift wind pressure. Two 12 in. wide decks were placed side-by-side and connected to the girder with four clamps, two on each panel. Load was applied by two hydraulic jacks, one on each side. Deflection was measured at the joint and at the middle of each panel. According to AASHTO LRFD (2005), the required ultimate capacity of each clamp is 0.76 kip. Figure 5.7 shows the test setup, mode of failure, and the load-deflection response. With a peak load of more than four times the required ultimate load, the clamps proved to be adequate for uplift. Failure occurred at the deck edge, while all clamps remained intact. Two solid pieces of deck edge, each of a length equal to that of the clamp were broken off. Failure was sudden, as indicated by the sharp load drop in Figure 5.7.

5.4.4 Lip Test (Tongue and Groove Test)

Strength of the tongue and groove connection is important for the transfer of load from one panel to the other. Failure of the tongue and groove connection may lead to excessive deflection and potential delamination of the wearing surface. Hence, it is imperative to determine the strength of this connection. A 12 in. long piece of deck panel was used along with two 4 ft long panels to perform the test. One string potentiometer was installed under the loading point at the middle of the section to monitor deflection. Figure 5.8 shows the test setup, mode of failure, and the load-deflection response. The 12 in. wide lip failed at 75 kips, which is twice the target load of 37.24 kips. In an actual bridge deck, lip failure is unlikely to occur, because the lip will be present along the

entire length of the panels. The high strength of the lips will ensure the development of panel action to effectively distribute the load in the lateral direction.

5.4.5 Fatigue and Residual Strength Tests

Fatigue is a major design consideration and a typical mode of failure for metal structures under repeated load cycles. Fatigue test of the aluminum deck panels was performed at the FDOT Structures Lab in Tallahassee. Two loading pads were placed at the center of each span at a center-to-center distance of 4 ft, which is more critical than the wheel spacing (6 ft) of an HS 20 truck. Deck panels were subjected to two million cycles of design truck single axel sinusoidal load in the range of 0.5-18 kips at a frequency of 4 Hz. The lower limit of 0.5 kips was set to prevent the pads from walking (Vyas et al. 2009). The test was run continuously for almost six days. Load, displacement, and strain data were recorded after every 1,000 cycles up to 10,000 cycles, and then after every 10,000 cycles up to 2 million cycles. At each interval, eight sinusoidal cycles were continuously recorded for all channels. During and after the test, the deck panels were monitored for cracks in the panels or connections. After the fatigue test, two static tests were performed on the panels to determine their residual strengths. Figures 5.9 and 5.10 show the instrumentation plan, loading configuration, and deflection growth under the fatigue loading. Fatigue loading developed tensile stresses ranging from 0.19 ksi to 2.1 ksi at the most critical location, which is the top fiber at the interior support section. Nominal fatigue resistance calculated based on AASHTO 7.6.1.2.4 was found to be 5.3 ksi, which is greater than the stress range developed in the deck. For the calculation of fatigue resistance it was assumed that the average daily traffic (ADT) is 20,000, only one lane is available for trucks, bridge is located on rural interstate and deck

falls in category A in the detail categories for fatigue (AASHTO Table 7.6.1.2.3-1). These assumptions provide the most conservative value of the fatigue resistance.

The panels showed no sign of cracking or failure after 2 million cycles of fatigue loading. The maximum deflection increased from 0.09 to 0.12 in. (L/508 to L/406). The bolt of the clamp holding the center panel on the interior support failed at about 200,000 cycles, and was replaced with a new one. Installation of the new bolt increased the stiffness of the system, as visible in Figure 5.10. There was only one clamp, instead of two, for each panel on every support because the top flanges of the supporting girders were only 4.5 in. wide and could not accommodate both clamps. Had there been two clamps on each support, as per the manufacturer's recommendation, this failure would not have occurred. All other bolts performed well throughout the fatigue test. Bolted connections have a tendency of loosening over time, and therefore, require routine inspection. Strains at all locations remained within the elastic range throughout the fatigue test. Based on the maximum stress level at all locations, the stress ratio was 0.1, which corresponds to an infinite fatigue life for the deck panels for the tested load range.

Figures 5.11 and 5.12 show the test setup and the load-deflection responses for the two residual strength tests. In the first test, one point load was applied on the lip joint, whereas in the second test the load was applied on the central panel, between the lip joints. The load-deflection responses for both configurations clearly show that deck panels remained within the linear elastic range. In both cases, the deck panels were loaded up to a level of 100 kips, which is nearly three times the target load of 37.24 kips. The maximum deflection reached 0.54 and 0.52 in., respectively, in the first and second tests. The panels and the connections remained intact and did not show any sign of

failure. However, some elastic local buckling was observed in the inclined plates. Deflections and strains in the panels adjacent to the loading panels indicate that the system was able to develop adequate panel action. This is by the virtue of the tongue and groove connection that distributes the loads in the lateral direction.

5.4.6 Coupon Tests

Two coupon tests were performed in a universal testing machine according to ASTM E8-99 to characterize material properties of the deck. Extensometer and strain gauge were used to record the elongation and strain. The middle portion of the plates were $\frac{1}{4}$ in. thick and 1 in. wide. Figure 5.13 shows the test setup, mode of failure, and stress-strain responses. The modulus of elasticity of aluminum was found to be 9,352 ksi, used for the finite element analysis.

5.5 Finite Element Analysis

A three-dimensional finite element (FE) model was developed using the general purpose nonlinear finite element program MSC.Marc 2005. Four-noded quadrilateral thin shell elements were used to model the aluminum plates of the deck section with different thicknesses. Solid elements were used to simulate the neoprene pad and the steel loading plate. Uniform nodal loads were applied on the top surface of steel plate to simulate the wheel load of an HS 20 truck. Modulus of elasticity of the steel plate and neoprene pad were taken as 29,000 ksi and 7.25 ksi, respectively. The material properties of aluminum were derived from the coupon test, as discussed in the previous section. The shell elements near supports were set as elastic to avoid the yielding of the material due to stress concentration.

Load-deflection responses for the simple-span and two-span continuous panels are compared with the experimental responses in Figures 3 and 4. The moment-strain responses are presented in Figure 14. Analytical load-deflection responses for both specimens closely trace the experimental responses, especially in the elastic range. Moment-strain responses also show a close agreement with the experimental results.

5.6 Conclusions

The selected aluminum deck system was subjected to a rigorous series of component, system, and fatigue load tests that demonstrated its feasibility as an alternative to open grid steel decks from both strength and serviceability points of view. Two million cycles of design truck wheel loading on the deck panels did not induce any global or local failure in the deck panels. Failure of a bolted connection during the fatigue testing is attributed to the fact that only half of the manufacturer-specified bolted clamps could be used in the test due to the narrow flanges of the girders. Even though the deck panels were loaded up to 100 kips in the two residual strength tests, the extreme fiber stresses remained well within their elastic range. In addition, the deck-to-girder connections proved adequate for the braking force and the uplift wind pressure, although sudden failure of connections was observed during the shear and uplift tests. The load-deflection and moment-strain responses predicted by the FE analysis showed very good agreement with the experimental results. A full-scale multi-unit FE model is still needed to predict the effective width of the deck and the load distribution among the deck panels.

While the aluminum deck system appears to be a promising system for field implementation in moveable bridges, the following issues still need to be further investigated. First, an evaluation is needed of available wear surfaces, such as Acrydur[®],

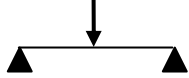

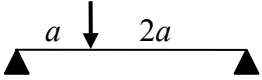
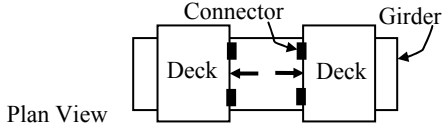
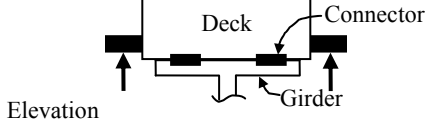
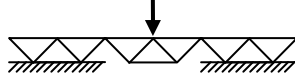

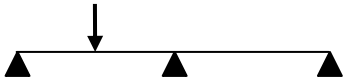
poured mastic asphalt, or ultra high performance concrete. Second, field monitoring of aluminum deck under ambient traffic and designated truck loading needs to be performed.

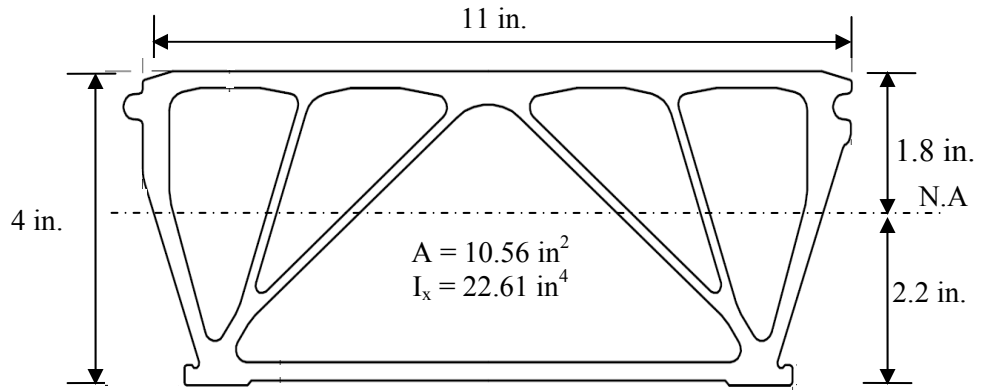
References

- Arrien, P., Bastien, J., and Beaulieu, D., 2001, "Rehabilitation of Bridges Using Aluminum Decks." *Canadian Journal of Civil Engineering*, 28(6), pp. 992-1002.
- AASHTO LRFD Bridge Design Specifications, 2005, American Association of State Highway and Transportation Officials, Washington, D.C.
- ASTM D5484-99, 1999, "Standard Specification for Steel Grid Bridge Flooring." ASTM International, West Conshohocken, PA.
- ASTM E8-99, 1999, "Standard Test Methods for Tension Testing of Metallic Materials." ASTM International, West Conshohocken, PA.
- Das, S.K., and Kaufman, J.G., 2007, "Aluminum Alloys for Bridges and Bridge Decks." The Minerals, Metals and Materials Society, Warrendale, PA, pp. 61-72.
- Dobmeier, J.M., Barton, F.W., Gomez, J.P., Massarelli, P.J., and McKeel, W.T., 2001, "Failure Study of an Aluminum Bridge Deck Panel." *Journal of Performance of Constructed Facilities*, ASCE, 15(2), pp. 68-75.
- Exodermic™, 2008, Brochure for Exodermic™ Bridge Deck Inc., North Baltimore, OH.
- Growdon, J.P., Riegel, R.M., and Tremplin, R.L. (1934). "Heavy Bridge Floor Replaced with Aluminum." *Civil Engineering*, ASCE, 4(3), pp. 113-117.
- Hoglund, T., and Nilsson, L., 2006, "Aluminum in Bridge Decks and in a New Military Bridge in Sweden." *Structural Engineering International*, 16(4), pp. 248-351.
- Mazzolani, F.M., 2006, "Structural Applications of Aluminium in Civil Engineering." *Structural Engineering International*, 16(4), pp. 1-4.
- Mirmiran, A., Saleem, M.A., Mackie, K. and Xia, J., 2009, "Alternatives to Steel Grid Decks." *Final Report*, Florida Department of Transportation, Tallahassee, FL.
- MSC.Marc User's Guide, 2005, MSC.Software Corporation, Los Angeles, CA.
- National Bridge Inventory, 2008, Federal Highway Administration, Washington, D.C.
- SAPA Bridge Decking System, 2008, SAPA Building Systems AB, Vetlanda, Sweden.
- Siwowski, T.W., 2009, "Structural Behavior of Aluminum Bridge Deck Panels." *Engineering Structures*, Elsevier, 31(7), pp. 1349-1353.

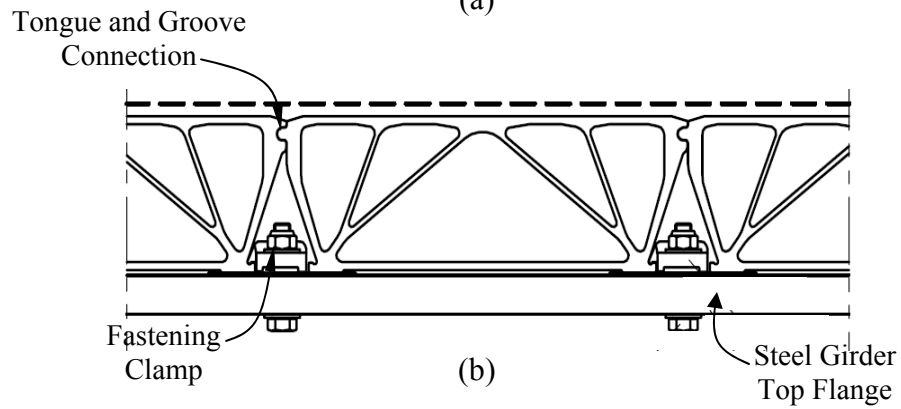
- Siwowski, T., and Zoltowski, P., 2003, "Analytical and Experimental Evaluation of Aluminum Bridge Deck." *Proceeding of European Bridge Engineering Conference*, Rotterdam, Netherlands.
- Soetens, F., and Straalen, V., 2003, "Aluminum Bridges, Aluminum Bridge Decks." *Proceeding of European Bridge Engineering Conference*, Rotterdam, Netherlands.
- Takkasila, M., and Reddy, H., 1996, "Structural Modification of Bascule Bridges for Noise Mitigation." *Final Report*, Florida Department of Transportation, Tallahassee, FL.
- Vyas, J.S., Zhao, L., Ansley, M.H. and Xia, J., 2009, "Characterization of a Low-Profile Fiber-Reinforced Polymer Deck System for Moveable Bridges." *Journal of Bridge Engineering*, ASCE, 14(1), pp. 55-65.
- Wright, W., 1997, "Building the Bridge to the 21st Century with Aluminum?" *Public Roads Magazine*, 60(4), pp. 30-33.

Table 5.1 Test Matrix

Serial No.	Description of Test	Schematics
1	Flexural Tests	
	<ul style="list-style-type: none"> Simple-Span Test 	
	<ul style="list-style-type: none"> Two-Span Continuous Test 	
	<ul style="list-style-type: none"> Simple-Span Inverted Panel Test 	
2	Shear Test for Connectors	 <p>Plan View</p>
3	Uplift Test for Connectors	 <p>Elevation</p>
4	Lip Test (Tongue and Groove Test)	
5	Fatigue and Residual Strength Tests	
	<ul style="list-style-type: none"> Fatigue Test 	
	<ul style="list-style-type: none"> Residual Strength Tests 	

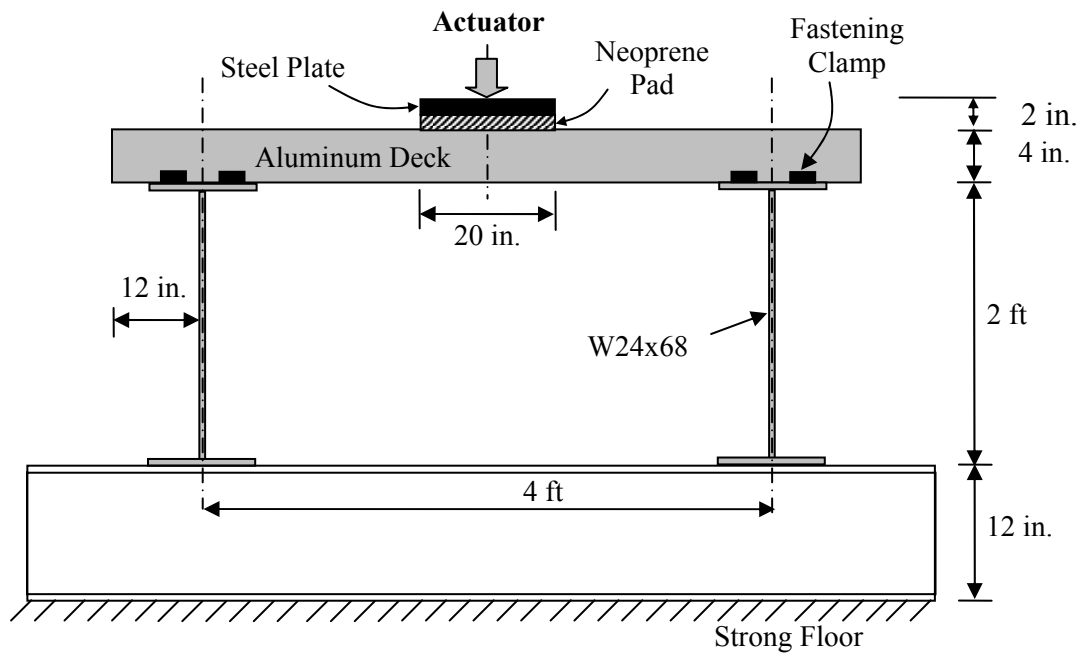


(a)

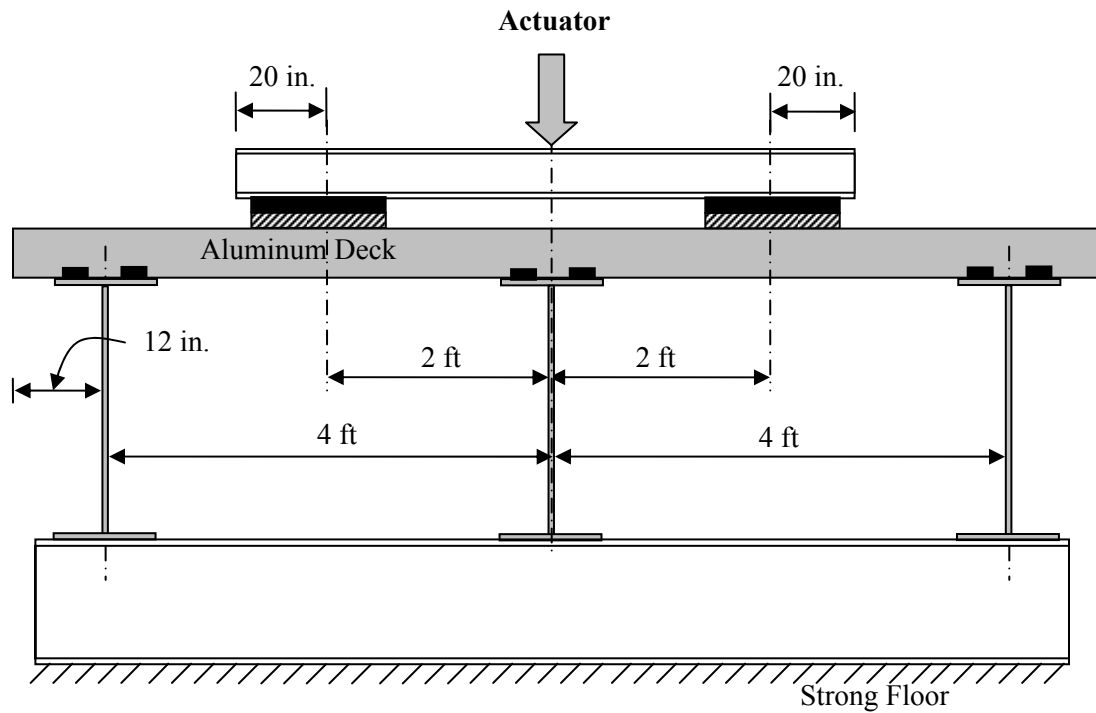


(b)

Figure 5.1 Aluminum Bridge Deck Panel: (a) Unit Cross Section; and (b) Assembled Deck (SAPA Bridge Decking System 2008)



(a)

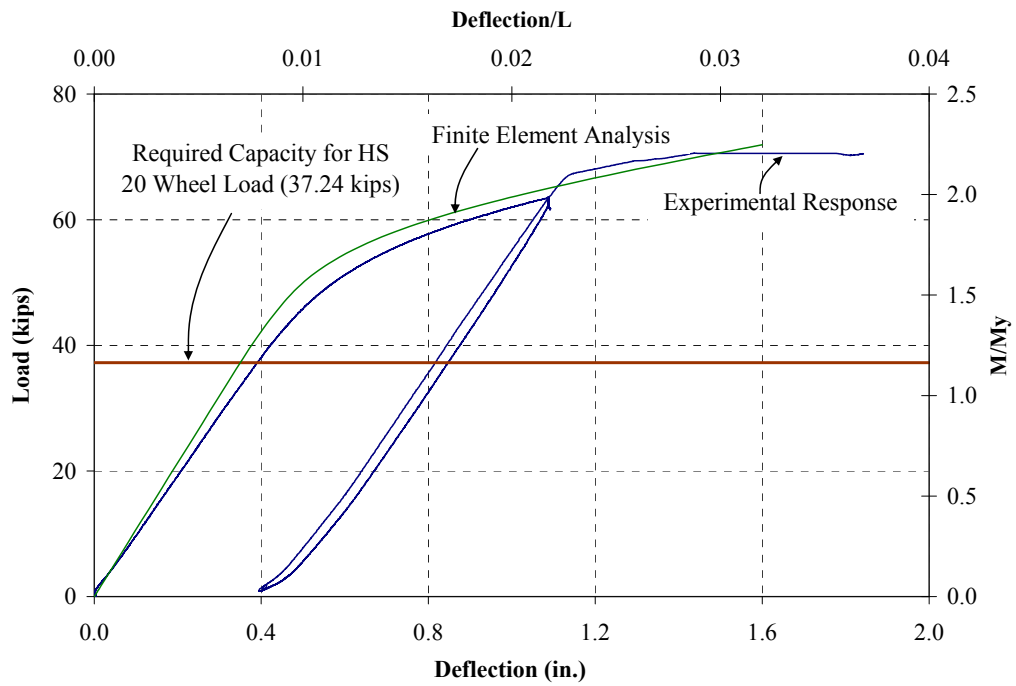


(b)

Figure 5.2 Test Setup for: (a) Simple-Span Panel; and (b) Two-Span Continuous Panel



(a)

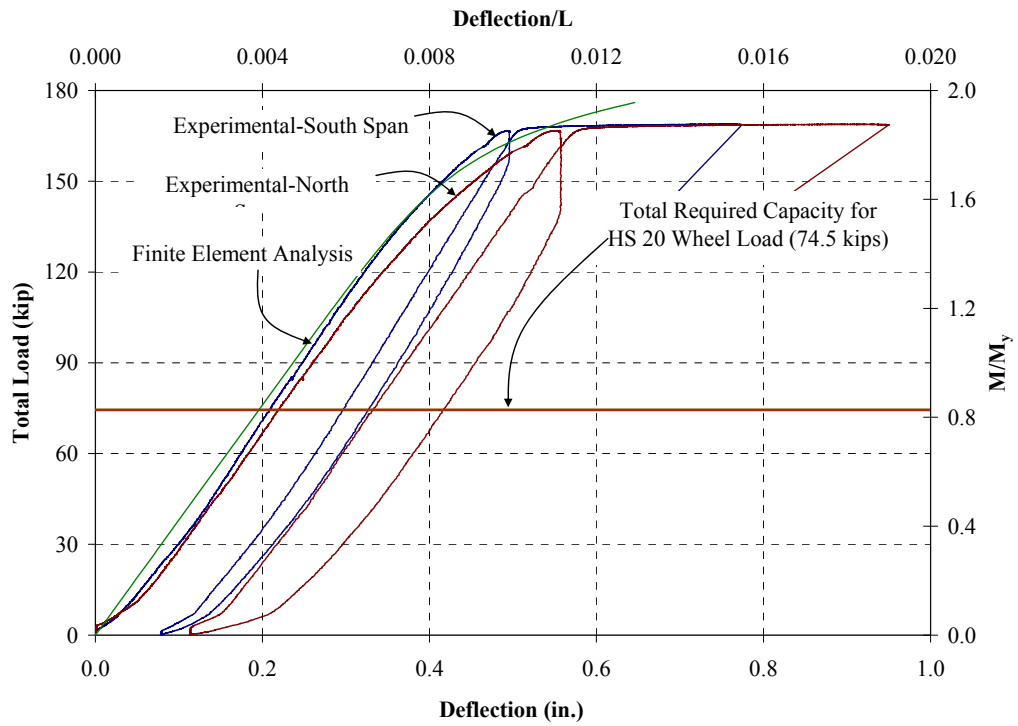


(b)

Figure 5.3 Simple-Span Panel: (a) Deformed shape; and (b) Mid-Span Load-Deflection Response



(a)

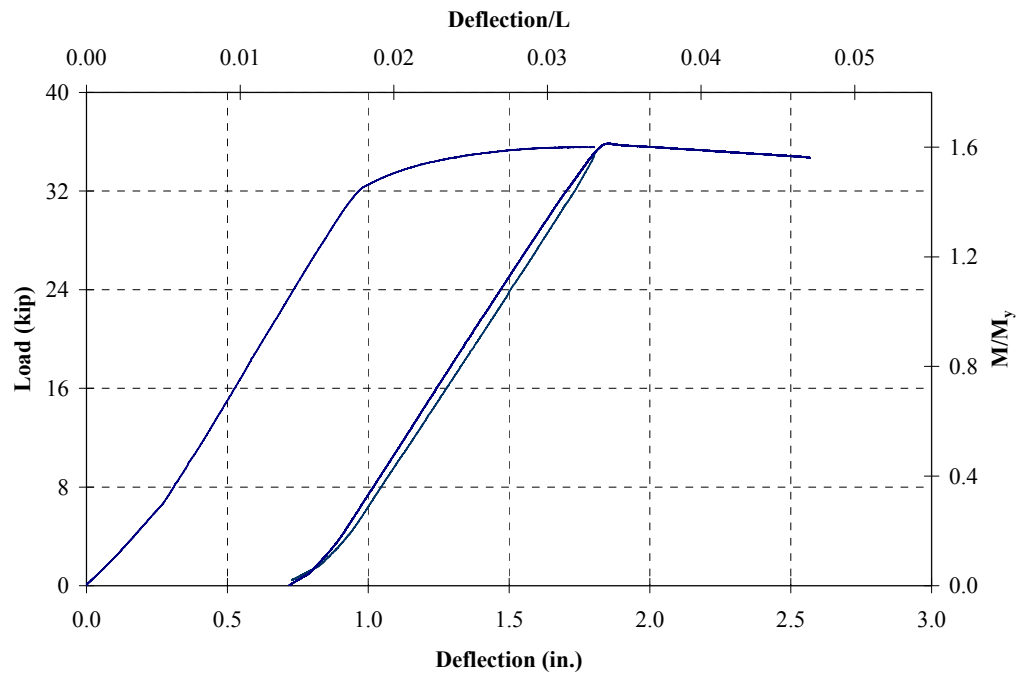


(b)

Figure 5.4 Two-Span Continuous Panel: (a) Deformed Shape; (b) Mid-Span Load-Deflection Response

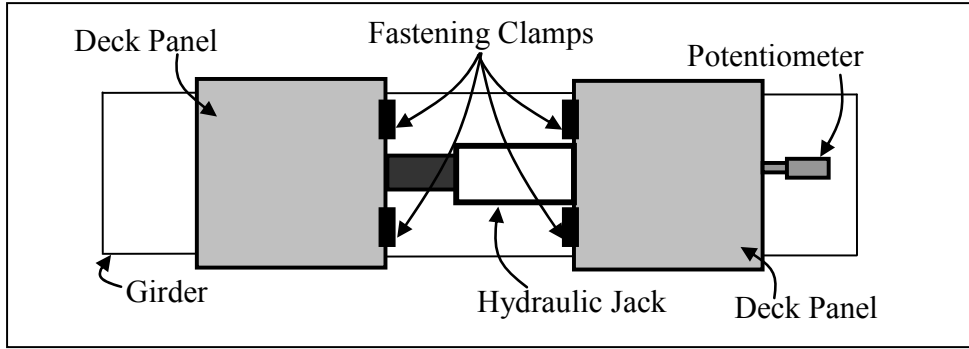


(a)

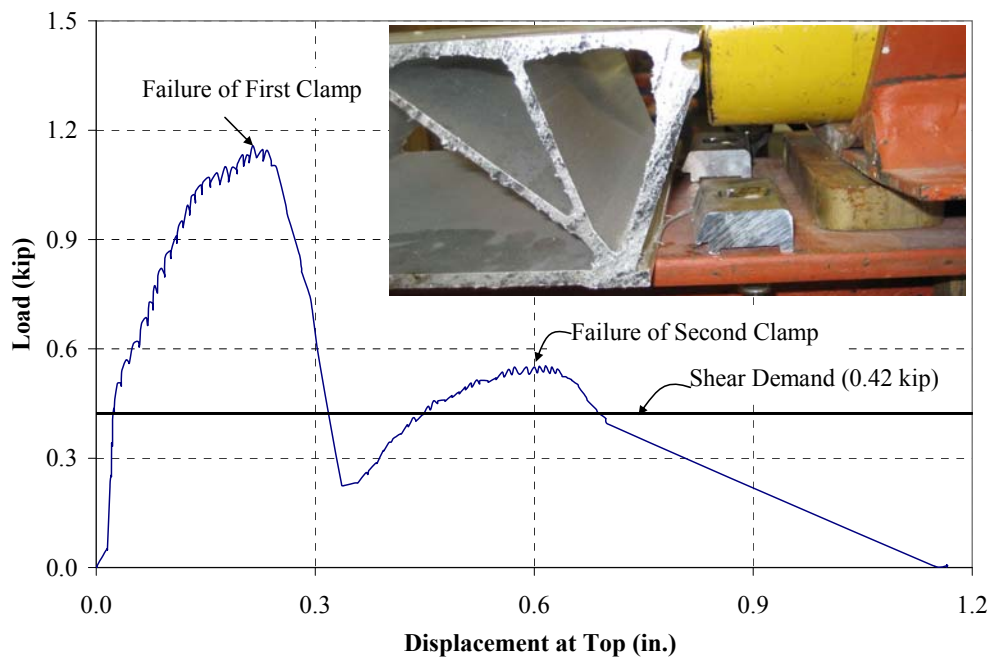


(b)

Figure 5.5 Simple-Span Inverted Panel: (a) Deformed Shape; (b) Mid-Span Load-Deflection Response



(a)



(b)

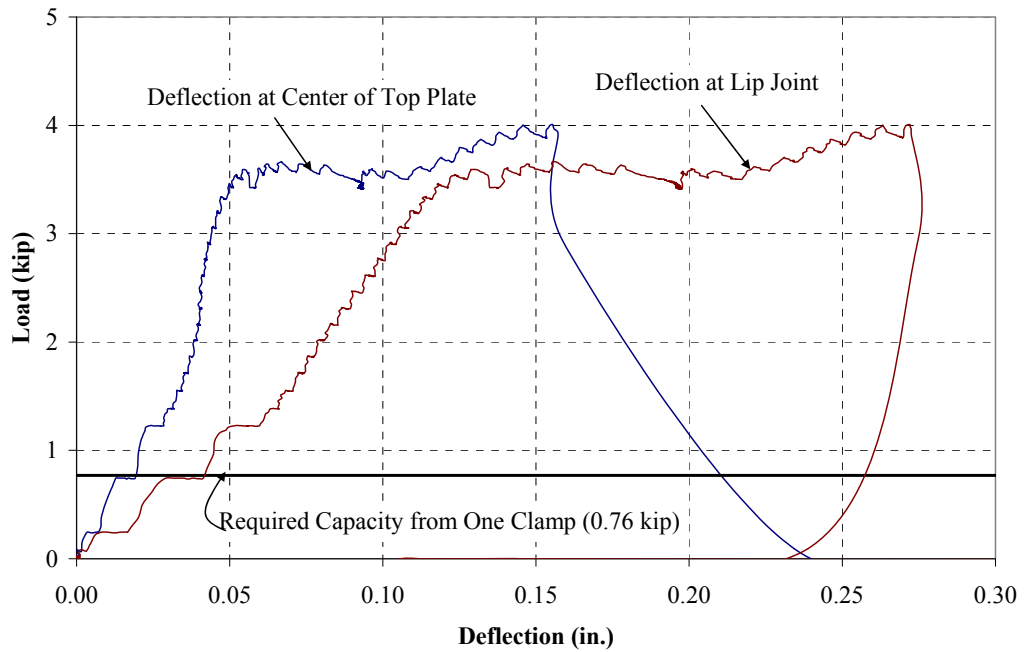
Figure 5.6 Shear Test for Connectors: (a) Test Setup; (b) Load-Displacement Response



(a)

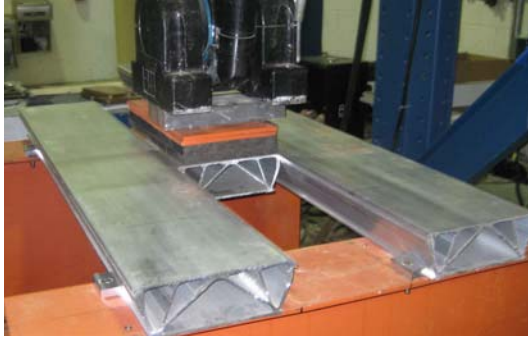


(b)



(c)

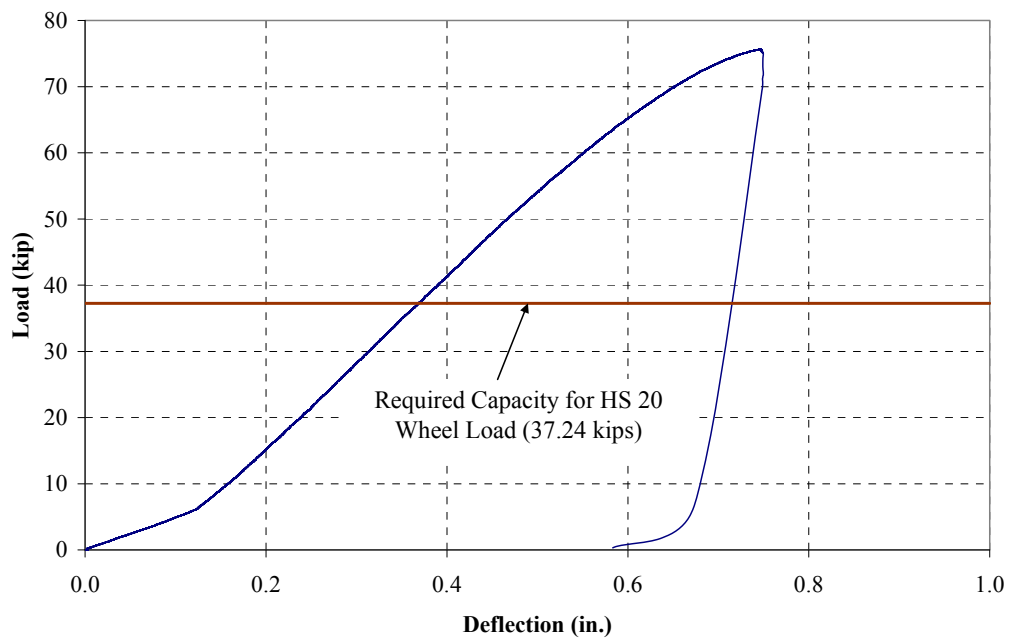
Figure 5.7 Uplift Test for Connectors: (a) Test Setup; (b) Failure Pattern; and (c) Load-Deflection Responses



(a)



(b)



(c)

Figure 5.8 Lip Test: (a) Test Setup; (b) Failure Pattern; and (c) Load-Deflection Response

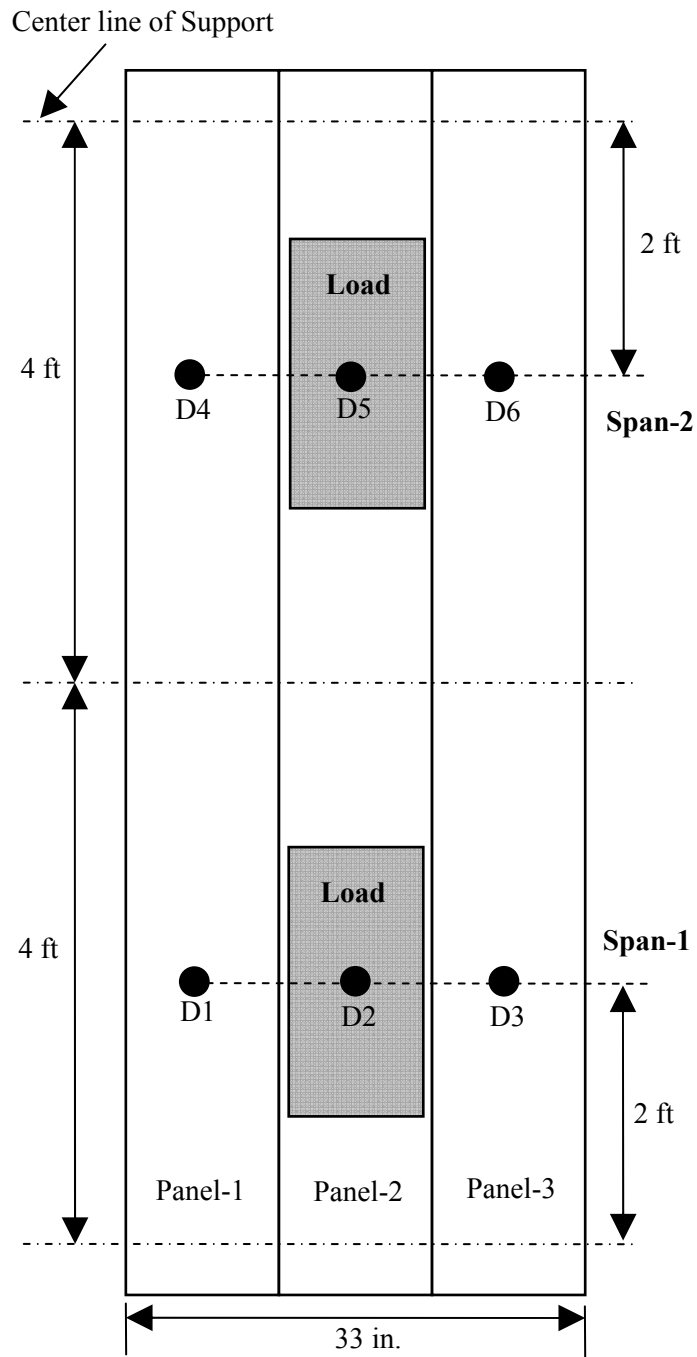
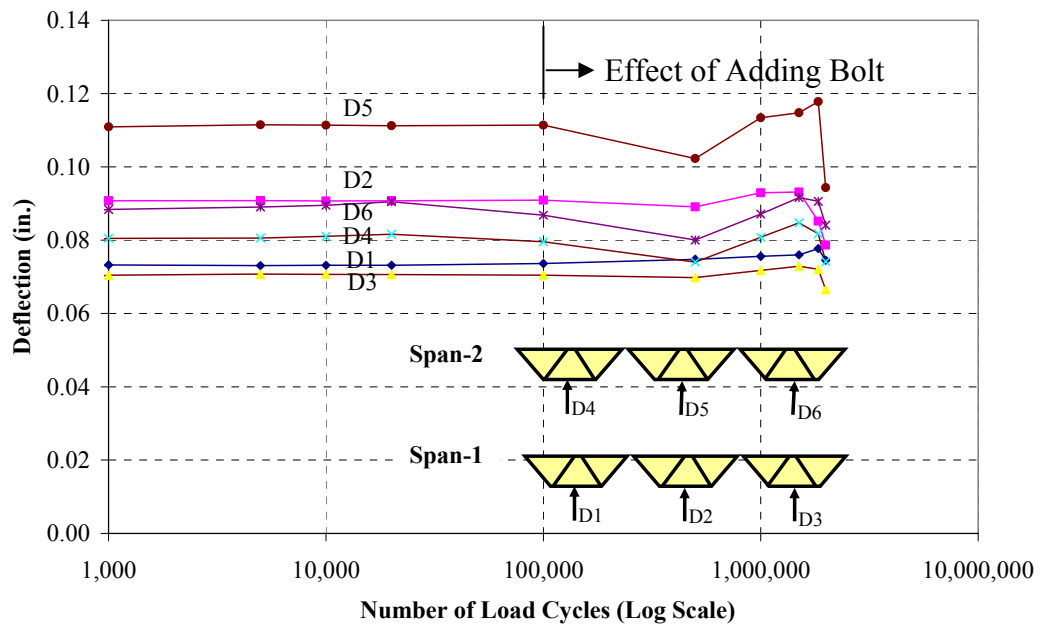


Figure 5.9 Instrumentation Plan and Loading Configuration for the Fatigue Test



(a)

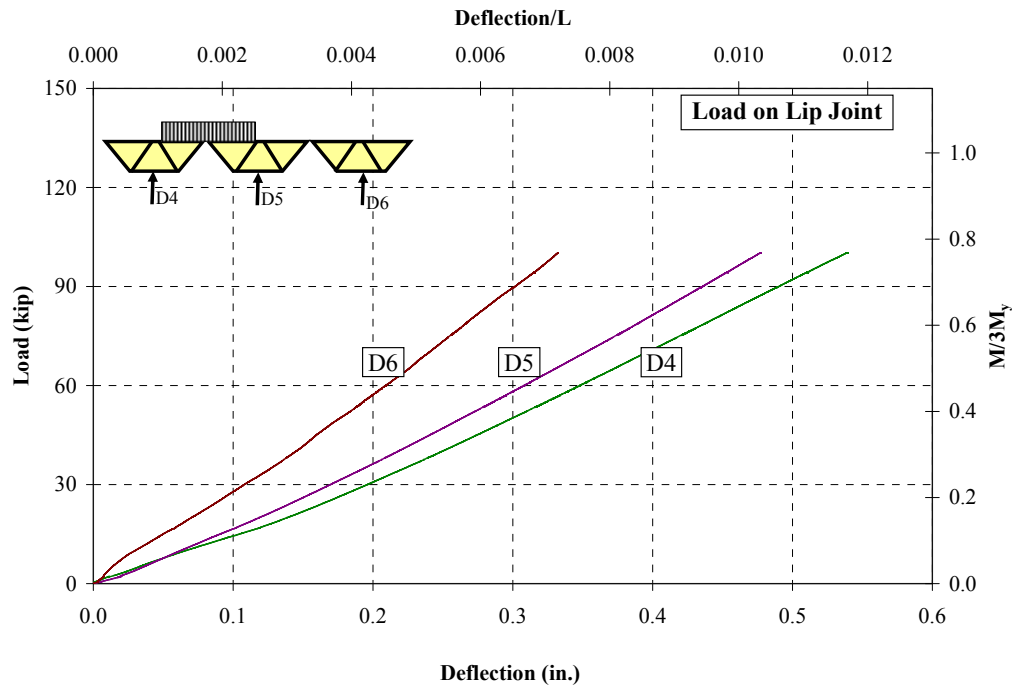


(b)

Figure 5.10 Fatigue Test: (a) Test Setup; and (b) Growth of Maximum Deflection under Fatigue Loading (Performed at FDOT Marcus Ansley Structures Research Laboratory)



(a)

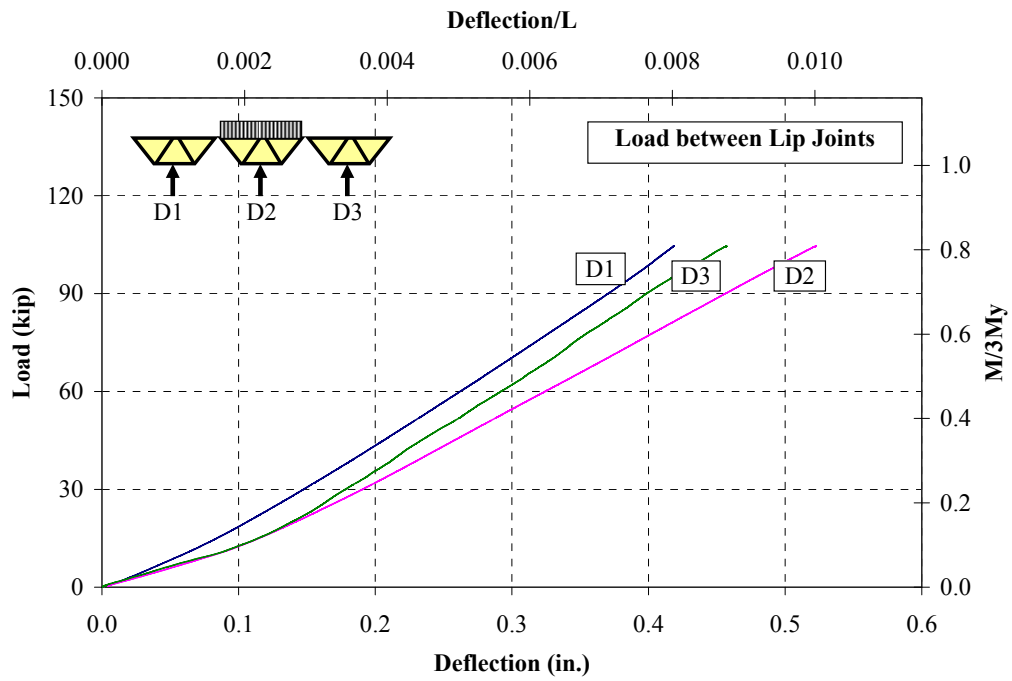


(b)

Figure 5.11 Residual Strength Test on Lip Joint: (a) Test Setup; and (b) Load-Deflection Responses (Performed at FDOT Marcus Ansley Structures Research Laboratory)



(a)

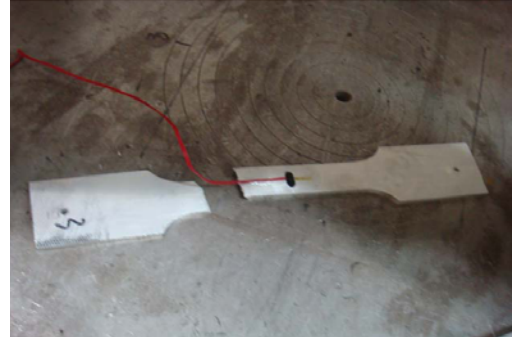


(b)

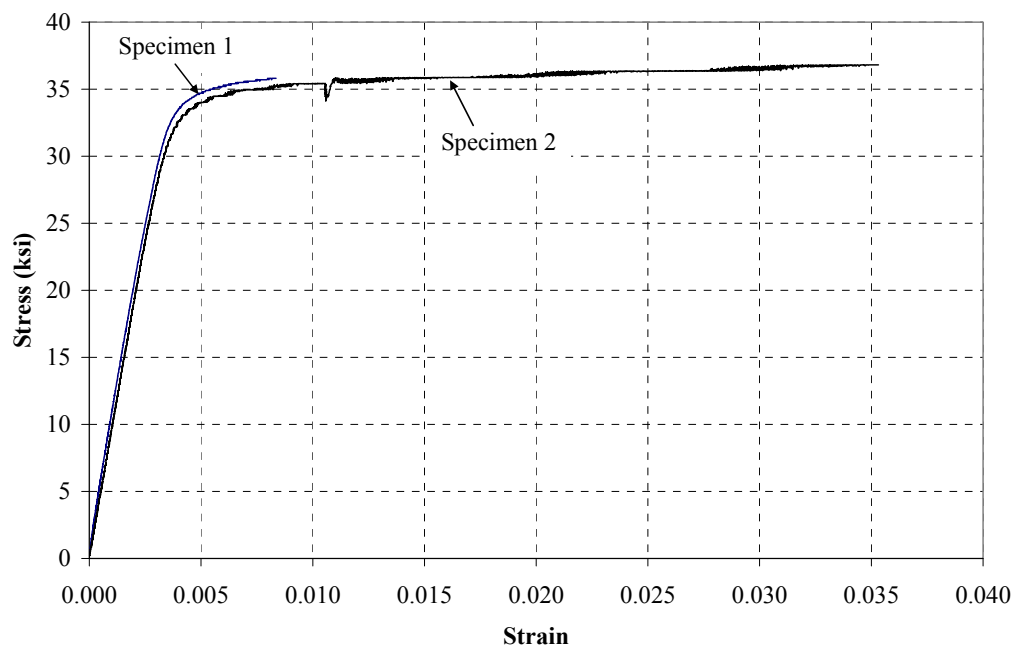
Figure 5.12 Residual Strength Test between Lip Joints: (a) Test Setup; and (b) Load-Deflection Responses (Performed at FDOT Marcus Ansley Structures Research Laboratory)



(a)

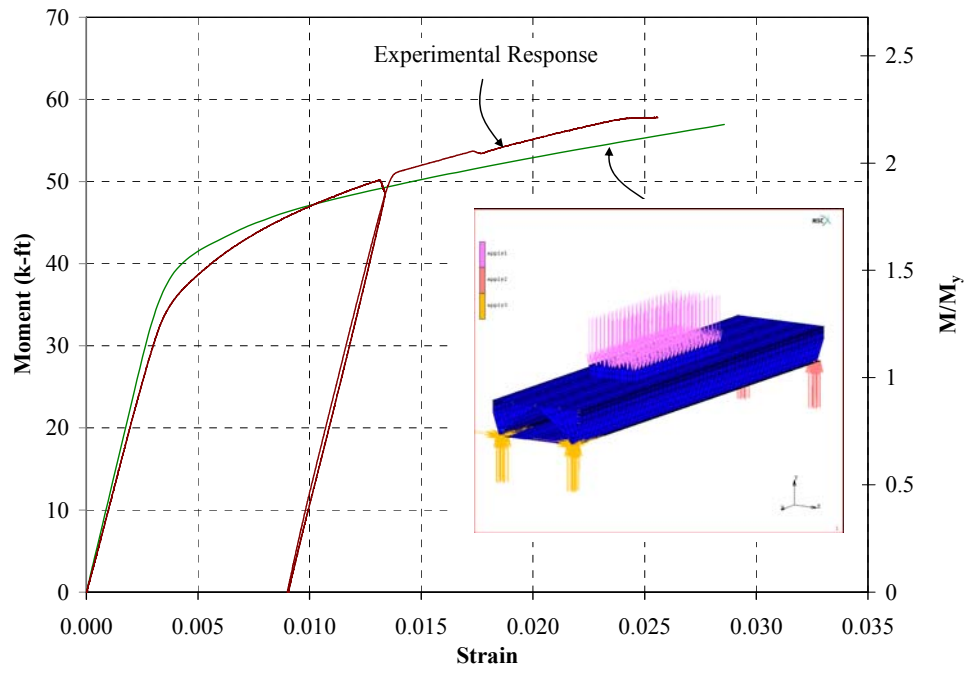


(b)

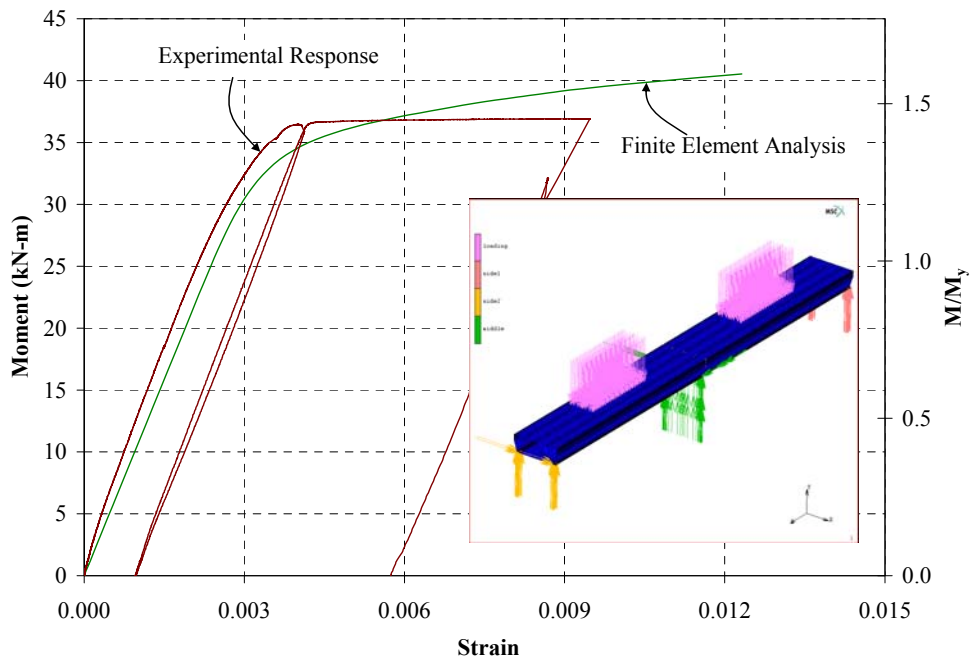


(c)

Figure 5.13 Tension Test: (a) Test Specimen; (b) Ruptured Specimen; (c) Stress-Strain Response



(a)



(b)

Figure 5.14 Comparison of Experimental and Analytical Load-Strain Responses: (a) Simple-Span Panel; and (b) Two-Span Continuous Panel

6. TUBE-BASED COMPOSITE DECK SYSTEM FOR MOVEABLE BRIDGES

Muhammad Azhar Saleem, Amir Mirmiran, Jun Xia, and Kevin Mackie

A Paper Appeared in the Proceedings of Concrete Bridge Conference 2010

Abstract

Open grid steel decks, commonly used on moveable bridges, have several disadvantages, including poor skid resistance, high maintenance costs and high noise levels, and susceptibility to vibration. It is therefore desirable to find alternative deck systems with solid surface. This research is focused on development of a composite deck made of ultra high performance concrete (UHPC) and fiber reinforced polymer (FRP) tubes. It resembles a hollow core slab but without any metallic reinforcement. FRP tubes take the tension, while the UHPC takes the compression and also serves as the wearing surface. This composite deck has an additive benefit of corrosion resistance as both materials used have very good corrosion resistance. A preliminary experimental testing program was undertaken to investigate the strength and serviceability of the deck system. Results from the ultimate load tests are presented in this paper. The findings indicate that the proposed system is a promising alternative to the open grid steel decks from both strength and serviceability standpoints.

Keywords: Ultra-high performance concrete, Bridge decks, FRP, Moveable bridges.

6.1 Introduction

Open grid steel decks are commonly used on moveable bridges throughout the U.S. Self-weight is the governing criterion for the selection of decks for these types of bridges. Open grid decks, being lighter in weight, are a suitable choice for moveable bridges. On average, these decks weigh less than 25 lb/ft²; while some can weigh as little

as 14 lb/ft². These decks, however, have a lower skid resistance, are costly to maintain, and produce high noise levels. Open grid decks polish over time, which further deteriorates their skid resistance, thus increasing the chances of accidents. To address these issues of safety and environmental quality, research is needed to develop alternative deck systems with a solid riding surface.

This paper presents the preliminary experimental work to develop an ultra high performance concrete (UHPC)-fiber reinforced polymer (FRP) tubes deck system, which represents an entirely new concept. Prestressed hollow core slabs made of regular concrete are commonly used in building structures but rarely as bridge decks. Researchers have worked on all-FRP bridge decks and concrete-filled FRP tubes, but none has combined UHPC and FRP tubes for a bridge deck. The idea behind combining UHPC with FRP tubes is to enhance the flexural capacity of UHPC. FRP tubes serve as tensile reinforcement both in the positive and negative moment regions, and help reduce the self-weight of the deck. Figure 6.1 shows the stress-strain behavior of glass FRP. Also shown in the figure, are the geometric properties of the FRP tube.

6.2 Literature Review

FRP composite materials have shown great potential as alternative construction materials, especially in the field of repair and rehabilitation of existing bridges, and to some extent in new bridge construction (Ehlen 1999). The acceptance of FRP composites in bridge industry is mainly due to their superior properties, such as high strength, long-term durability, and good corrosion and fatigue resistance (Zhang et al. 2006). Moreover, FRPs are well suited for mass production of structural shapes because of their light weight, which allows rapid installation of FRP modular decks on bridges (Plunkett 1997).

An FRP bridge deck weighs approximately 80% less than a concrete deck (Mu et al. 2006). The lightweight FRP deck could be especially beneficial for movable bridges, in which spans have to be lifted for the passage of vessels.

In the past decade there have been numerous examples of new bridges using FRP decks, or old bridge decks replaced by new FRP decks. For example, replacement of an existing conventional concrete deck on a 60-year old Warren steel truss bridge, which was funded by New York DOT (Jerome et al. 2000). Currently, a total of nine states DOTs including Delaware, Illinois, Kansas, Maryland, New York, North Carolina, Ohio, Oregon and Pennsylvania are using FRP bridge deck panels. In Oregon, FRP bridge deck panels have been used to replace an existing timber deck on a moveable bridge (Hong and Hastak 2006). Florida is also in the midst of installing an FRP bridge deck. Several researchers including Robinson and Kosmatka (2008), Alagusundaramoorthy et al. (2006), Prachasaree et al. (2006), Stiller et al. (2006), Aluri et al. (2005), and Hutcheson and Sheppard (2003) have conducted laboratory experiments on decks with different FRPs and connection types to characterize their static and dynamic behavior.

6.3 Preliminary Design

Based on the self-weight limit of 25 lb/ft², two design schemes were proposed, one with a uniform cross section and other with a tapered section. Figure 6.2 shows the schematics of the two design configurations. The first design has the entire tube section embedded in a 3½ in. thick UHPC section. The estimated self-weight would be 26.8 lb/ft². For the second design configuration, concrete on the tension face was considered ineffective and therefore, was removed from the section. The resulting shape was tapered along the span yielding a self-weight of 25.8 lb/ft². The section design was based on

moment-curvature analysis of the first design configuration. The minimum thickness of UHPC portion was designed as 1 in. to prevent punching shear failure, based on previous results in the literature (Harris and Roberts 2005). The UHPC material model used in the design is shown in Figure 6.3 (Graybeal 2006). According to the AASHTO LRFD Highway Bridge Design Specifications (2005) the service wheel load for an HS 20 truck is 16 kips and the required ultimate load including the impact becomes 37.24 kips.

Assuming perfect bond between UHPC and FRP tubes, the moment-curvature analysis of a 4 in. wide uniform deck section was performed. The assumption of perfect bond was used to estimate the upper bound capacity of the system. However, as will be discussed later in this paper, the experiments confirmed slippage between UHPC and FRP. The section loses its moment capacity when UHPC reaches its compressive strength or the FRP tube ruptures in tension.

6.4 Experimental Work

A preliminary experimental work was carried out to characterize the behavior of UHPC-FRP tube hollow core deck. Both specimens were prepared in one casting. Compressive strength of UHPC was 27 ksi which is based on the testing of three cylinders. No heat treatment was used because the required temperature (194 °F) could not be achieved in the lab. Both deck panels were subjected to a single load at the mid-span. Load was applied on an AASHTO prescribed footprint of an HS 20 truck dual tire wheel (20 in. x 10 in.). Displacement control procedure was adopted with a displacement rate of 0.015 in./min. Surface-mounted strain gauges and string potentiometers were installed at strategic locations to gather strain and deflection data along with loading data from the actuator.

6.4.1 Uniform Section Deck Specimen

Figures 6.4 to 6.6 show the instrumentation plan, test setup and failure pattern of the uniform section UHPC-FRP deck specimen. Originally, the design depth of the section was 3½ in. However, due to floating of the tubes at the time of casting, this height could not be maintained. With some extra cover at top and bottom, the actual depth of the section turned out to be 4¼ in. Increased depth affected the ultimate load as well as the self-weight. Figures 6.7 and 6.8 show the load-deflection and load-strain responses, respectively. Also shown in Figure 6.7 is the slippage of the center tube with respect to the UHPC section. The first flexural crack appeared at 10.3 kips at the mid-span. Two more flexural cracks appeared at the later stage, and kept on growing until failure. In addition to three major cracks, several small flexural cracks were also observed. The specimen failed at 37 kips. The three FRP tubes failed suddenly in compression one after the other. Figure 6.7 shows that there was no slippage in the tubes up to a load of 20 kips, after which the tubes started slipping inwards because of the opening of flexural cracks at the mid-span. Figure 6.8 shows that the compressive strain of concrete was well above its crushing strain of 0.0035.

6.4.2 Tapered Section Deck Specimen

Figures 6.9 to 6.14 show the instrumentation plan, test setup and failure pattern of the tapered section deck specimen. The deck failed suddenly in compression at 27 kips. Figures 6.15 to 6.18 show the load-deflection and load-strain responses. The failure initiated on the compression side of concrete, and then cracks penetrated into FRP tubes leading to a sudden compression burst failure. At 4 kips, the bond between UHPC and tubes at the mid-span failed, leading to the loss of composite action at mid-span, and

subsequently degradation of the global stiffness and abrupt changes in caused the slopes of S1, S2, S3 curves (Figure 6.16). This debonding progressed to the end of the beam, with gradual changes of the slopes of S4 and S6 curves (Figure 6.16), as compared to those of S1, S2 and S3. The slippage at the end took place at around 12 kips, as shown in Figure 6.15. The compressive stress between the UHPC and the tube at the end support helped increase the bond strength. It is believed that a considerable amount of load was transferred through the interface at the end support even after the tube began to slip. Figure 6.16 shows that the tension fibers of FRP tubes remained intact up to failure. The maximum tensile strain in FRP tubes at mid-span (Figure 6.16) reached 0.032, which is 2.8 times the ultimate strain provided by the manufacturer. However, the tubes did not show any sign of tensile fracture. The maximum compressive strain in concrete at mid-span reached 0.0052, clearly indicating the crushing of concrete, which was also observed during the test.

6.5 Conclusions

The preliminary experimental work on UHPC-FRP tubes deck specimens has led to the following conclusions:

1. The system has shown good promise to replace the conventional open steel grid decks. Based on the ultimate loads of the two simple-span specimens, it can be inferred that the multi-unit system would achieve the target load.
2. Both specimens failed suddenly in compression. However, the uniform section deck specimen had significant tensile cracks, as opposed to the tapered section deck that showed no tensile fracture.

3. Greater composite behavior between UHPC and FRP tubes was observed for the uniform section deck specimen, mainly because the FRP tubes were fully encased in UHPC throughout the span length.

Since the system has shown significant promise, the experimental work should be expanded to multi-unit multi-span specimens. The connections between adjacent deck panels and as well with girders should be designed and tested. Moreover, fatigue behavior of the deck needs to be evaluated.

References

- Ehlen, M.A., 1999, "Life-Cycle Costs of Fiber-Reinforced-Polymer Bridge Decks." *Journal of Materials in Civil Engineering*, ASCE, Volume 11, Issue 3, pp. 224-230.
- Zhang, Y., Cai, C.S., Shi, X., and Wang, C., 2006, "Vehicle-Induced Dynamic Performance of FRP versus Concrete Slab Bridge." *Journal of Bridge Engineering*, ASCE, Volume 11, Issue 4, pp. 410-418.
- Plunkett, J.D., 1997, "Fiber-Reinforced Polymer Honeycomb Short Span Bridges for Rapid Installation." *IDEA Project Final Report*, Transportation Research Board, Washington, D.C.
- Mu, B., Wu, H., Yan, A., Warnemuende, K., Fu, G., Gibson, R.F., and Kim, D., 2006 "FEA of Complex Bridge System with FRP Composite Deck." *Journal of Composite for Construction*, ASCE, Volume 10, Issue 1, pp. 79-86.
- Jerome, S., Connor, O., Hoyos, H., Yannotti, A., and Wagh, V., 2000, "Installing an FRP Deck on a Truss Bridge." *Proceedings of the 17th Annual Meeting*, International Bridge Conference, Pittsburgh, PA.
- Hong, T., and Hastak, M., 2006, "Construction, Inspection, and Maintenance of FRP Deck Panels." *Journal of Composites for Construction*, ASCE, Volume 10, Issue 6, pp. 561-572.
- Robinson, M.J., Koamatka, J.B., 2008, "Light-Weight Fiber-Reinforced Polymer Composite Deck Panels for Extreme Applications." *Journal of Composites for Construction*, ASCE, Volume 12, Issue 3, pp. 344-354.
- Alagusundaramoorthy, P., Harik, I., and Choo, C., 2006, "Structural Behavior of FRP Composite Bridge Deck Panels." *Journal of Bridge Engineering*, ASCE, Volume 11, Issue 4, pp. 384-393.
- Prachasaree, W., GangaRao, H.V.S., and Shekar, V., 2006, "Performance Evaluation of FRP Bridge Deck Component under Torsion." *Journal of Bridge Engineering*, ASCE, Volume 11, Issue 4, pp. 430-442.
- Stiller, W.B., Gergely, J., and Rochelle, R., 2006, "Testing, Analysis, and Evaluation of a GFRP Deck on Steel Girders." *Journal of Bridge Engineering*, ASCE, Volume 11, Issue 4, pp. 394-400.
- Aluri, S., Jinka, C., and GangaRao, H.V.S., 2005, "Dynamic Response of Three Fiber Reinforced Polymer Composite Bridge." *Journal of Bridge Engineering*, ASCE, Volume 11, Issue 6, pp. 722-730.

- Hutcheson, D., and Sheppard, M., 2003, "Sandwich Panel Performance Optimizing with 3D Fiber Reinforcing Core Architecture." *SAMPE Journal*, Volume 39, Issue 6, pp. 68-75.
- Harris, D.K., and Roberts, C.L., 2005, "Characterization of the Punching Shear Capacity of Thin Ultra-High Performance Concrete Slabs." Virginia Transportation Research Council, Charlottesville, VA.
- Graybeal, B. A., 2006, "Structural Behavior of Ultra-High Performance Concrete Prestressed I-Girders," *Final Report*, Federal Highway Administration, McLean, VA
- AASHTO LRFD Bridge Design Specifications, 2005 Interim Revisions, American Association of State Highway and Transportation Officials, Washington, D.C.
- AASHTO LRFD Moveable Highway Bridge Design Specifications, 2008 Interim Revisions, American Association of State Highway and Transportation Officials, Washington, D.C.
- ASTM C39, 2003, "Standard Specification for Flow Table for Use in Tests of Hydraulic Cement." ASTM International, West Conshohocken, PA.
- Ductal[®] Mechanical Performances, "http://www.ductal-lafarge.com/lafarge_DUCTAL/PUBLICATION/20041228/Perf_meca_annex_uk.pdf." Lafarge North America, Canada.
- EXTREN Properties Guide, "<http://www.strongwell.com/PDFfiles/Extren /EXTREN %20 Properties.pdf>." Strongwell Corporation, Bristol, VA.

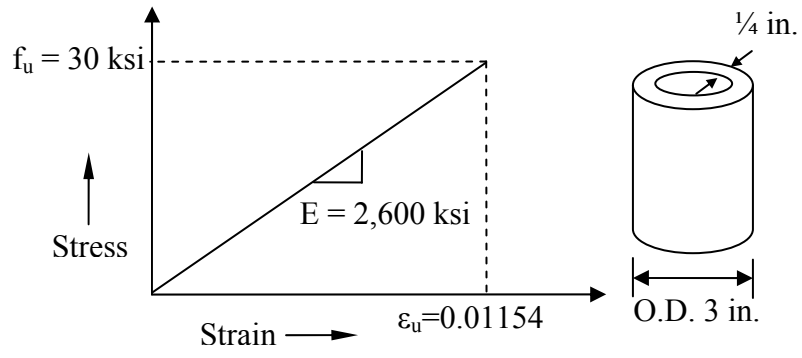


Figure 6.1 Stress-Strain Response of Glass FRP Tubes

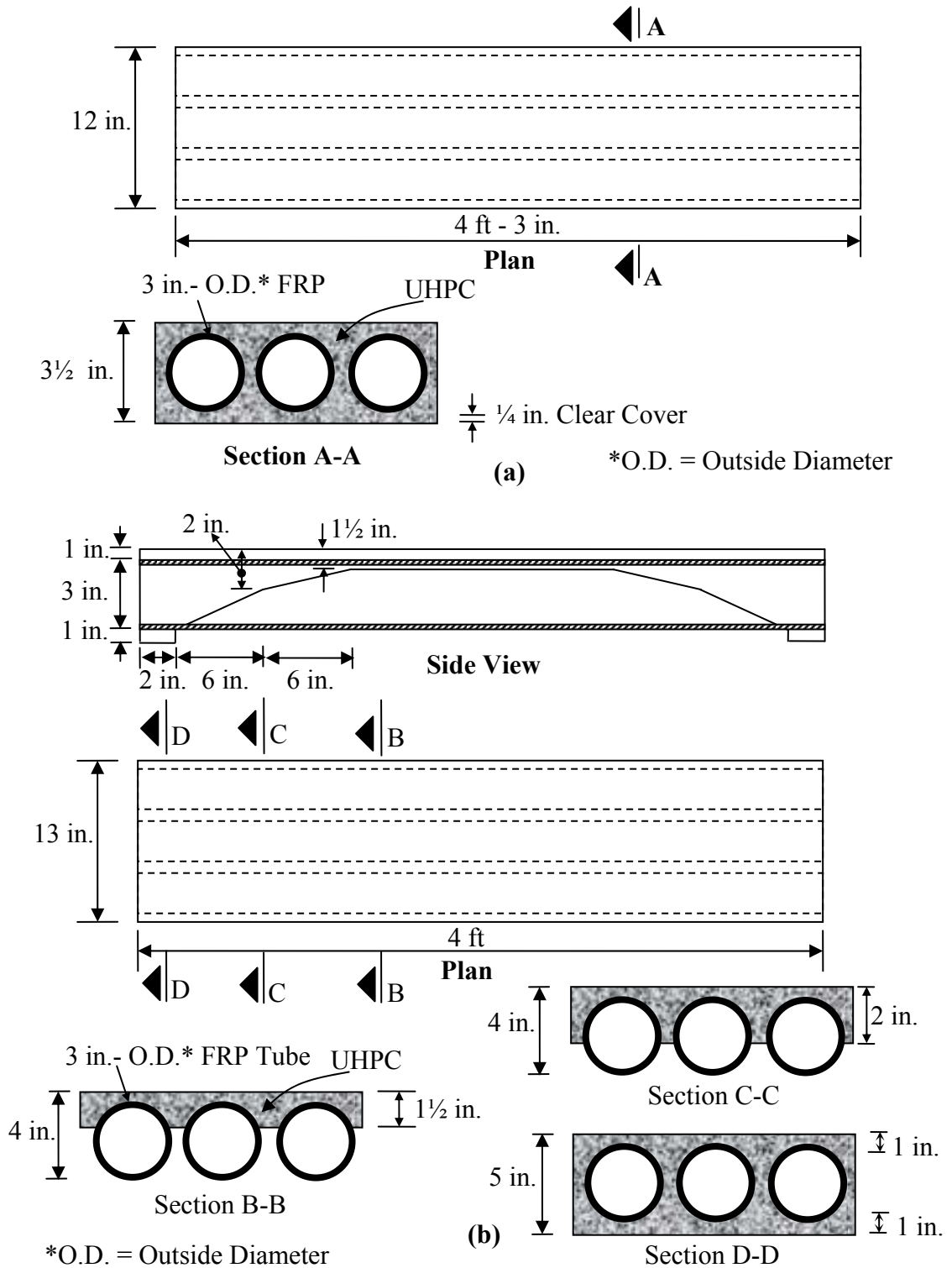


Figure 6.2 Geometry of Deck Sections: (a) Uniform Section, and (b) Tapered Section

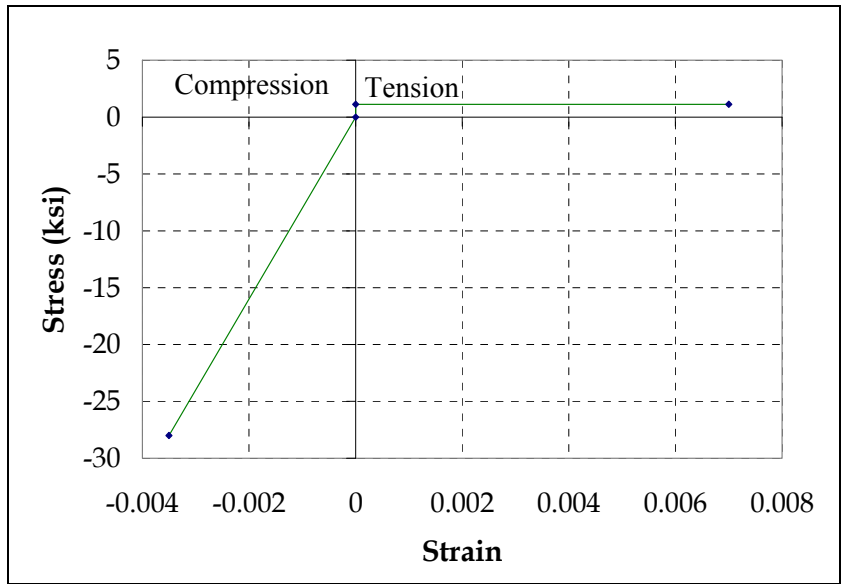


Figure 6.3 Stress-Strain Relationship for UHPC

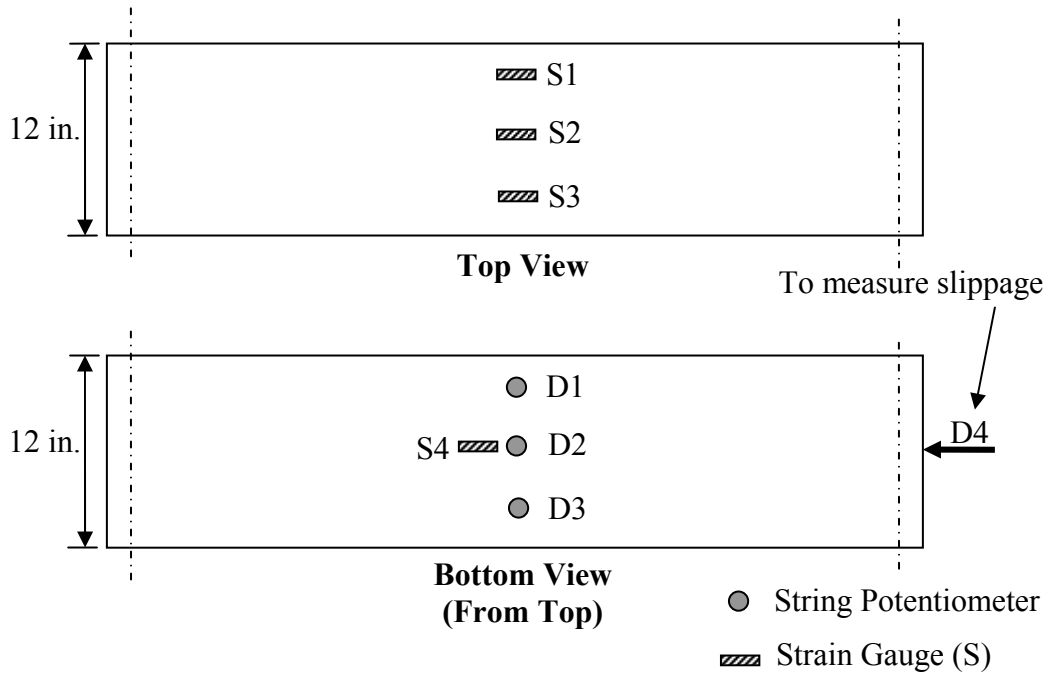


Figure 6.4 Instrumentation Plan for the Uniform Section UHPC-FRP Deck Specimen



Figure. 6.5 Test Setup for the Uniform Section UHPC-FRP Deck Specimen



Figure 6.6 Flexural Cracks near Ultimate Load

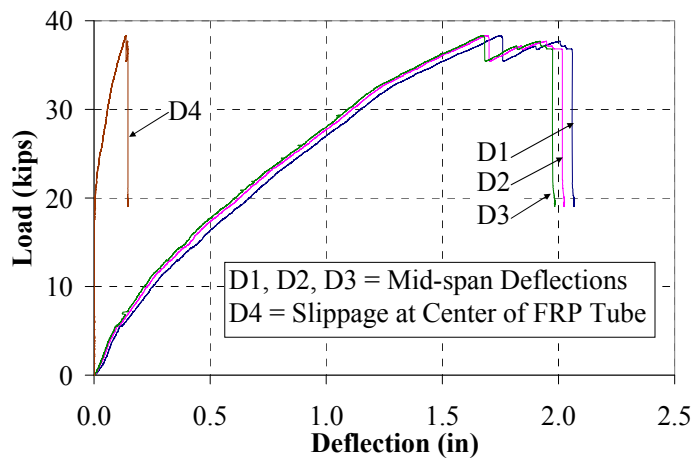


Figure 6.7 Load-Deflection and Load-Slippage Responses

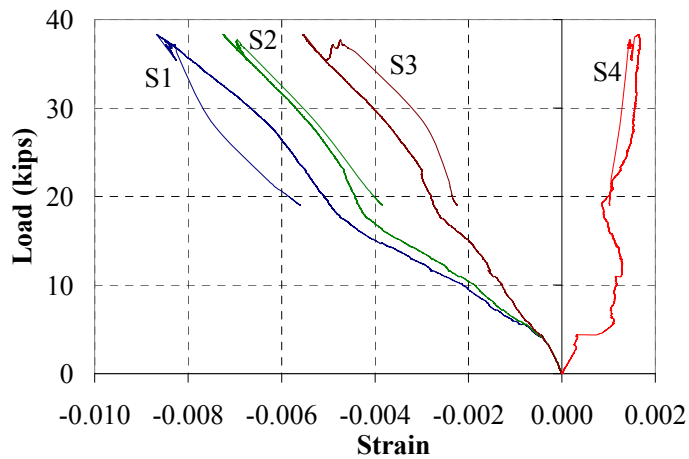


Figure 6.8 Load-Strain Responses

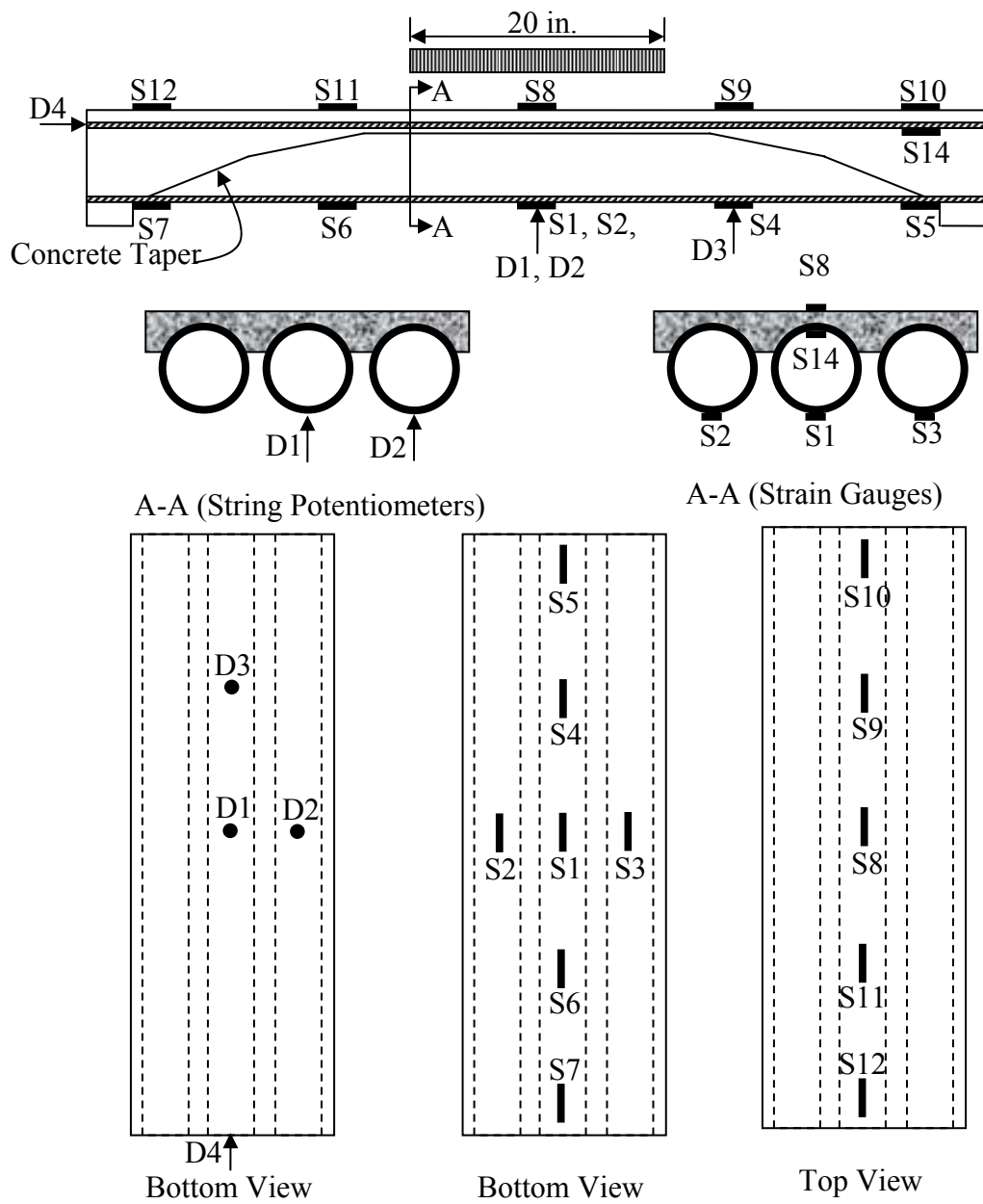


Figure 6.9 Instrumentation Plan for the Tapered Section UHPC-FRP Deck Specimen

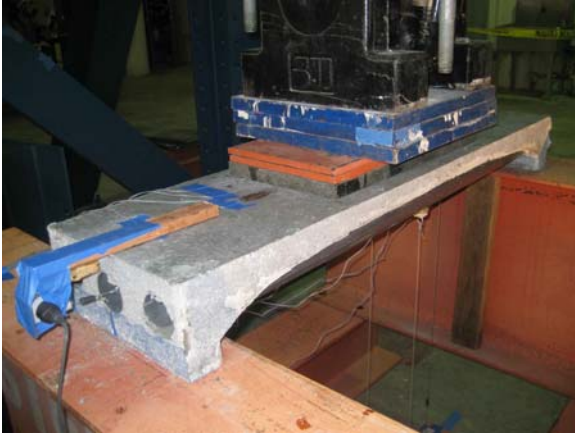


Figure 6.10 Test Setup for the Tapered Section UHPC-FRP Deck Specimen



Figure 6.11 Failure Pattern



Figure 6.12 Compression Failure



Figure 6.13 Un-cracked Tension Face

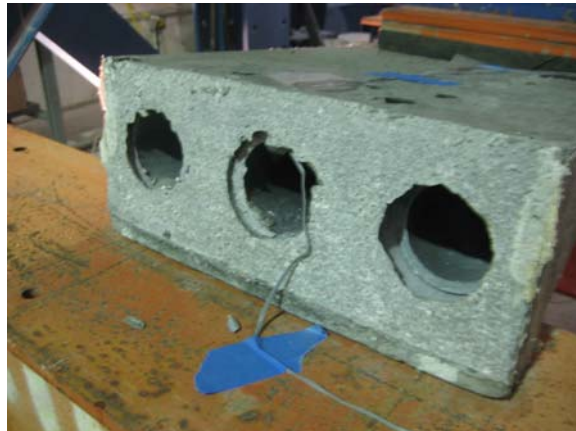


Figure 6.14 Slippage of FRP Tubes

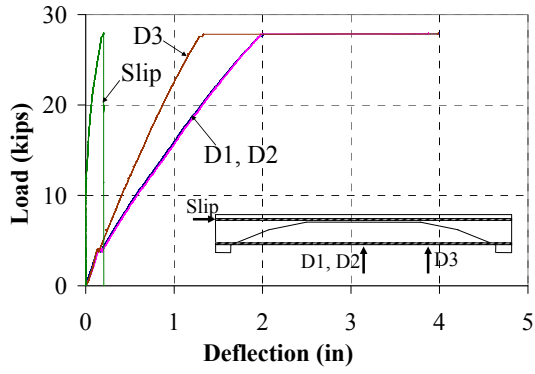


Figure 6.15 Load-Deflection and Load-Slippage Responses

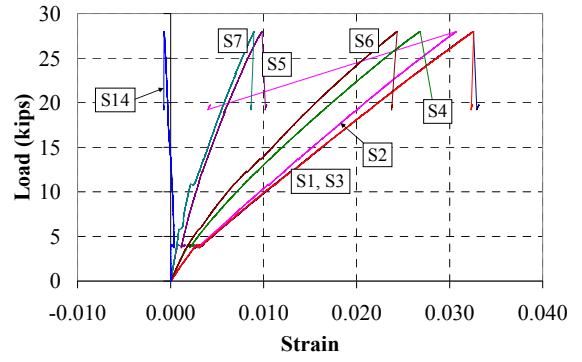


Figure 6.16 Load-Strain Responses

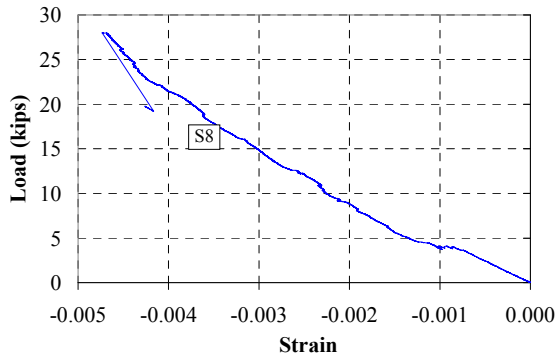


Figure 6.17 Load-Strain Response

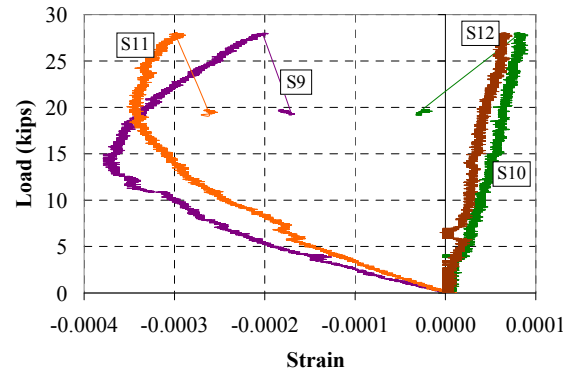


Figure 6.18 Load-Strain Responses

7. SUMMARY AND CONCLUSIONS

The major objective of this research was to develop alternative bridge deck systems to open grid steel deck. The alternative deck systems should address the rideability and environmental concerns, while meeting the strict self-weight limit of 25 lb/ft². The three systems considered in this study included UHPC deck, aluminum deck, and UHPC-FRP tube deck. Detailed studies of the three systems have led to the conclusions and recommendations, as summarized in the following sections.

7.1 UHPC Bridge Deck

The proposed deck system was developed using UHPC and HSS. It is composed of longitudinal and transverse ribs. Longitudinal ribs span between the girders and act as primary load-carrying members, whereas the smaller transverse ribs run parallel to the direction of traffic and connect the longitudinal ribs. Detailed experimental and analytical work on the UHPC bridge deck system led to the following conclusions:

1. The system is a viable alternative to the open grid steel decks and is ready for implementation. Deck panels and connections successfully endured two million cycles of fatigue loading and had a residual strength of at least 47% higher than the target load.
2. Inadequacy of load transfer across the tongue and groove connection during the initial static loading before the fatigue test demonstrated the need for epoxy grouting of the tongue and groove joint.
3. The dominant mode of failure in most flexural specimens was shear, except for the first two simple-span specimens which suffered from shear-bond failure.

4. Use of standard 180° hooks at both ends of flexural reinforcement helped effectively avoid bond failure.
5. Shear reinforcement and reduced flexural steel did not change the failure mode from shear to flexure. The specimen with shear reinforcement, however, exhibited higher stiffness and a more distributed crack pattern than its counterparts.
6. Deck-to-girder and deck-to-deck connections proved to be more than adequate for the loading conditions expected from and HS 20 truck and wind forces.
7. When the load is applied directly on a rib most of it would be taken by that rib and the ribs immediately next to it on either side. The rib under the load, on average, takes 34% of the total load. With the increase in the applied load, the rib under the loading pad attracts more load, which ultimately leads to punching failure.
8. Development lengths for #3 and #7 HSS rebars embedded in UHPC were found as $12d_b$ and $18d_b$ respectively. These values should be considered as an estimate and may require further verification.
9. Development lengths calculated based on the equations provided by the ACI-408R-03 reasonably agree with the values suggested by the present study. On the other hand, ACI 318-08 greatly overestimates the development length for HSS rebars embedded in UHPC.
10. Pullout tests provide reasonable results for smaller rebars but not for the large rebar sizes, especially when the concrete cover is small. Beams tests are recommended for such cases. However, the configurations of specimens, test

setup and method of loading should be carefully selected to avoid premature failure.

11. The FE model showed reasonable agreement with the experimental results. However, the model needs further refinement to help capture the cracking load and the load drop after the peak.

While the system appears ready for implementation, the following issues may need further investigations:

1. Evaluation of UHPC as wearing surface.
2. Field implementation and monitoring under ambient traffic and/or designated truck loading to ensure constructability and acceptable performance.
3. Potential for use of other types of high-strength steel, including stainless steel.
4. Pullout and beam tests with various rebar sizes to develop a database, which could then be used to propose an equation for calculating development lengths for HSS embedded in UHPC.

7.2 Aluminum Bridge Deck

This light-weight aluminum bridge deck system is made up of five voided extrusions that are attached to each other using tongue and groove connections, and are mechanically fastened to steel girders. The extruded panel weighs 14 lb/ft², which more than satisfies the self-weight requirement for replacing an open grid steel deck. The deck system went through a rigorous set of component, system, and fatigue load testing and analysis, which led to the following conclusions:

1. Aluminum bridge deck panel is a feasible alternative to the open grid steel decks from both the strength and serviceably points of view.

2. Two million cycles of AASHTO-specified fatigue loading on deck panels did not show any sign of global or local failure in the deck panels. Failure of a bolted connection during the fatigue testing was attributed to the fact that only half of the manufacturer-specified bolted clamps were used in the tests due to the narrow flanges of the stringers.
3. Even though deck panels were loaded up to 100 kips in the two residual strength tests, the extreme fiber stresses remained well within their elastic range.
4. Deck-to-girder connections proved adequate for the braking force and the uplift wind, although sudden failure of connections was observed in shear and uplift tests.

While the this deck system appears quite ready for implementation, perhaps even as a test section on an existing bridge deck, the following issues still need to be further investigated:

1. Evaluation of available wearing surfaces, such as Acrydur[®], poured mastic asphalt, or UHPC.
2. Field monitoring of aluminum deck under ambient traffic and designated truck loading.
3. Evaluation of deck-to-girder connection for the uplift force developed due to wind while the bridge is open.

7.3 UHPC-FRP Bridge Deck

This is a composite deck system made of UHPC and FRP tubes. It resembles a hollow core slab but without any metallic reinforcement. FRP tubes take the tension, while the UHPC takes the compression and also serves as the wearing surface. This

composite deck has an additive benefit of corrosion resistant as both materials used have very good corrosion resistance. From a couple of pilot tests on the UHPC-FRP tube deck system, one can make the following conclusions:

1. The system has shown good promise to replace the conventional open steel grid decks. Based on the ultimate loads of the two simple-span specimens, it can be inferred that the multi-unit system will achieve the target load.
2. Both specimens failed suddenly in compression. However, the uniform section deck specimen had significant tensile cracks, as opposed to the tapered section deck that developed no tensile cracks.
3. Greater composite behavior between UHPC and FRP tubes was observed for the uniform section deck specimen, mainly because the FRP tubes were fully encased in UHPC throughout the span length.

Since the system has shown significant promise, the experimental work should be expanded to multi-unit two-span specimens. The connections between adjacent deck panels and as well with girders should be designed and tested. Moreover, fatigue behavior of the deck needs to be evaluated.

VITA

MUHAMMAD AZHAR SALEEM

Aug. 11, 1981	Born, Lahore, Pakistan
1999-2003	B.Sc. Civil Engineering University of Engineering and Technology Lahore, Pakistan
2003-2005	M.Sc. Civil Engineering University of Engineering and Technology Lahore, Pakistan
2007-2011	Ph.D. Candidate, Civil Engineering Florida International University Miami, Florida, US
2003-2007	Lecturer University of Engineering and Technology Lahore, Pakistan
2005-2007	Structural Engineer Republic Engineering Corporation Lahore, Pakistan
2007-2011	Research/Teaching Assistant Florida International University Miami, Florida, US